Check for updates

Received: 28 February 2026 | Accepted: 18 September 2026

DOI: 10.1111/syen.70073

ORIGINAL ARTICLE

Systematic Entomology

# The origin and evolution of Dolichoderinae, a dominant ant clade (Hymenoptera: Formicidae)

Ziv E. Lieberman [1] | Jill T. Oberski [2,3] | Brendon E. Boudinot [3]

[1]Department of Entomology & Nematology, University of California, Davis, California, USA

[2]Senckenberg Forschungsinstitut und Naturmuseum Frankfurt, Senckenberg – Leibniz Institution for Biodiversity and Earth System Research, Frankfurt am Main, Germany

[3]Department of Biology, Hope College, Holland, Michigan, USA

**Correspondence**
Ziv E. Lieberman, Department of Entomology & Nematology, University of California, Davis, One Shields Ave, 95616, Davis, California, USA.
Email: zlieberman@ucdavis.edu

**Funding information**
National Science Foundation, Grant/Award Number: DEB-1932062; University of California, Davis

## Abstract

Although the phylogeny of ants (Hymenoptera: Formicidae) has been extensively studied with phylogenomic techniques, the species-rich subfamily Dolichoderinae has never been treated with genomic data. The subfamily is ecologically diverse and known for morphological homogeneity coincident with cases of extreme derivation in taxa such as *Dolichoderus* Lund. To study these evolutionary and ecological dynamics, a modern, comprehensive phylogenetic framework is necessary. Here, we address this gap using ultraconserved elements and 131 terminals including all genera of Dolichoderinae except *Ecphorella* Forel. Our results both substantiate the monophyly of tribes and most genera and recover novel relationships, facilitating a new classification of genus groups. We recover the aberrant genus *Anillidris* as sister to the Neotropical depauperon *Paranillidris relicta* (**gen. nov.**, **comb. nov.**) within the *Leptomyrmex* genus group. Morphological reinvestigation reveals synapomorphies for this and other clades and illuminates patterns of homoplasy. Divergence dating and historical biogeographic analyses support an origin of Dolichoderinae in Eurasia near the Cretaceous–Tertiary boundary, with most tribes and genus groups arising in the Palaeogene. Some clades show high geographic fidelity, while others have complicated histories including multiple dispersals among bioregions. We compare model performance, highlighting areas in need of conceptual and operational attention. We synonymize the genera *Arnoldius* Dubovikoff (**syn. nov.**) and *Chronoxenus* Santschi (**stat. rev.**) under *Bothriomyrmex* Emery and treat *Iridomyrmex anceps* (Roger) as a senior synonym of *Anonychomyrma glabrata* **syn. nov**. We also propose the following new and revised combinations: *Tapinoma indicum* Forel **comb. rev.**; *Technomyrmex epinotalis* (Karavaiev) **comb. nov.**; *Technomyrmex flavidus* (André) **comb. nov.**; *Technomyrmex incisus* (Stitz) **comb. nov.**; *Ochetellus democles* (Walker) **comb. nov.**; †*Schismiscapus caritatis* (Brandão and Baroni Urbani) **comb. nov**. and †*Schismiscapus hispaniolae* (Wilson) **comb. nov**. Finally, we provide a synopsis of genus groups, including a suite of new diagnostic male characters, and an updated, illustrated key to workers of extant genera.

KEYWORDS
divergence dating, historical biogeography, palaeoentomology, phylogenomics, systematics

This is an open access article under the terms of the Creative Commons Attribution-NonCommercial License, which permits use, distribution and reproduction in any medium, provided the original work is properly cited and is not used for commercial purposes.

© 2026 The Author(s). *Systematic Entomology* published by John Wiley & Sons Ltd on behalf of Royal Entomological Society.

## INTRODUCTION

The spectacular diversity of ants (Hymenoptera: Formicidae) (Bolton, 2026; Boudinot et al., 2025; Hölldobler & Wilson, 1990; Oberski, Griebenow et al., 2025) is unevenly distributed in space, through time and across the phylogeny. Just five of 16 extant subfamilies contain some 93% of species richness: Dolichoderinae, Dorylinae, Formicinae, Myrmicinae and Ponerinae (Bolton, 2026). Among these 'big five', the Dolichoderinae comprises ca. 730 extant species (Bolton, 2026), but its members are often numerically and/or ecologically dominant in the myrmecofauna, especially in the Neotropical and Australasian regions (e.g., Andersen, 1995). These ants are also frequently conspicuous, their visibility enhanced by the propensity of most species to forage epigeically, arboreally or both – and sometimes in very large numbers, as in the perennial trunk trails of the Holarctic genus *Liometopum* Mayr, which can reach 80 m in length (del Toro et al., 2009; Wang et al., 2010). The 'odorous ants' (Dolichoderinae) are additionally diagnosable by the production of volatile iridoid terpenoids and other compounds by the hypertrophied pygidial glands (Billen, 1986, 1994, 2009) and the synapomorphic Pavan's gland (Billen, 1986; Pavan, 1955).

A number of dolichoderine species are popular study systems for insect ecologists due to extensive symbioses with plants and hemipterans. The Neotropical genus *Azteca* Forel is especially recognized for obligate associations with myrmecophytes, including species of *Cordia* L., *Cecropia* Löf., *Duroia* L.f., *Patima* Aublet, *Remijia* DC., *Tachigalia* Aubl. and *Triplaris* Löf. (Longino, 1989, 1996; Wheeler, 1942), but myrmecophytic partnerships occur in many regions and with a diversity of plant and ant partners. *Philidris* Shattuck ants in Indomalaya and Australasia inhabit domatia of *Myrmecodia* Jack, tubers of *Hydnophytum* Jack, rhizomes of *Lecanopteris* Reinw. and the bursate 'ant leaves' of *Dischidia* R. Br. (Bequaert, 1922; Janzen, 1974; Peeters & Wiwatwitaya, 2014). In the Afrotropics, certain species of *Axinidris* Weber and *Technomyrmex* Mayr occupy swollen stems of *Canthium* Lam. and *Cuviera* DC. (Wheeler, 1922), and leaf pouches of *Scaphopetalum* Mast. (Dejean & Djieto-Lordon, 1996). *Anonychomyrma* Donisthorpe in the New Guinea highlands may tend coccid scales within myrmecophytic *Myristica* Gronov. (Gullan et al., 1993).

Mutualisms with sternorrhynchan hemipterans are common, reaching their obligate apotheosis in the 'wandering herdsmen' or '*Wanderhirten*' of the *Dolichoderus cuspidatus* (Smith) clade, which are unique among ants as nomadic symbionts of coevolved pseudococcid mealybugs (Dill et al., 2002). Dolichoderines are also well known in the public consciousness due to a number of human-mediated globe-trotting species such as the household pest *Tapinoma melanocephalum* (Fabricius) or 'ghost ant', and the highly destructive and supercolonial adventive *Linepithema humile* (Mayr) or 'Argentine ant.' The latter is considered one of '100 of the world's worst invasive species' ((Lowe et al., 2019); see also Hughes et al. (2024)), and has spread from its humble Neotropical origins to six continents in the last century. Supercoloniality is also a biological factor in the spread of the 'great gland ant' ('große Drüsenameise', *Tapinoma magnum* Mayr and kin) in Central Europe (Seifert et al., 2017), whose infamy is due to their ability to damage public and private infrastructure.

The taxonomic history of the Dolichoderinae has been convoluted, and a number of lineages lack modern or comprehensive revisions. The subfamily is readily diagnosable, although many characters are convergently shared with the Formicinae, including the usually thin and weakly sculptured cuticle; the unpetiolated third and unconstricted fourth abdominal segments; the lack of an injective sting; and certain features of the proventriculus (Bolton, 1994; Boudinot et al., 2025; Eisner, 1957; Matte et al., 2025). Important characters for general recognition were already noted by Forel (1878), specifically the transverse cloacal orifice (often incorrectly called the 'anus' or 'anal opening'), which contrasts with the tubular, coronulate acidopore of Formicinae; and the often vertical, tilted or keel-shaped seventh abdominal sternite. Workers are additionally characterized by a combination of the usual presence of dentition on the basal mandibular margin, and a number of abdominal characters including the sessile petiole, and the strongly emarginate helcial tergite (Bolton, 1994; Shattuck, 1992a); for further anatomical detail, see Boudinot, Borowiec, & Prebus (2022). Males are diagnosed by the unique conformation of the gonopod ('paramere'), with a reduced gonostylus ('telomere') which does not extend proximoventrally below the distal gonocoxital ('basimeral') margin, and by a further combination of several characters of the wing and soma (Boudinot, 2015) (for discussion and comparison of genital terminology, cf. Boudinot, 2013, dal Pos et al., 2023, Griebenow et al., 2023, and Boudinot et al., 2024). Juvenile characters, including loss of the pupal cocoon and reduction of the maxillary palps in larvae, were also evinced as synapomorphies in cladistic analysis (Shattuck, 1992b).

While these characters provide strong criteria for recognizing the Dolichoderinae, discriminating genera and species has historically been much more difficult. Dolichoderines are known for broad-scale morphological homogeneity, both within and among genera, which in some cases is superficial, but often represents extensive homoplasy at multiple anatomical scales. The combination of misinterpretation of convergent traits with limited understanding of variation due to undersampling led to the establishment of a number of wastebasket genus-group taxa. For example, *Iridomyrmex* Mayr at one time encompassed species now classified in *Anonychomyrma*, *Chronoxenus* Santschi, *Doleromyrma* Forel, †*Eldermyrmex* Shattuck (= †*Ctenobethylus* Brues), *Gracilidris* Wild & Cuezzo, *Linepithema* Mayr, *Ochetellus* Shattuck, *Papyrius* Shattuck, *Philidris* and †*Yantaromyrmex* Dlussky & Dubovikoff. The taxonomic histories of *Dorymyrmex* Mayr and *Dolichoderus* Lund (among others) are similarly convoluted at the levels of genus, subgenus, species and subspecies. Coincident with overall morphological similarity are limited examples of clearly derived lineages such as *Dolichoderus* and *Leptomyrmex* Mayr, which are mostly distinguished by autapomorphies, problematizing their affinities in morphological phylogenies. Several dolichoderines are also critically understudied because of the lack of material, due to exceptional rarity or highly cryptic habits. The most enigmatic dolichoderine is surely *Ecphorella wellmani* (Forel), still known only from the holotype worker over a century after its discovery (Forel, 1909). Ecological crypsis and autapomorphic morphology coincide in the blind, aberrant *Anillidris bruchi* Santschi, known from scant collections beneath stones or in soil

13653113, 2026, 4, Downloaded from https://resjournals.onlinelibrary.wiley.com/doi/10.1111/syen.70073 by Readcube (Labtiva Inc.), Wiley Online Library on [06/11/2026]. See the Terms and Conditions (https://onlinelibrary.wiley.com/terms-and-conditions) on Wiley Online Library for rules of use; OA articles are governed by the applicable Creative Commons License

to a depth of 50 cm (Borgmeier, 1937; Santschi, 1936, 1937; Schmidt et al., 2013).

Considerable taxonomic clarity across the Dolichoderinae was provided by the generic revision of Shattuck (1992a), whose genus concepts are mostly stable and largely substantiated by the present work, with the few exceptions being made in the light of more recently described material and new molecular evidence. Nevertheless, many questions of both higher classification and interspecific relationships remain. The extant Dolichoderinae has been divided into one to five tribes since the first considerations by Emery (1913). Shattuck (1992a), recognizing that previous tribal limits were inaccurate, and further observing 'phenetic gaps among genera' to be 'fairly uniformly distributed throughout the subfamily' (p. 6), eschewed tribes entirely, implicitly treating the subfamily as a single tribe Dolichoderini. The current four tribe system was established in the most recent molecular phylogeny of Dolichoderinae (Ward et al., 2010). This study was fundamental to the contemporary understanding of dolichoderine evolution and provided independent evidence for the monophyly of tribes and genera. Ward et al. (2010) also performed the first divergence dating and biogeographic inference for the subfamily, while demonstrating both the importance of its relict sister taxon *Aneuretus* Emery (Aneuretinae) in topological inference, and the effects of alignment partitioning. However, the phylogeny of Ward et al. (2010) was constrained by available sequencing technologies, being based on a limited 10-gene dataset, and had moderate taxon sampling density.

Overall, the Dolichoderinae has been phylogenetically neglected in the era of high-throughput sequencing, especially considering the proliferation of recent systematic studies in ants. The advent of phylogenomic techniques has facilitated robust inference of higher ant taxonomy (e.g., Branstetter et al., 2017; Romiguier et al., 2022), and the relationships of subfamilies are now considered highly stable (with the exception of the earliest-branching lineages Leptanillinae Emery and Martialinae Rabeling & Verhaagh with respect to the remaining Formicidae or 'Euformicia'). Similarly, the internal phylogenies of most 'big five' subfamilies have been partially or exhaustively studied using broad sampling and ultraconserved elements (UCEs). The taxonomically challenging Ponerinae was recently investigated at an unprecedented scale, with comprehensive sampling (Doré et al., 2025), and the Formicinae and Dorylinae have seen similar attention (Blaimer et al., 2015; Borowiec, 2019; Ward et al., 2016). The megadiverse Myrmicinae was addressed with a multilocus dataset (Ward et al., 2015), and subsequent studies have questioned the tribal relationships recovered therein (Branstetter et al., 2017; Romiguier et al., 2022), but phylogenomic analyses of major myrmicine tribes provide significant additional resolution (Blaimer et al., 2018; Prebus & Rabeling, 2025). In contrast, of the Dolichoderinae, only *Dorymyrmex* has been studied phylogenomically with extensive taxon sampling (Oberski, 2022, 2024); this study also including a representative sample of *Forelius* Emery and *Leptomyrmex*. A recent phylogeographic study of *Tapinoma* Foerster was also recently performed with UCEs (Pérez-Flores et al., 2025) but was largely constrained in terms of sampling and scope by a focus on *T. melanocephalum*. Other phylogenomic data have been generated in a few restricted cases, most pertinently for *Technomyrmex* (Hsu et al., 2025), but only applied to population-genetic study. The need for a comprehensive analysis of tribal and generic relationships in the Dolichoderinae is therefore apparent, especially given the long-standing and well-known difficulties of morphological classification in the subfamily (e.g., Shattuck, 1992b).

With regard to divergence dating and historical biogeography, the Dolichoderinae benefits from an unusually rich fossil record, with 141 valid extinct species (Bolton, 2026) in 21 genera, of which 15 are extinct. These fossil taxa often have compellingly different distributional patterns compared with contemporary ranges (although these apparent patterns are surely affected by sampling bias towards certain fossil Lagerstätten). Modern dolichoderines are globally distributed, attaining their greatest richness in the Neotropical, Indomalayan and Australasian bioregions, with relative species paucity in the Palearctic and low genus richness throughout the Holarctic. By contrast, dolichoderines are copiously represented in Holarctic ambers and impressions, especially of Eocene age, as well as in Neotropical ambers of the Miocene. In these Lagerstätten, dolichoderines may account for a substantial proportion of known species, individuals or both. For example, in the Middle Eocene Green River impressions, Dolichoderinae accounts for 61% of ant material, while the figure is 62.6% for the Florissant Formation of the earliest Oligocene (Dlussky & Rasnitsyn, 2003). In Baltic Amber, about 20% of species and 63.7% of individuals are dolichoderines (Dlussky & Rasnitsyn, 2003). This abundance is sometimes highly biased; for example, 25% of the Green River material is †*Dolichoderus kohlsi* Dlussky & Rasnitsyn (Dlussky & Rasnitsyn, 2003). Famously, the species †*Ctenobethylus goepperti* (Mayr) was originally estimated to represent a third of all ants found in Baltic amber (Mayr, 1868), a number increased to nearly half (46.5%) with greatly expanded sampling (Wheeler, 1915). The same species constitutes a third of contemporaneous Rovno Amber material (31%; Dlussky & Perkovsky, 2002). Similarly, dolichoderines dominate Miocene Dominican amber, in which †*Azteca alpha* Wilson represents one third to one half of all material (Johnson et al., 2001; Wilson, 1985). In addition to information from geographic distribution and abundance, fossils provide ecomorphological evidence that illuminates extant dolichoderine diversity. For example, it has been inferred that besides faunal dominance, the commonality of †*C. goepperti* in amber, as well as its likely sistergroup relationship to *Liometopum*, indicates arboreal nesting (Boudinot et al., 2026; Dlussky, 1997), a niche often filled by formicines in the present-day northern hemisphere.

With the benefit of genomic data and increased material availability, we here revisit basic questions of dolichoderine evolution: Are current tribes and genera monophyletic, and what are their relationships? When and where did major clades of Dolichoderinae evolve, and what biogeographic patterns explain extant distributions? What taxonomic changes best reflect the phylogeny? We use a primary dataset of ultraconserved elements (Faircloth et al., 2012) from 131 terminals representing 128 species spanning the entire Dolichoderinae, along with its sister subfamily Aneuretinae and their closest relatives, the Myrmeciomorpha. In order to test the robustness of the

13653113, 2026, 4, Downloaded from https://resjournals.onlinelibrary.wiley.com/doi/10.1111/syen.70073 by Readcube (Labtiva Inc.), Wiley Online Library on [06/11/2026]. See the Terms and Conditions (https://onlinelibrary.wiley.com/terms-and-conditions) on Wiley Online Library for rules of use; OA articles are governed by the applicable Creative Commons License

data to modelling choices, we infer phylograms under a variety of alignments and model conditions, including maximum likelihood and Bayesian inference, concatenation with several partitioning schemes and the multispecies coalescent model, as well as using alignments of exonic sequences extracted from the UCE data. We recover highly supported trees with strong topological congruence among treatments at all but selected shallow nodes. Our phylogenetic results facilitate a discussion of morphological homoplasy and synapomorphy within and among several key clades, including the *Leptomyrmex* genus group as newly recognized.

To explore divergence dates and historical biogeography, we combine re-evaluated fossil data with our extant phylogeny to infer node-calibrated chronograms. From our model comparisons and by reference to simulation studies, we discuss limitations and opportunities in prior design and model behaviour, highlighting the need for explicit choices and the value of empirical model testing. We reconstruct ancestral areas and discuss possible biogeographic histories in major clades. Finally, we provide a taxonomic synopsis with revised diagnoses for major extant and extinct groups, including new male characters, along with an updated, illustrated global key to dolichoderine genera.

## MATERIALS AND METHODS

Detailed methods are provided in File S1.

### Taxon sampling

Our molecular dataset includes 125 ingroup taxa, representing one or more species of all extant genera of Dolichoderinae except *Ecphorella* (Table S1). We sampled a single specimen per species, with three exceptions in which we included two terminals each: two sequences of *Anillidris bruchi*, due to this species' rarity in collections, its highly derived morphology and because it has not previously been included in a molecular phylogeny of Dolichoderinae; two specimens identified morphologically as *Forelius pruinosus* (Roger) from disparate localities, which were recently recovered as non-sister taxa (Oberski, 2024); and two specimens of *Tapinoma jandai* Seifert from disparate localities, originally identified morphologically as different species, the identity of which was clarified during manuscript preparation following Seifert (2025). For genera with more than two species, our sampling density is approximately proportional to genus-level species richness. We chose terminals to span demonstrated and hypothetical nodes, and to represent morphological and geographical diversity. We informed our sampling using integrative systematic work for *Dorymyrmex* (Oberski, 2022, 2024) and *Leptomyrmex* sensu lato (Barden et al., 2017; Boudinot et al., 2016; Lucky, 2011), and morphological studies for *Iridomyrmex* (Heterick & Shattuck, 2011), *Leptomyrmex* (Lucky & Ward, 2010; Smith & Shattuck, 2009), and *Technomyrmex* (Bolton, 2007). We selected *Dolichoderus* species based on preliminary results of an ongoing phylogenomic study of the genus (Lieberman, unpublished).

The sister relationship between Dolichoderinae and *Aneuretus simoni* Emery (Aneuretinae), that is, the Dolichoderomorpha, has been robustly recovered, as has the sister relationship of Dolichoderomorpha to the Myrmeciomorpha (Myrmeciinae + Pseudomyrmecinae) (Borowiec et al., 2019, 2025; Branstetter et al., 2017; Romiguier et al., 2022; Ward et al., 2010); for clade names see Oberski, Griebenow et al. (2025). Therefore, we used *A. simoni* as an 'inner outgroup' and chose two species of *Myrmecia* Fabricius (Myrmeciinae) and one species of each genus of Pseudomyrmecinae (*Myrcidris epicharis* Ward, *Pseudomyrmex oculatus* (Smith) and *Tetraponera natalensis* (Smith)) as 'outer outgroups'. Sampling localities are visualized in Figure 1.

### Material

We obtained specimens from the following repositories. Abbreviations follow Bolton (2026), available at www.antcat.org/institutions. A full list of material, including collection and deposition information, is given in Table S1.

CASC California Academy of Sciences; San Francisco, CA, USA
JKWC Jim K. Wetterer collection, USA.
JTLC John T. Longino Research Collection; University of Utah; Salt Lake City, UT, USA
PSWC Philip S. Ward Research Collection; University of California, Davis, Davis, CA, USA

No new collections were made for this study, and all material was originally collected following relevant local permits and regulations, hence no further authorizations were required. Each molecular sequence is represented by a physical voucher, which for adults is usually the extracted specimen itself. Immatures, which were destroyed during extraction, are vouchered by an adult from the same nest or collection series. Each voucher received two unique identifying numbers, one for the DNA extraction (e.g., D####) and one for the specimen (e.g., CASENT#######). All vouchers were imaged and uploaded to AntWeb.org, which provides collection data and repository for all vouchers.

The new genus established here has been registered as a nomenclatural act in ZooBank. The ZooBank publication record for this paper is: https://zoobank.org/urn:lsid:zoobank.org:pub:979F6919-CC7E-406B-AA7B-8B4176966F16

### Imaging and visualization

Specimen images were acquired as focus stacks using either a Keyence VHX-970F digital microscope (Keyence Corporation of America, Itasca, IL, USA); a Leica MZ16A stereomicroscope with a Leica DMC2900 camera (Leica Microsystems Inc., Deerfield, IL, USA); or a Leica M205C stereomicroscope with a Leica MC190 HD sensor. We plotted trees and distributions using FigTree v1.4.4 (Rambaut, 2018), and the packages 'MCMCtreeR' (Puttick, 2019; Puttick & Title, 2019),

13653113, 2026, 4, Downloaded from https://resjournals.onlinelibrary.wiley.com/doi/10.1111/syen.70073 by Readcube (Labtiva Inc.), Wiley Online Library on [06/11/2026]. See the Terms and Conditions (https://onlinelibrary.wiley.com/terms-and-conditions) on Wiley Online Library for rules of use; OA articles are governed by the applicable Creative Commons License

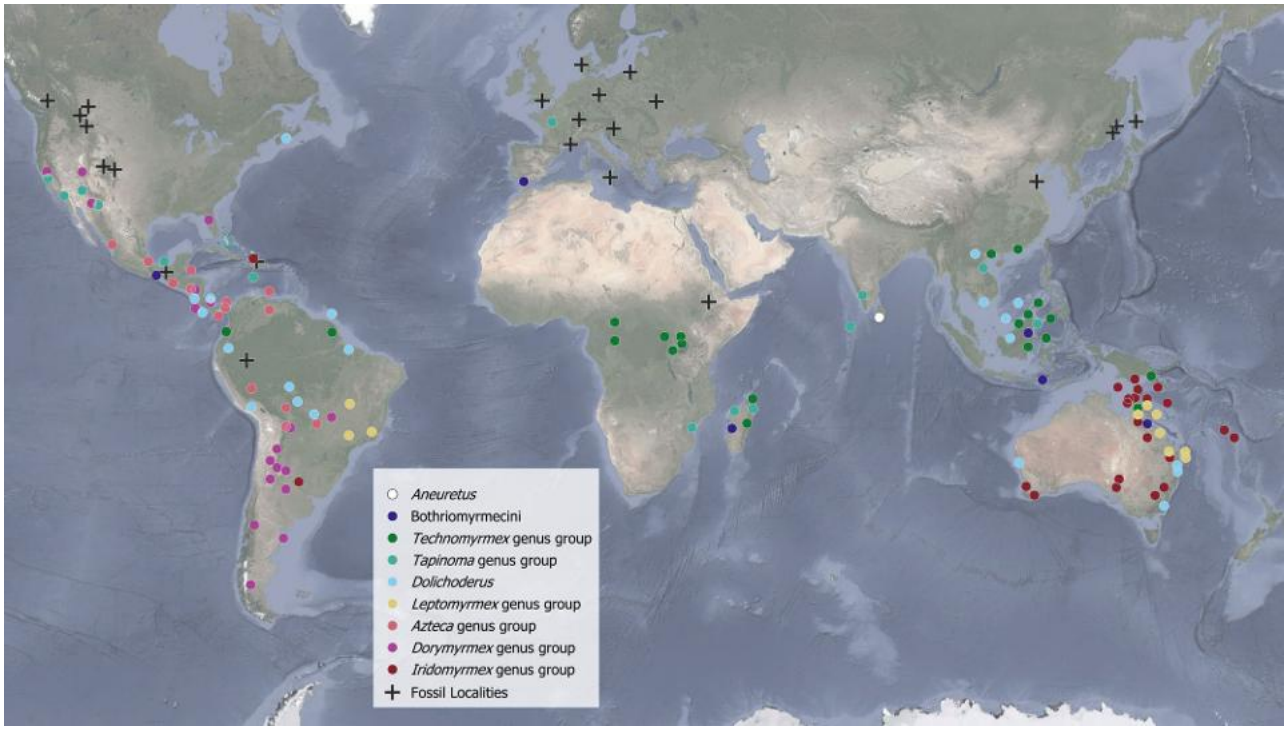



**FIGURE 1** Localities of sampled ingroup terminals, plus *Aneuretus* (coloured circles) and important fossil localities (black crosses). Colours correspond to genus groups as shown in the inset legend. Points corresponding to the same locality or very close coordinates are jittered to reduce visual overlap.

'ggtree' (Yu et al., 2017) and 'RevGadgets' v1.2.1(Tribble et al., 2023) in R v4.3.1 (R Core Team, 2023). The locality map was made in QGIS 3.40.14 (QGIS Association, 2026). Photomicrographs were levels-adjusted and sharpened in Adobe Photoshop CC 2025, and figures were composed in Adobe Illustrator CC 2025 (Adobe Inc., San Jose, CA, USA).

## External sequence data

One sequence of *Anillidris* (DZUP517233) was previously published (Camacho et al., 2022), as were all sequence data for *Dorymyrmex*, *Forelius* and *Leptomyrmex* (Oberski, 2022, 2024), except *Forelius chalybaeus* CASENT0106157. All other sequence data were newly generated, either by re-sequencing previously extracted aliquots or from new extractions (Table S2).

## DNA extraction and shearing

We re-sequenced 28 aliquots from DNA extractions performed by Ward et al. (2010) (Table S2). These aliquots were housed in the Ward Lab at UC Davis. The majority of extractions were newly performed using QIAGEN DNeasy Blood and Tissue Kits (Qiagen, Valencia, CA, USA) with slight modification (see File S1). We nondestructively extracted from individual adults (workers, queens or males) or destructively from immatures (usually pupae), which were ground with a plastic pestle in Buffer ATL prior to the first incubation step (Table S1). We sheared DNA to a target fragment length of around 300–600 base pairs in a Qsonica Q800R3–110 sonicator (Qsonica Inc., Newtown, CT, USA) or for a minority of samples, with a Diagenode Bioruptor (Diagenode LLC., Denville, NJ, USA).

## Library preparation, target enrichment and sequencing

We obtained ultraconserved elements (UCEs) through a combination of target enrichment and in silico capture from low-coverage whole-genome sequencing (WGS). Library preparation and target enrichment were either performed in-house or under similar conditions at RAPiD Genomics (Gainesville, FL, USA), Novogene Inc. (Sacramento, CA, USA) or the University of Utah Genomics Core (Table S2). In-house library preparation generally followed Faircloth et al. (2015) as modified by Branstetter et al. (2017). For target enrichment, we used myBaits reagent kits (Daicel Arbor Biosciences, Ann Arbor, MI, USA) and the myBaits UCE Hymenoptera 2.5Kv2A v2-ant-specific probes designed by Branstetter et al. (2017). We followed the myBaits v4.01 protocol until the 24-h 65°C incubation; for the remaining enrichment and quantification we followed the method available at www.ultraconserved.org/#protocols. Final pools were sequenced on either an Illumina HiSeq 2500 or a NovaSeq X at the University of Utah

13653113, 2026, 4, Downloaded from https://resjournals.onlinelibrary.wiley.com/doi/10.1111/syen.70073 by Readcube (Labtiva Inc.), Wiley Online Library on [06/11/2026]. See the Terms and Conditions (https://onlinelibrary.wiley.com/terms-and-conditions) on Wiley Online Library for rules of use; OA articles are governed by the applicable Creative Commons License

Genomics core; an Illumina HiSeq 4000 at Novogene or a NovaSeq X at RAPiD Genomics LLC (Table S2).

## Data processing and alignment

Data were demultiplexed by the sequencing company and provided as 'raw' reads in .fastq.gz format. We processed these data using Phyluce v1.6.7 and its codistributed utilities (Faircloth, 2016). We cleaned reads and trimmed adapters using illumiprocessor (Faircloth, 2013), a wrapper for trimmomatic (Bolger et al., 2014), with default settings. We assembled contigs using SPAdes v.3.12.0–3.14.1 (Bankevich et al., 2012), or, for a few taxa, with Trinity v.2013-02-25 (Grabherr et al., 2011) (Table S2), matching contigs to UCE probes with a minimum identity of 80%. We aligned loci with MAFFT v7.407 (Katoh & Standley, 2013), retaining loci present in a minimum of three taxa and using -no-trim. We trimmed ambiguously aligned and nonconserved regions with Gblocks (Castresana, 2000; Talavera & Castresana, 2007) under relaxed block settings as follows: minimum proportion of sequences for a conserved sequence (−b1) 0.5; minimum proportion of sequences for a flank position (−b2) 0.5; maximum number of contiguous nonconserved positions (−b3) 12; minimum block length (−b4) 7. After determining the number of loci in matrices of varying coverage with *phyluce_align_get_align_summary_data*, we created two matrices by removing loci not represented by a minimum of 85% or 90% of taxa, and concatenated per-locus alignments into two .phylip files. We generated further summary statistics per alignment and per taxon with AMAS v1.0 (Borowiec, 2016) (Tables S3 and S4). Inferential methods detailed below are summarized in Figure S1.

## Alignment selection

In order to determine if the smaller but more complete 90% alignment was suitable for tree inference and downstream analyses, we examined congruence in topology and support between trees inferred from both matrices. We used IQ-TREE2 v2.3.2 (Minh et al., 2020) for maximum likelihood (ML) inference under equivalent model parameters (see below). We obtained identical topologies with negligible differences in branch support, indicating robustness to missing data thresholds. We therefore selected the 90% matrix for further analysis.

## Data partitioning

We implemented three partitioning strategies: unpartitioned, per-locus partitioning and Sliding Window Site Characteristics (SWSC)-based partitioning, the latter reducing dimensionality while preserving site heterogeneity (Tagliacollo and Lanfear, 2018). Locus partitioning used the 1,742 UCE loci in the 90% alignment. For SWSC partitioning, we used the site-entropies method (SWSC-en), implemented in parallel using the UCERegion program in CURE (Freitas et al., 2023). This method subdivides each UCE locus into three parts, representing the high percent-identity core and the more variable left and right flanks. The 5,226 partitions output from SWSC-en were input to ModelFinder (Kalyaanamoorthy et al., 2017) in IQ-TREE2 using the parameter -m TESTMERGEONLY to merge partitions with similar rates without proceeding to tree inference, and using the fast relaxed clustering algorithm from PartitionFinder2 (Lanfear et al., 2017) with the parameter -rclusterf 10 to consider only the best 10% of schemes. We used -merge-model GTR and -merge-rate G during partition merging, in order to restrict model space and improve computational tractability; and additionally because we later used ExaBayes (Aberer et al., 2014), which only implements the generalized time-reversible (GTR) model of nucleotide site evolution. We performed model selection after merging, allowing both models accounting for among-site rate variation using a four-category discretized gamma distribution (+G4) and proportion of invariable sites (+I), because IQ-TREE2 implements the optimization heuristic of Nguyen et al. (2018) to account for parameter competition. IQ-TREE2 output 215 partitions, which we tested for assumptions of stationarity and homogeneity using the matched-pairs tests of symmetry (Naser-Khdour et al., 2019) in IQ-TREE2 with the parameter -symtest. We retained only partitions passing these tests ($n = 126$), thereby minimizing model violation.

## Exon extraction

In systematic studies, UCEs are valued for their phylogenetic utility, rather than for functional properties. Nevertheless, many UCEs are at least partially located in exons, for example, 48.6% in some Hymenoptera (van Dam et al., 2021). To examine topological effects of data reduction and data type, we extracted protein-coding sequences from our full dataset using the program uce-to-protein (Borowiec, 2019) to match unaligned contigs to all available protein sequences ($n = 29{,}009$) from the reference sequence genome assembly for the dolichoderine *Linepithema humile* (Pan et al., 2024) available on NCBI (RefSeq GCF_040581485.1). Uce-to-protein outputs three unaligned .fasta files for each match: as nucleotide (NT) sequences, NTs with the third codon positions removed and as amino acid (AA) sequences. We did not use the files with the third codon positions removed.

We used MACSE v2.07 (Ranwez et al., 2018) to clean sequences and perform codon- and frameshift-aware alignment. We closely followed the steps in the MACSE_ALFIX pipeline but did not implement the pipeline utilities. We pre-trimmed the unaligned NT and AA sequences and generated homologous masks, then aligned each data type. To ensure that we stringently accounted for alignment and sequencing errors, we input the AA alignments into HMMCleaner v0.243280 (di Franco et al., 2019). We used these filtered AA alignments and the NT alignments to produce filtered NT alignments, and exported final alignments of both types. We used Phyluce as described above to create matrices of 50% and 90% taxon coverage. We also partitioned the 90% matrix by locus and performed model selection as above but with -m MFP + MERGE.

13653113, 2026, 4, Downloaded from https://resjournals.onlinelibrary.wiley.com/doi/10.1111/syen.70073 by Readcube (Labtiva Inc.), Wiley Online Library on [06/11/2026]. See the Terms and Conditions (https://onlinelibrary.wiley.com/terms-and-conditions) on Wiley Online Library for rules of use; OA articles are governed by the applicable Creative Commons License

## Maximum likelihood inference

All ML tree inference was performed in IQ-TREE2. We used several model and support estimation approaches for different datasets and partition schemes:

*UCE concatenation.*— For each unpartitioned UCE analysis (alignments 126.5 t-85p and 126.5 t-90p), we used a single GTR + G4 model with empirical site frequencies (+F), and assessing branch support with ultrafast bootstrapping (UFB; Minh et al., 2013; Hoang et al., 2018) and Shimodaira–Hasegawa approximate likelihood ratio tests (SH-alrt; Shimodaira & Hasegawa, 1999; Anisimova et al., 2011), using 1000 replicates for each. For the UCE locus-partitioned inference, we omitted the computationally intensive partition model step due to the high number of partitions, instead providing each partition with its own GTR + F + G4 model. Similarly, we omitted the SH-alrt, using only UFB. We inferred a tree using the 90% UCE alignment and the 215 merged SWSC-en partitions with selected models, UFB and SH-alrt. We used the symmetry-tested reduced alignment (126.5 t-90.swscen.best_model.nex.good.phy) with the 126 partitions and selected models, with UFB and SH-alrt.

*Exon concatenation.*—The 50% exon alignment was assigned a single GTR + F + G4 model; the 90% alignment with locus partitions used a GTR + F + G4 model for each partition; and the 90% alignment with merged loci used the selected models. Support for all exon alignments was assessed only with UFB.

## Multispecies coalescent

To examine concordance of integrated gene-tree and concatenated species-tree inference, we ran IQ-TREE2 in parallel on per-locus alignments using the script *estimate-trees.sh* in CURE (Freitas et al., 2023), which also concatenates trees into single treefiles for input to multispecies coalescent models. Because CURE outputs locus trees with both UFB and SH-alrt supports, we split the concatenated treefile into two by removing one or the other support value from Newick trees. We inferred integrated trees under the multispecies coalescent model (MSC) using ASTER* to run parallelized weighted ASTRAL (wASTRAL) (Yin et al., 2019; Zhang & Mirarab, 2022). Weighted ASTRAL weights the quartet-based species-tree inference method in ASTRAL through the user's choice of metric, in order to account for low quartet support and long terminal branches. We used the hybrid method, incorporating branch lengths and branch supports from locus trees.

## Bayesian inference

We used the 90% concatenated alignment and the merged SWSC-en symmetry-tested partition scheme as input for Bayesian inference (BI) in ExaBayes, removing the model block from the partition Nexus file as ExaBayes only includes the GTR + G model. We conducted four independent inferences with identical settings, except for the number of generations, which we varied after examining convergence and effective sampling of the first runs. Each analysis had linked branch lengths across the 126 partitions, and comprised four runs with four coupled chains and four swaps per generation; we treated the first 10% of each chain as burn-in. We ran the first analysis to 488,000 generations per chain for a combined total of 1758,500 states. The three subsequent analyses were run for 300,000 generations per chain, for a combined total of 1,080,000 states per analysis. We assessed the number of effective samples (ESS), and examined convergence and mixing visually, in Tracer v1.7.2 (Rambaut et al., 2018).

## Divergence dating

For divergence dating, we first vetted all valid fossil dolichoderine species for which literature, specimen images and/or material were accessible and which could provide valid node-age priors, according to best practices (Parham et al., 2012). We used the package PAML (Yang, 2007) to infer node-calibrated chronograms. In order to take advantage of our large alignment while maintaining computational tractability, we used the likelihood approximation approach in MCMCtree, which can be three orders of magnitude faster than exact likelihood calculation (Battistuzzi et al., 2011). We used the same alignment as for ExaBayes, that is, the 90% SWSC-en merged symmetry-tested matrix (126.5 t-90.good.phy), but unpartitioned. We used 1 time unit = 100 million years (hecto-Megaannum, hMa) to obtain node ages in the range 0.01–10.0. The gamma prior on average substitution rate among branches was parameterized with location ($\alpha$) = 1.5 and scale ($\beta$) = 8.192022, using the method recommended in the PAML documentation (dos Reis et al., 2014); see File S1. We parameterized sigma2_gamma with $\alpha = 1$ and $\lambda = 10$ for a large variance in the logarithm of the rate.

We used the GTR model and a G4 distribution for ASRV with an alpha parameter of 0.5. Equal priors were specified on speciation and extinction rate, and extant sampling fraction was calculated from our uniquely sampled species and the extant species richness of Dolichoderomorpha (Bolton, 2026), although this does not account for undescribed species, for example, Oberski (2024). We ran inferences using both the conditional (Yang & Rannala, 2006) and multiplicative constructions (Heled & Drummond, 2012, 2015) of the joint time and birth-death-sampling prior (see Results and Discussion).

Prior to inference, we checked effective priors by running both multiplicative and conditional models without data (usedata = 0) and found that despite several differences in results, no effective priors severely violated minimum constraints. We ran three independent chains for each construction, using burnin = 1e6 and nsample = 20,000 for both, and varying sampfreq from 500 to 600 after observing mixing of the first runs. We combined each triplet of replicate runs into a single trace file for each construction using LogCombiner (Bouckaert et al., 2014). The combined traces had 27,001,000 states each with ESS between 450 and 10,517. To generate dated trees, we used the combined traces, the input topology and the parameter print = −1 in the control file.

13653113, 2026, 4, Downloaded from https://resjournals.onlinelibrary.wiley.com/doi/10.1111/syen.70073 by Readcube (Labtiva Inc.), Wiley Online Library on [06/11/2026]. See the Terms and Conditions (https://onlinelibrary.wiley.com/terms-and-conditions) on Wiley Online Library for rules of use; OA articles are governed by the applicable Creative Commons License

**TABLE 1** Parameters of node-age priors for calibration densities.

| Clade | Distribution | Location (ζ) | Scale (ω) | Shape (α) | PAML syntax |
|---|---|---|---|---|---|
| Dolichoderomorpha | Skew-normal | 0.722 | 0.2 | 10 | 'SN(0.722, 0.20, 10)' |

| Clade | Distribution | Minimum age ($t_L$) | Mode (offset; $p$) | Tail decay (scale; $c$) | Left-tail probability ($p_L$) | PAML syntax |
|---|---|---|---|---|---|---|
| Bothriomyrmecini + Tapinomini | Truncated Cauchy | 0.4807 | 0.1 | 0.1 | 0.025 | 'L(0.4807,0.1,0.1,0.025)' |
| *Ravavy* + *Loweriella* | Truncated Cauchy | 0.1598 | 0.1 | 0.25 | 0.025 | 'L(0.1598,0.1,0.25,0.025)' |
| *Tapinoma* genus group | Truncated Cauchy | 0.339 | 0.1 | 0.1 | 0.025 | 'L(0.339,0.1,0.1,0.025)' |
| *Technomyrmex* genus group | Truncated Cauchy | 0.1598 | 0.1 | 0.25 | 0.025 | 'L(0.1598,0.1,0.25,0.025)' |
| *Dolichoderus* | Truncated Cauchy | 0.4807 | 0.1 | 0.1 | 0.025 | 'L(0.4807,0.1,0.1,0.025)' |
| *Dolichoderus sulcaticeps* + *quadripunctatus* spp. groups | Truncated Cauchy | 0.339 | 0.1 | 0.1 | 0.025 | 'L(0.339,0.1,0.1,0.025)' |
| *Dolichoderus bidens* + *bispinosus* spp. groups | Truncated Cauchy | 0.1382 | 0.3 | 0.3 | 0.025 | 'L(0.1382,0.3,0.3,0.025)' |
| Leptomyrmecini | Truncated Cauchy | 0.1598 | 0.1 | 0.25 | 0.025 | 'L(0.1598,0.1,0.25,0.025)' |
| *Leptomyrmex* genus group | Truncated Cauchy | 0.1382 | 0.3 | 0.3 | 0.025 | 'L(0.1382,0.3,0.3,0.025)' |
| *Azteca* genus group | Truncated Cauchy | 0.1382 | 0.3 | 0.3 | 0.025 | 'L(0.1382,0.3,0.3,0.025)' |

Abbreviations: Clade, calibrated node is the MRCA of the given clade; Distribution, type of statistical distribution used; PAML syntax, calibration densities exactly as specified in the calibration topology.

Calibration parameters are summarized in Table 1. We removed node and branch labels from the ExaBayes consensus tree to produce the fixed input topology, then trimmed Myrmeciomorpha while retaining *Aneuretus*. In addition to the root, we calibrated 10 internal nodes, including clades from all four tribes. We derived deposit and stratum ages mainly from the Paleobiology Database (see citations therein), checked against the International Chronostratigraphic Chart v2024/12 (Cohen et al., 2013). When multiple potential calibrations were available for a given clade and its subclades, we generally chose the most tipward (least inclusive) clade. Conversely, we generally calibrated the parent node of the constrained taxon to allow fossils to be part of total clades. We designed calibration densities semi-subjectively, in that we used the ages of fossiliferous strata or amber deposits for minimum bounds and to inform subjective distribution parameters. We designed priors with greater density towards the middle of stratigraphic ages, with soft minima to account for uncertainty in stratigraphic information, and long right tails to allow for large gaps between speciation and fossilization events. Our calibrated taxa are as follows, in descending node order; see File S1 for justification and details of prior distributions for internal nodes:

1. Dolichoderomorpha root: †*Chronomyrmex medicinehatensis*, from the Campanian Grassy Lake amber (72.2–83.6 Ma).
2. MRCA Bothriomyrmecini + Tapinomini: an undescribed species from Ypresian Hat Creek amber (56.0–48.07 Ma), previously ascribed to *Technomyrmex* (Archibald et al., 2018; Poinar et al., 1999).
3. MRCA of *Ravavy* Fisher + *Loweriella* Shattuck: the only bothriomyrmecine fossil is †*Ravavy goldmani* Boudinot & Perrichot, from Early Miocene Ethiopian amber spanning the Aquitanian to the lower Burdigalian (23.04–15.98 Ma) (Bouju & Perrichot, 2020; Perrichot et al., 2018, 2022).
4. MRCA *Tapinoma* genus group (*Aptinoma* Fisher + (*Liometopum* + *Tapinoma*)): †*Ctenobethylus goepperti*, from Priabonian Baltic and Rovno ambers (37.7–33.90 Ma).
5. MRCA *Technomyrmex* genus group (*Technomyrmex* + *Axinidris* Weber): †*Technomyrmex svojtkai* Perrichot & Engel, from Miocene Ethiopian amber (23.04–15.98 Ma).
6. Crown *Dolichoderus*: an undescribed species of *Dolichoderus* from Hat Creek amber figured by Archibald et al. (2018), Figure 10k.
7. MRCA *Dolichoderus sulcaticeps*- and *quadripunctatus* species groups, represented in our trees by *D. patens* (Mayr) and *D. taschenbergi* (Mayr) respectively: several contemporaneous species of *Dolichoderus* from Priabonian Baltic and Rovno ambers: †*D. polonicus* Dlussky, †*D. tertiarius* (Mayr) and †*D. zherichini* Dlussky.
8. MRCA *Dolichoderus bispinosus*- and *bidens* groups sensu lato: †*Dolichoderus prolaminatus* (Wilson) from Burdigalian-Langhian Dominican Amber (20.45–13.82 Ma).
9. MRCA Leptomyrmecini: †*Schismiscapus exstinctus* Varela-Hernández et al. in Aquitanian-Burdigalian Chiapas amber (23.04–15.98 Ma); see also *Systematic Palaeontology* below.
10. MRCA *Leptomyrmex* genus group (*Leptomyrmex* + (*Anillidris* + *Paranillidris*)): †*Paranillidris neotropica* (Baroni Urbani) (=†*Leptomyrmex neotropicus*), from Dominican amber.
11. MRCA *Azteca* genus group (*Azteca* + *Gracilidris*): †*Azteca alpha* and †*Gracilidris humiloides* (Wilson), from Dominican amber.

Internal nodes were semi-arbitrarily calibrated with soft-truncated Cauchy distributions (Inoue et al., 2010); see Table 1 and File S1 for details.

13653113, 2026, 4, Downloaded from https://resjournals.onlinelibrary.wiley.com/doi/10.1111/syen.70073 by Readcube (Labtiva Inc.), Wiley Online Library on [06/11/2026]. See the Terms and Conditions (https://onlinelibrary.wiley.com/terms-and-conditions) on Wiley Online Library for rules of use; OA articles are governed by the applicable Creative Commons License

**TABLE 2** Summary statistics for alignments used in phylogram inference.

| Alignment | Number of Loci/ partitions | Number of sites | Proportion missing data | Proportion variable sites | Proportion parsimony informative |
|---|---|---|---|---|---|
| 85% UCE matrix | 1984 UCEs | 16,74,398 | 0.20 | 0.64 | 0.49 |
| 90% UCE matrix | 1742 UCEs | 14,70,372 | 0.19 | 0.64 | 0.49 |
| 90% SWSC-en partitioned, merged, symmetry-tested matrix | 126 partitions | 7,94,469 | 0.20 | 0.64 | 0.49 |
| Full exon MACSE-aligned matrix | 1734 exonic loci | 16,40,076 | 0.65 | 0.36 | 0.23 |
| 50% exon MACSE-aligned matrix | 1368 exonic loci | 14,02,371 | 0.61 | 0.37 | 0.24 |
| 90% exon MACSE-aligned matrix | 375 exonic loci | 3,15,588 | 0.53 | 0.35 | 0.24 |

*Note*: Full statistics for each alignment and sequence are given in Tables S3–S7.

## Historical biogeography

We inferred historical biogeography under ML in BioGeoBEARS (Matzke, 2018) and under BI in RevBayes (Höhna et al., 2016). In both programs, we used the MCMCtree chronogram inferred under the conditional joint prior construction (CC), rescaled to units of 1 Ma; and collapsing the terminal pairs of *Anillidris bruchi* and *Tapinoma jandai*. We also used the MC chronogram in BioGeoBEARS to test sensitivity to node ages. We coded distributions for each terminal using six biogeographic regions: Nearctic (R); Neotropical (T); Palearctic (P); Afrotropical (including Malagasy; A); Indomalayan (I); and Australasian (U) (Cox, 2001). Differing from Cox (2001), we considered Weber's line as the boundary between Indomalaya and Australasia (Mayr, 1944). The inclusion of Sulawesi in the Indomalayan region (i.e., partitioned by the Wallace Line sensu Mayr (1944)) more accurately represents ant distribution (Ward et al., 2025), while the inclusion of the Lesser Sunda Islands reflects the distribution of dolichoderine genera including *Leptomyrmex*, *Papyrius* and *Turneria*, and of species groups in *Dolichoderus*. To account for changing geological connectivity over time, we stratified the models into five time bins with breakpoints of 66.0, 48.07, 33.9 and 23.04 Ma, then constructed five corresponding area-adjacency matrices (Table S8) by reference to palaeogeographic maps (Crowley, 2012; Lawver & Gahagan, 2003; Scotese, 2021). BioGeoBEARS requires an upper age for the oldest bin, for which we used 100 Ma.

We ran BioGeoBEARS under six models: Dispersal-extinction-cladogenesis (DEC); DIVALIKE; BAYAREALIKE; and the same models but including founder-event or jump speciation events (+J). We compared models using likelihood ratio tests based on the corrected Akaike information criterion (AICc) (Hurvich & Tsai, 1989). In RevBayes, we implemented the DEC and DEC + J model; for prior details, see File S1. We used the same parameters for both models except for the inclusion of +J. Each pair of areas had the same dispersal and extirpation rates. Based on extant distributions, we restricted inferred range occupancy to a maximum of three regions, and we constrained the root frequencies to the simplex of adjacent regions in the oldest adjacency matrix. We ran each model to 35,000 generations, regarding the first 10% as burnin, and examined mixing and effective sampling in Tracer. To compare relative model fit, we estimated marginal likelihoods in RevBayes with power posterior analysis and calculated Bayes factors.

# RESULTS AND DISCUSSION

Newly generated sequence data had a mean of 6,675,264 reads (median 5,534,586). Alignment statistics are summarized in Table 2; full alignment statistics are given in Table S3, and per-sequence statistics for various alignments in Tables S4–S7. The combined trace from Bayesian phylogram inference had 4,998,500 states and ESS values between 1401 and 10,013. Full trace files for each chain for each analysis are provided in the supplementary data.

## Model comparison

### Phylograms: Topology and support

Differences in topology and support are summarized in Figures S1 and S2; individual trees are in Figures 2 and S3–S12. We recovered generally high congruence in topology and support across alignments and inferential methods. Our six concatenated UCE-based analyses produced identical topologies (hereafter, the 'consensus topology') under ML and BI (Figures 2 and S1–S7). Branch support in these analyses was maximal or high (>90% bootstrap support, BS) at all but three nodes. The node subtending *Papyrius nitidus* (Mayr) was weakly to unsupported with no more than 71% BS in ML trees but had 1.0 posterior probability (PP) in BI (Figure S2). Two shallow nodes in the Southern clade of *Forelius* were unsupported in the 85% matrix only (53% BS) (Figures S2 and S3). Multispecies coalescent (MSC) inferences showed minor topological variance among one another, and with the consensus topology, at several shallow nodes in *Forelius* and *Technomyrmex* (Figures S1, S2 and S7–S9). The MSC also recovered a sister relationship between *Paranillidris relicta* (Boudinot et al.) and *Anillidris bruchi* + *Leptomyrmex*, rather than the sister relationship between *Paranillidris* and *Anillidris*. Support for this arrangement varied from 0.66 local posterior probability (LPP) in unweighted ASTRAL to 0.95 LPP in SH-aLRT based wASTRAL. Exon-based concatenation

13653113, 2026, 4, Downloaded from https://resjournals.onlinelibrary.wiley.com/doi/10.1111/syen.70073 by Readcube (Labtiva Inc.), Wiley Online Library on [06/11/2026]. See the Terms and Conditions (https://onlinelibrary.wiley.com/terms-and-conditions) on Wiley Online Library for rules of use; OA articles are governed by the applicable Creative Commons License

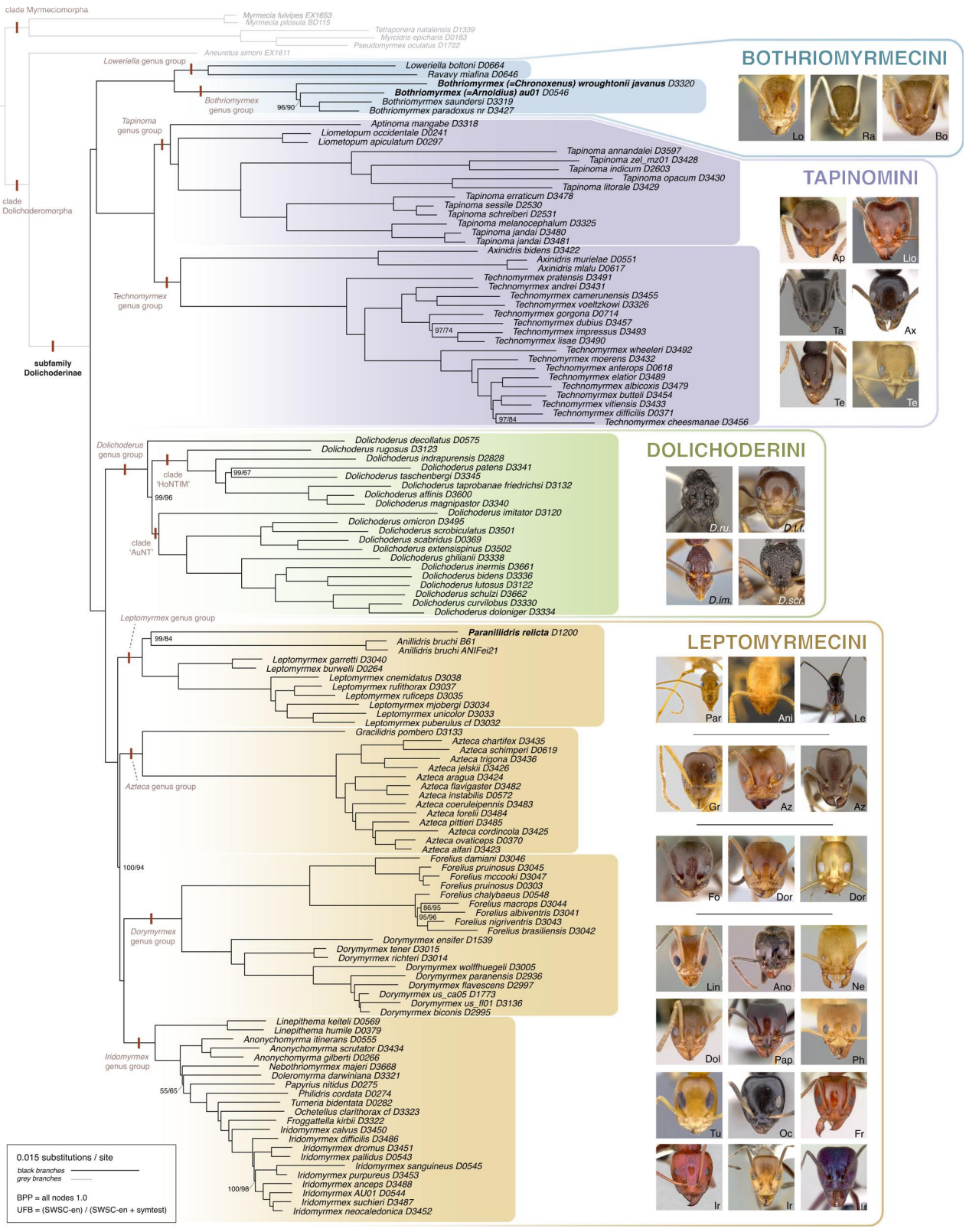



**FIGURE 2** Consensus phylogram from Bayesian inference. All nodes maximally supported (BPP = 1.0) under Bayesian inference; support values for select nodes are from maximum likelihood inferences (90p_swscen-merged-partitioned / 90p_symtest-partitioned) where UFB < 100. Colours correspond to tribes; shaded boxes indicate genus groups. Pictured taxa are abbreviated: Lo = *Loweriella*, Ra = *Ravavy*, Bo = *Bothriomyrmex*, Ap = *Aptinoma*, Lio = *Liometopum*, Ta = *Tapinoma*, Axe = *Axinidris*, Te = *Technomyrmex*, *D. ru* = *Dolichoderus rugosus*, *D. t. f.* = *Dolichoderus taprobanae friedrichsi*, *D. im* = *Dolichoderus imitator*, *D. scr* = *Dolichoderus scrobiculatus*, Par = *Paranillidris*, Ani = *Anillidris*, Le = *Leptomyrmex*, Gr = *Gracilidris*, Az = *Azteca*, Fo = *Forelius*, Dor = *Dorymyrmex*, Lin = *Linepithema*, Ano = *Anonychomyrma*, Ne = *Nebothriomyrmex*, Dol = *Doleromyrma*, Pap = *Papyrius*, Ph = *Philidris*, Tu = *Turneria*, Oc = *Ochetellus*, Fr = *Froggattella*, Ir = *Iridomyrmex*. All photos courtesy of AntWeb (www.antweb.org); for full specimen data and photographer credits, see Table S13.

13653113, 2026, 4, Downloaded from https://resjournals.onlinelibrary.wiley.com/doi/10.1111/syen.70073 by Readcube (Labtiva Inc.), Wiley Online Library on [06/11/2026]. See the Terms and Conditions (https://onlinelibrary.wiley.com/terms-and-conditions) on Wiley Online Library for rules of use; OA articles are governed by the applicable Creative Commons License

trees showed the most variability, including discordant tribal relationships (Figures S1, S2 and S10–S12). In contrast to all other trees, exon-based alignments produced a balanced *Bothriomyrmex*, with a clade of *B.* (=*Arnoldius*) au01 plus *B.* (=*Chronoxenus*) *wroughtonii javanus* Forel, sister to *B.* sensu stricto. Minor topological disagreements also occurred in *Dorymyrmex*, *Forelius*, *Iridomyrmex* and *Technomyrmex*, and in the early branches of *Dolichoderus*, with widely variable support (Figures S1, S2 and S10–S12).

The discordance between UCE-based topologies was mostly concentrated at shallow nodes and short branches. While exon-based alignments produced differences at deeper nodes, they suffered from high proportions of missing data and low proportions of parsimony-informative sites (Figure S1; Tables 2 and S3). Additionally, gene concordance vectors for the UCE alignment and consensus topology were improved compared with either exon alignment, with higher concordance and reduced discordance due to polyphyly (Figure S13, Tables S9 and S10). The difference in intertribal topologies, and correspondence between the 50% exon tree and Ward et al. (2010), may be attributable to the type of data (exonic sequences here and protein-coding genes in Ward et al. (2010)) and/or to missing data. Because exon capture was sparse, missing data and data type are confounded in our analyses.

It is possible that MSC inferences were more accurate than UCE analyses at shallow nodes in *Forelius*, *Technomyrmex* and *Iridomyrmex*, given that the short branches involved may have precluded sufficient time for deep coalescence. Therefore, any topology in these groups of species should be considered provisional for the present. Nevertheless, given the robustness of our UCE concatenated analyses to alignment, partition and model approaches, we used the consensus topology for downstream analyses. Among these trees, support was similar between the 90% SWSC-en partitioned tree and the 90% symmetry-tested reduced tree under ML and BI. While the BI tree had 1.0 PP at all nodes, BI posterior probabilities are expected to be higher than ML bootstrap supports (Erixon et al., 2003), hence we display the BI tree with support values from these three inferences in Figure 2.

## Divergence dating

Our data-free analyses to assess effective priors found that both constructions of the joint time and tree process priors had variable behaviour across nodes (Figures S14–S26). Most notably, for three calibrated nodes (the MRCAs of the *Technomyrmex*, *Leptomyrmex* and *Azteca* genus groups), the conditional construction (CC) produced strongly bimodal effective priors (Figures S18 and S23–S24). Each had a density peak within the calibrated distribution, and another at older ages, speculatively representing different contributions of the calibration and birth-death-sampling densities. Effective priors at the same nodes under the multiplicative construction (MC) were all unimodal but skewed towards older ages than the calibration density. (Figures S18 and S23–S24). A similar skew in MC occurred at the MRCAs of Bothriomyrmecini + Tapinomini (Figure S15), *Dolichoderus* (Figure S19), and the *Tapinoma* genus group, which was also diffuse and weakly bimodal (Figure S17). At the other calibrated nodes, both CC and MC effective priors were overall comparable to one another and to the specified densities. At uncalibrated nodes, almost all effective priors were also strongly bimodal under CC (Figure S25).

Since both constructions seemingly had strengths and weaknesses based on data-free analyses, and no effective priors strongly violated minimum age constraints, we ran inferences with data under both methods. All CC posterior distributions were unimodal (Figure 3), except at the MRCA of *Loweriella* + *Ravavy*, which was unusually trimodal, with a geometric mean of 29 Ma and minor peaks in density at around 18 and 36 Ma, the younger peak overlapping with the calibration density. The skew towards older ages in MC priors was recapitulated in posterior estimates across the tree, except at the root (Figure S27): the mean difference between MC and CC posterior mean estimates was +5 Ma (11–0.6 Ma), while the root node was around 15 Ma younger in MC (Figures S28 and S29; Table S11). MC posteriors were also overall somewhat diffuse (Figure S28).

In the absence of definitive criteria for evaluating results, we consider that the posterior estimates under CC were overall more realistic. For example, the 95% highest posterior density (HPD) for the root under MC was 79–67 Ma, while the calibrating fossil stratum is minimally 72.2 Ma; by comparison, the CC 95% HPD for the root was 111–70 Ma (Figure S29). Several major clades had mean ages older than the Cretaceous-Tertiary boundary, or very shortly after, under MC, which we consider a priori unlikely. Specifically, the Bothriomyrmecini + Tapinomini had a mean age of 70 Ma, Bothriomyrmecini a mean age of 64 Ma, Dolichoderini + Leptomyrmecini a mean age of 68 Ma and the clade comprising the *Azteca*, *Dorymyrmex* and *Iridomyrmex* genus groups had a mean age of 63 Ma (Figure S29). We therefore focus below on results from the CC inference (Figure 3), which we also selected for biogeographic inferences.

## Historical biogeography

BioGeoBEARS likelihood ratio tests under CC narrowly favoured BAYAREALIKE+J ('BALJ') (Table 3), while under MC the best fitting model was DEC + J. Inferred areas for CC BALJ were the same as MC DEC + J at most nodes, with only a few differences at nodes in the *Technomyrmex* genus group (Supplementary Data). We therefore focus on CC BALJ, because we also used the CC chronogram for Bayesian inference. Bayes factors from power posterior analysis, calculated using stepping stones and path sampling, were equivocal between Bayesian DEC ('BDEC') over Bayesian DEC + J ('BDECJ') (Table 4) following the approximate scale of Jeffreys (1961).

## Summary of tribes and genus groups

To aid in the following report and discussion, we here introduce informal names for monophyletic groups of genera. For a complete taxonomic synopsis, including taxonomic actions, see *Extant Taxonomy* and *Systematic Palaeontology* below.

13653113, 2026, 4, Downloaded from https://resjournals.onlinelibrary.wiley.com/doi/10.1111/syen.70073 by Readcube (Labtiva Inc.), Wiley Online Library on [06/11/2026]. See the Terms and Conditions (https://onlinelibrary.wiley.com/terms-and-conditions) on Wiley Online Library for rules of use; OA articles are governed by the applicable Creative Commons License

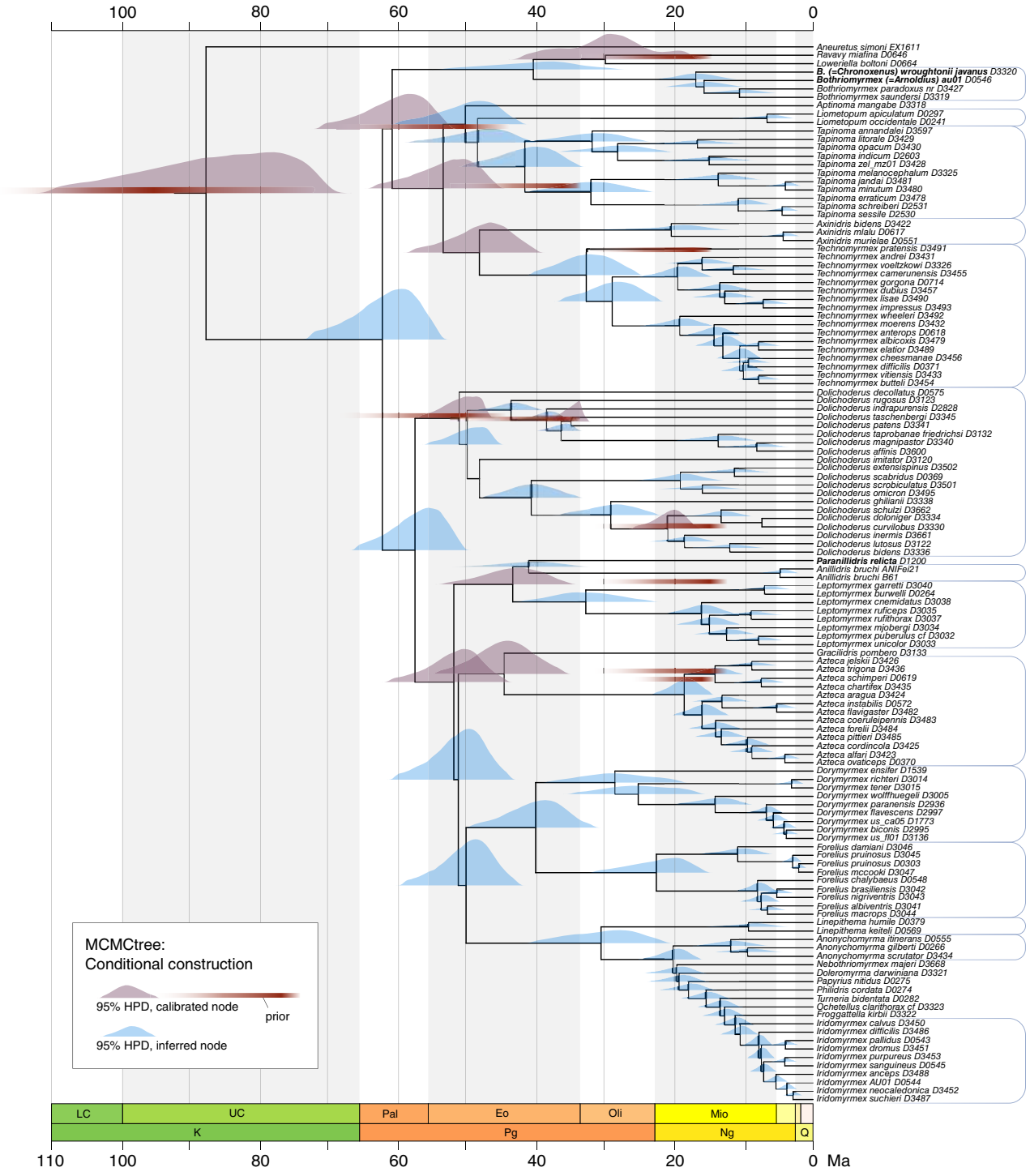



**FIGURE 3** Chronogram inferred under the conditional joint prior in MCMCtree with posterior distributions shown at nodes. Horizontal axis, tip and bottom: Absolute ages (Ma); horizontal axis, lower: Geological periods and epochs. Purple distributions = 95% highest posterior density distribution for calibration nodes. Red bars = calibration priors. Blue distributions = 95% highest posterior density distribution for non-calibration nodes. Geological periods: K = Cretaceous; Pg = Palaeogene; Ng = Neogene. Geological epochs: LC = Lower Cretaceous, UC = Upper Cretaceous, Pal = Palaeocene, Eo = Eocene, Oli = Oligocene, Mio = Miocene. Geological periods: K = Cretaceous, Pg = Palaeogene, Ng = Neogene, Q = Quaternary.

I. Tribe Bothriomyrmecini
   1. *Bothriomyrmex* genus group: *Bothriomyrmex* (including *Arnoldius* and *Chronoxenus*)
   2. *Loweriella* genus group: *Loweriella; Ravavy*

II. Tribe Tapinomini
   3. *Tapinoma* genus group: *Aptinoma*; †*Ctenobethylus*; *Liometopum*; *Tapinoma*.
   4. *Technomyrmex* genus group: *Axinidris; Technomyrmex*.

13653113, 2026, 4, Downloaded from https://resjournals.onlinelibrary.wiley.com/doi/10.1111/syen.70073 by Readcube (Labtiva Inc.), Wiley Online Library on [06/11/2026]. See the Terms and Conditions (https://onlinelibrary.wiley.com/terms-and-conditions) on Wiley Online Library for rules of use; OA articles are governed by the applicable Creative Commons License

**TABLE 3** Summary statistics of biogeographic models in BioGeoBEARS.

| Model | LnL | # parameters | *d* | *e* | *j* | AIC | AIC_wt |
|---|---|---|---|---|---|---|---|
| DEC | −254.5 | 2 | 0.025 | 0.013 | 0 | 513 | 1.20E-43 |
| DEC + J | −156.3 | 3 | 0.0039 | 1.00E-12 | 0.028 | 318.6 | 0.19 |
| DIVALIKE | −254.8 | 2 | 0.026 | 0.013 | 0 | 513.6 | 8.80E-44 |
| DIVALIKE+J | −157.1 | 3 | 0.0044 | 1.00E-12 | 0.026 | 320.2 | 0.088 |
| BAYAREALIKE | −287.6 | 2 | 0.031 | 0.029 | 0 | 579.1 | 5.20E-58 |
| BAYAREALIKE+J | −155 | 3 | 0.003 | 1.00E-07 | 0.029 | 316 | 0.72 |

Abbreviations: # params, number of free parameters; +J, with jump/founder event speciation parameter; AIC, Akaike information criterion; AIC_wt, AIC weights; d, e, j, maximum likelihood estimates of dispersal (d), extinction (e) and jump speciation (j) rates; DEC, dispersal-extinction-cladogenesis model; LnL, log likelihood.

**TABLE 4** Summary statistics of biogeographic models in RevBayes.

| Model | P(allopatry) | P(sympatry) | P(jump) | log10 background rate | Extirpation rate | Marginal likelihood, s.s. | Marginal likelihood, p.s. |
|---|---|---|---|---|---|---|---|
| BDEC | 0.639 [0.200, 1.00] | 0.343 [7.18E-3, 0.844] | NA | −2.48 [−2.64, −2.323] | 4.85 [0.771, 10.1] | −194.886 | −195.0215 |
| BDEC + J | 0.529 [0.0832, 0.999] | 0.676 [0.267, 0.999] | 0.0184 [3.88E-3, 0.034] | −2.99 [−3.27, −2.73] | 1.21 [0.272, 2.57] | −186.699 | −186.7732 |
| | | | | | | **Bayes factor: 0.9580** | **Bayes factor: 0.9577** |

*Note*: Posterior estimates are given in the form mean [lower limit of 95% highest posterior density, upper limit of 95% highest posterior density]. The values marked in bold refer to the Bayes factor for stepping stone estimation and Bayes factor for path sampling estimation respectively.
Abbreviations: +J = with jump/founder event speciation parameter; BDEC, Bayesian dispersal-extinction-cladogenesis model; marginal likelihood p.s., log marginal likelihood calculated with path sampling; marginal likelihood s.s., log marginal likelihood calculated with stepping stone sampling; P(allopatry), probability of allopatric speciation event; P(jump), posterior probability of jump speciation event; P(sympatry), probability of sympatric speciation event.

III. Tribe Dolichoderini
   5. *Dolichoderus* genus group: †*Damzenomyrmex*; *Dolichoderus*
IV. Tribe Leptomyrmecini
   6. *Leptomyrmex* genus group: *Anillidris; Leptomyrmex*; *Paranillidris*
   7. *Azteca* genus group: *Azteca; Gracilidris*.
   8. *Dorymyrmex* genus group: *Dorymyrmex; Forelius*.
   9. *Iridomyrmex* genus group: *Linepithema*; *Anonychomyrma; Nebothriomyrmex* Dubovikoff; *Doleromyrma*; *Papyrius; Philidris; Turneria* Forel; *Ochetellus; Froggattella* Forel; *Iridomyrmex*.

## Topology

Here, we discuss the consensus topology (Figure 2) in descending node order. We recover the expected relationships within and between Myrmeciomorpha and Dolichoderinae: Myrmeciomorpha is resolved as a clade ((*Myrmecia fulvipes* Roger, *M. pilosula* Smith), (*Tetraponera natalensis*, (*Myrcidris epicharis*, *Pseudomyrmex oculatus*))), sister to the Dolichoderomorpha (*Aneuretus simoni*, Dolichoderinae). Dolichoderinae comprises four mutually monophyletic tribes, divided into two clades: Bothriomyrmecini + Tapinomini and Dolichoderini + Leptomyrmecini. The Bothriomyrmecini includes the *Loweriella* genus group (*Loweriella* + *Ravavy*) and *Bothriomyrmex* (including *Arnoldius* and *Chronoxenus*), while the Tapinomini includes the sister *Tapinoma* and *Technomyrmex* genus groups. The only extant member of the Dolichoderini is *Dolichoderus*, which is robustly monophyletic. In Leptomyrmecini, the first basal clade is the *Leptomyrmex* genus group. The next node divides the *Azteca* genus group from the *Dorymyrmex* + *Iridomyrmex* genus groups.

Our taxon sampling was not comprehensive enough to fully elucidate the interspecific relationships of the more species-rich genera. Nevertheless, our results do provide the first phylogenomic insights into the internal phylogeny of a number of genera and provide an opportunity to compare these backbones with previous morphology-based hypotheses. Here we comment on the topology of genera and genus groups.

*Bothriomyrmex*.—We infer *Bothriomyrmex* (=*Chronoxenus* **comb. rev**.) to be sister to a clade comprising *B.* (=*Arnoldius* **syn. nov**.) plus a monophyletic *Bothriomyrmex* sensu stricto.

*Tapinoma* genus group.—In the *Tapinoma* genus group, we find a novel sister relationship of *Aptinoma* to *Liometopum* + *Tapinoma*. Within *Tapinoma* we recover two main clades and five major lineages. The unusually dimorphic *T. annandalei* (Wheeler), representative of the erstwhile genus *Zatapinoma* Wheeler, is sister to the remainder of the first main clade.

*Technomyrmex*.—Our results show varying degrees of agreement with the species group hypotheses of Bolton (2007), although we were not able to sample many of the 16 groups established therein.

13653113, 2026, 4, Downloaded from https://resjournals.onlinelibrary.wiley.com/doi/10.1111/syen.70073 by Readcube (Labtiva Inc.), Wiley Online Library on [06/11/2026]. See the Terms and Conditions (https://onlinelibrary.wiley.com/terms-and-conditions) on Wiley Online Library for rules of use; OA articles are governed by the applicable Creative Commons License

We recover *T. pratensis* (Smith) (*pratensis* group) sister to the remainder of the sampled terminals, which form two major clades. The first includes two subclades comprising members of Bolton's (2007) *bicolor*, *camerunensis* and *textor* groups, which are mutually paraphyletic. *Technomyrmex wheeleri* (Emery), in Bolton's *grandis* group, is sister to the *albipes* group sensu lato.

*Dolichoderus*.—We recover three major lineages in *Dolichoderus*. The earliest-branching species is the Neotropical *Dolichoderus decollatus*, part of the distinctive *Dolichoderus* sensu stricto species group (i.e., the *D. attelaboides* (Fabricius) species complex + *D. decollatus* species complex sensu MacKay (1993)). The other two major clades, 'HoNTIM' and 'AuNT', include diverse and sometimes morphologically unintuitive groups of species. The earliest branch of the 'HoNTIM' clade (Holarctic, Neotropical, Indomalayan) is the monotypic, Neotropical *D. rugosus* (Smith). The next branch is *D. indrapurensis* Forel, which either represents a clade also containing *D. beccarii* Emery, or may be a junior synonym of the latter. The species *D. taschenbergi*, representing the unequivocally monophyletic, Holarctic *quadripunctatus* species group, is sister to *D. patens*, in the similarly cohesive Indomalayan *sulcaticeps* group. The remainder of 'HoNTIM' comprises the artificial '*thoracicus* species group', rendered paraphyletic by the monophyletic *cuspidatus* clade as represented by *D. magnipastor* Dill (Dill et al., 2002). The 'AuNT' clade has a generally analogous branching structure to 'HoNTIM'. The basal node separates the very long-branched, morphologically unique *D. imitator* Emery from a 'core AuNT' clade comprising an Australasian and a Neotropical clade. In the Australasian clade, we find a split between the unarmed *D. omicron* Shattuck & Marsden and *D. scrobiculatus* (Mayr) (the *scrobiculatus* species group) and the spinose *D. scabridus* Roger and *D. extensispinus* Forel (*doriae* and *scabridus* species groups (Shattuck & Marsden, 2013)). The Neotropical core AuNT clade comprises a comb of species, including a monophyletic *D. bispinosus* (Olivier) group (Mackay, 1993) (*D. curvilobus* (Lattke), *D. doloniger* (Roger)).

*Leptomyrmex genus group*.—Our most unanticipated result pertains to the composition of the *Leptomyrmex* genus group as newly defined. Our molecular results robustly locate *Anillidris* nested within the traditional *Leptomyrmex*, specifically as sister to the recently discovered *Paranillidris relicta* **comb. nov**. (=*Leptomyrmex relictus*). These Neotropical species, situated at the end of long branches, are together sister to the remainder of the otherwise strictly Australian-Indomalayan *Leptomyrmex*. *Leptomyrmex* comprises a 'micro' clade of species with short appendages and a 'macro' clade with greatly elongated appendages (Lucky & Ward, 2010; Smith & Shattuck, 2009). The 'macro' clade is geographically structured; see *Comparison to Prior Studies*. The membership of this genus group is supported by morphology in addition to molecular results; see *Morphological Implications*.

*Azteca*.—Our results largely corroborate previous molecular and morphological investigation (Ayala et al., 1996; Benson, 1985; Longino, 1989, 1991, 1996, 2007). We recover two main clades, the first of which is entirely bifurcating, while the second main clade is largely pectinate.

*Forelius*.—We recover a deep split between a South American or 'Southern' clade (*F. chalybaeus*, (*F. brasiliensis*, *F. nigriventris*), (*F. albiventris*, *F. macrops*)) and a 'Northern' clade of widespread, mostly Central and North American species which only range into South America as far as Colombia. As in Oberski (2024), we find *F. pruinosus* D0303 from northwestern Arizona to be sister to *F. mccooki* from southeastern Arizona, rather than to *F. pruinosus* D3045 from Costa Rica. Taxonomic revision of these widely distributed and morphologically homogeneous species or populations, with further model testing, is strongly indicated, especially given the variable topology and support recovered by different methods here (see *Model Comparison* above).

*Dorymyrmex*.—We find a pectinate series comprising *D. ensifer* and the *tener*, *wolfhuegeli* and *pyramicus* groups (Oberski, 2024). Unexpectedly, we recover *D. flavescens* Mayr as sister to the Nearctic clade of the *pyramicus* group, rather than in the basal clade with *D. ensifer* Forel in the *flavescens* group (Oberski, 2024). Given the results of prior research (Oberski, 2024), this is almost certainly an artefact, although the exact source of error is not immediately clear; see *Comparison to Prior Studies*.

*Iridomyrmex* genus group.—We recover this clade, previously informally referred to as 'L(DNA)PPTOFI' after the first letters of the constituent genera (Ward et al., 2010) to properly be 'LANDPPTOFI', that is, we recover a pectinate relationship between *Anonychomyrma*, *Nebothriomyrmex* and *Doleromyrma* rather than finding these genera in a clade together (Ward et al., 2010). It must be noted that, although highly supported, the branches subtending *Nebothriomyrmex* and its sister clade (DPPTOFI) and *Doleromyrma* and its sister clade (PPTOFI) are extremely short.

*Anonychomyrma*.—This genus has never been holistically revised and is somewhat poorly studied in general. Our inclusion of only three out of 27 species provides little information for the larger phylogeny of the group. We do note that the species *A. gilberti* (Forel) and *A. scrutator* (Smith), which we recover as sisters, share a distribution in Queensland, New Guinea and the Maluku Islands and are more similar to one another regarding cephalic proportions and overall pilosity than to *A. itinerans* (Lowne), which is strictly Australian.

*Iridomyrmex*.—We recover a mostly pectinate relationship among terminals. The charismatic 'meat ants', or *I. purpureus* (Smith) group, form a well-nested clade, as do the species *I. dromus* Clark and *I. pallidus* Forel, which differ from most other congeners by being primarily nocturnal (Heterick & Shattuck, 2011). Although this large genus has seen considerable study and was most recently revised by Heterick and Shattuck (2011), it has not been molecularly investigated in any depth. Additionally, species group classification has been somewhat fluid and was only partially adopted by Heterick and Shattuck (2011), making comparison of our results to prior hypotheses somewhat difficult.

## Divergence dates and biogeography

Confidence intervals were quite wide for many nodes. Therefore, we report ages in the form $\mu$: *a*-*b* where $\mu$ is the mean and *a* and *b* are the older and younger limits of the 95% HPD, all rounded to the nearest

13653113, 2026, 4, Downloaded from https://resjournals.onlinelibrary.wiley.com/doi/10.1111/syen.70073 by Readcube (Labtiva Inc.), Wiley Online Library on [06/11/2026]. See the Terms and Conditions (https://onlinelibrary.wiley.com/terms-and-conditions) on Wiley Online Library for rules of use; OA articles are governed by the applicable Creative Commons License

**TABLE 5** Posterior estimates for node ages at selected nodes.

| Node number | Node | Conditional construction mean: 95%HPD | Multiplicative construction mean: 95%HPD | Calibration minimum age | Calibration expected value/mode |
|---|---|---|---|---|---|
| 127 | Dolichoderomorpha Root | 88: 111–70 | 73: 79–67 | 72.2 | 92 |
| 128 | Crown Dolichoderinae | 63: 73–54 | 72: 78–66 | – | – |
| 129 | Bothriomyrmecini+Tapinomini | 61: 72–53 | 70: 76–64 | 48.07 | 53 |
| 130 | Bothriomyrmecini | 41: 54–29 | 50: 62–38 | – | – |
| 131 | *Loweriella* genus group | 30: 43–17 | 39: 51–25 | 15.98 | 18 |
| 135 | Tapinomini | 54: 64–46 | 64: 70–57 | – | – |
| 136 | *Tapinoma* genus group | 51: 61–43 | 60: 67–53 | 33.9 | 37 |
| 149 | *Technomyrmex* genus group | 49: 54–40 | 58: 65–51 | 15.98 | 18 |
| 168 | Dolichoderini + Leptomyrmecini | 58: 66–51 | 67: 74–61 | – | – |
| 169 | *Dolichoderus* | 51: 57–47 | 59: 65–52 | 48.07 | 53 |
| 171 | *Dolichoderus* HONTIM | 44: 49–40 | 48: 55–53 | - | - |
| 174 | *Dolichoderus quadripunctatus* + *sulcaticeps* groups | 33: 38–33 | 37: 41–33 | 33.9 | 37 |
| 177 | *Dolichoderus* AUNT | 49: 55–44 | 55: 61–49 | – | – |
| 183 | *Dolichoderus bidens* + *bispinosus* groups | 21: 26–17 | 30: 37–23 | 13.82 | 18 |
| 188 | Leptomyrmecini | 52: 62–45 | 63: 70–56 | 15.98 | 18 |
| 189 | *Leptomyrmex* genus group | 44: 54–35 | 54: 63–45 | 13.82 | 18 |
| 199 | Remaining Leptomyrmecini | 52: 61–44 | 62: 69–56 | – | – |
| 200 | *Azteca* genus group | 45: 55–36 | 55: 63–46 | 13.82 | 18 |
| 214 | *Dorymyrmex* genus group | 40: 50–32 | 50: 58–48 | – | – |
| 231 | *Iridomyrmex* genus group | 31: 41–21 | 41: 52–31 | – | – |
| 233 | Australasian *Iridomyrmex* genus group | 20: 25–16 | 29: 36–23 | – | – |

*Note*: Ages are given in units of 1 million years. Node numbers correspond to labels in Figure S32. Calibration expected value/mode = mean (node 127); mode (all other nodes).

Ma. Selected major node ages are compared between CC and MC in Table 5; all node ages are given in Table S11. We discuss biogeographic results from Bayesian DEC (BDEC) (Figure S30) and Bayesian DEC + J (BDECJ) (Figure S31) in addition to BAYAREALIKE+J (BALJ) (Figure 4). Because support varied widely across models at some nodes, we give posterior probabilities for the stated model, rounded to two digits; all inferred state posterior probabilities are given in Table S12. In general, ancestral areas in Bothriomyrmecini + Tapinomini are more poorly supported than in the Dolichoderini + Leptomyrmecini, concordant with the range diversity of extant species in the former clade.

*Dolichoderomorpha and Dolichoderinae*.—We infer the Dolichoderomorpha to have evolved in the middle of the Upper Cretaceous, but as early as the Albian and as late as the late Campanian (88: 111–70 Ma). The clade had a northern hemisphere origin encompassing the Palearctic and Indomalaya (BDEC:0.76, BDECJ:0.86), or solely Indomalayan (BALJ:0.87). The distinction between these regions is less meaningful at the inferred age than at younger intervals, with the boundaries of the Palearctic varying throughout the confidence interval due to the fluctuating, sometimes highly extensive coverage of the fragments of Laurasia by shallow seas throughout the Late Cretaceous. Crown Dolichoderinae probably emerged soon after the K-Pg extinction event (63: 73–54 Ma); the ancestral area is poorly supported but may have been Indomalayan (BALJ:0.74, BDECJ:0.40), or Indomalayan and Neotropical (BDEC:0.59). The two major dolichoderine clades appeared soon thereafter, the Bothriomyrmecini + Tapinomini arising around the mid-Palaeocene (61: 72–53 Ma), most likely in Indomalaya (though with weak support; BALJ:0.79; BDEC:0.67; BDECJ:051) and the Dolichoderini + Leptomyrmecini just prior to the Palaeocene–Eocene boundary (58: 66–51 Ma) in the Neotropics (BALJ:1.0; BDEC:0.88; BDECJ:0.96).

*Bothriomyrmecini and Tapinomini*.—The Tapinomini are considerably older than the Bothriomyrmecini, with all tapinomine genus groups appearing prior to the crown bothriomyrmecines: Tapinomini 54: 46–64 Ma; *Tapinoma* genus group 51: 60–43 Ma; *Technomyrmex* genus group 49: 54–40 Ma; Bothriomyrmecini 41: 54–29 Ma. The oldest biogeographic history of Bothriomyrmecini + Tapinomini is complicated by the presence of an undescribed member of this clade in southwestern Canadian Hat Creek amber (56.0–48.07 Ma). This species could represent an early Beringian dispersal or provide evidence that the ancestral range included the Nearctic as well as Indomalaya. In either case, though, this old Nearctic lineage left no other

13653113, 2026, 4, Downloaded from https://resjournals.onlinelibrary.wiley.com/doi/10.1111/syen.70073 by Readcube (Labtiva Inc.), Wiley Online Library on [06/11/2026]. See the Terms and Conditions (https://onlinelibrary.wiley.com/terms-and-conditions) on Wiley Online Library for rules of use; OA articles are governed by the applicable Creative Commons License

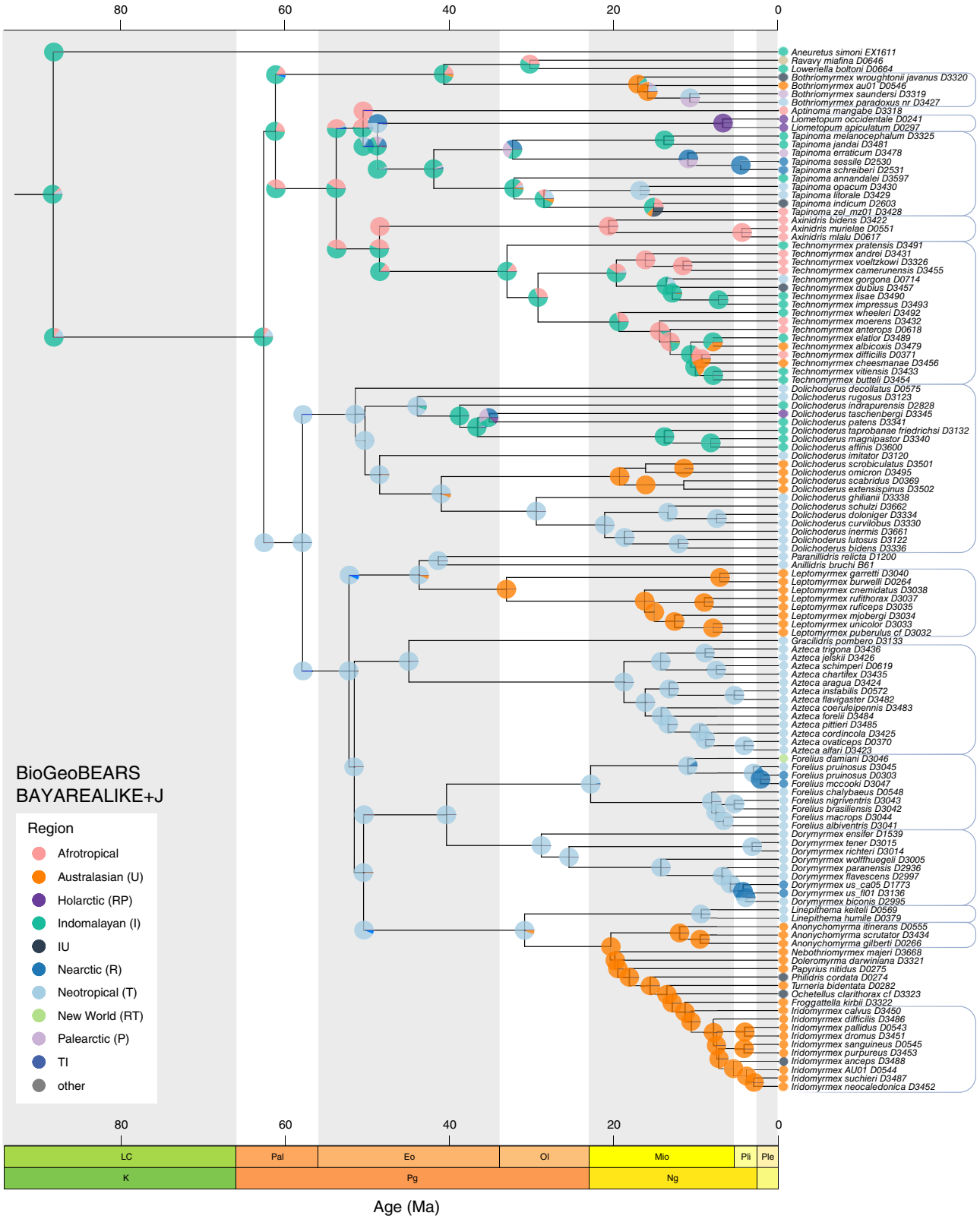



**FIGURE 4** Biogeographic ancestral range reconstruction tree inferred in BioGeoBEARS under the BAYAREALIKE + J model using the conditional chronogram from MCMCtree. Horizontal axis, top and lower: Absolute ages (Ma); horizontal axis, bottom: Geological periods and epochs. Coloured circles at nodes represent inferred ranges, with internal areas corresponding to proportional likelihoods. Coloured circles at tips represent extant distributions as coded. Colours correspond to ranges, as detailed in the inset legend. R = Nearctic; T = Neotropical; P = Palearctic; A = Afrotropical; I = Indomalayan; U = Australasian. Geological periods: K = Cretaceous; Pg = Palaeogene; Ng = Neogene. Geological epochs: LC = Lower Cretaceous; UC = Upper Cretaceous; Pal = Palaeocene; Eo = Eocene; Oli = Oligocene; Mio = Miocene; Pli = Pliocene; Ple = Pleistocene.

13653113, 2026, 4, Downloaded from https://resjournals.onlinelibrary.wiley.com/doi/10.1111/syen.70073 by Readcube (Labtiva Inc.), Wiley Online Library on [06/11/2026]. See the Terms and Conditions (https://onlinelibrary.wiley.com/terms-and-conditions) on Wiley Online Library for rules of use; OA articles are governed by the applicable Creative Commons License

fossil record yet known; there is an approximately 20 Ma gap to the next definitive evidence of any Nearctic bothriomyrmecine or tapinomine, when †*Liometopum scudderi* Carpenter and †*L. miocenicum* Carpenter were fossilized in Priabonian Florissant sediments (37.7–33.9 Ma).

*Bothriomyrmecini*.— Among the bothriomyrmecines, the age of the *Loweriella* genus group had a particularly broad confidence interval (30: 43–17 Ma), as well as a poorly resolved posterior distribution. The ancestral area of Bothriomyrmecini is inferred to be Indomalayan, albeit with weak support (BALJ:0.78; BDEC:0.61; BDECJ:0.66). The *Loweriella* genus group is also inferred to be Indomalayan, with moderate to high support in BDEC (0.91 PP) and BDECJ (0.84 PP), but with low support in BALJ (0.59 PP). *Bothriomyrmex* is inferred to be 17: 22–12 Ma and to have arisen in Australasia (BALJ:0.85), or both Indomalaya and Australasia (BDECJ:0.66); in BDEC the node was unresolved (all PP <0.25). The range of the ancestor of the Palearctic and Neotropical species, 11: 16–6 Ma may have been Neotropical (BALJ:0.51), Palearctic (BDECJ:0.51), or both (BDEC:0.49). The inferred ages exclude a trans-Antarctic dispersal from Australia to South America, but otherwise it appears that this node cannot be resolved without new fossils. Conflicting results in age and area inferences are not unexpected given the relatively young age of the genus relative to the calibrating fossil; the clade's extant distribution in the Palearctic, Indomalaya and Australasia; the scope of our sampling; and the lack of a fossil record.

*Tapinoma genus group*.— The *Tapinoma* genus group is inferred to be ancestrally Indomalayan, but with poor support (BALJ:0.59; BDEC: 0.65; BDECJ:0.45). The second most probable state in all models was the Afrotropics. *Liometopum* is recovered as Holarctic with high or moderate support in BALJ:0.99 and BDECJ:0.81 and poor support in BDEC:0.53. The presence of the lineage in both the Nearctic and Palearctic during the Priabonian is demonstrated by †*Ctenobethylus goepperti* and †*Liometopum oligocenicum* Wheeler in Baltic and Ukrainian Rovno ambers, and †*L. miocenicum* in the Florissant Formation of Colorado. It is unclear whether the total *Liometopum* clade experienced two intercontinental dispersals, via Beringia, then a North Atlantic Land Bridge (NALB) between western Eurasia and eastern North America, or a single westward dispersal, but the long stem leading to extant *Liometopum* suggests that intermittent connections could be available for both routes.

*Tapinoma* is inferred to have arisen in Indomalaya, 42: 34–51 Ma (BALJ:0.93; BDEC:0.79; BDECJ:0.76). The two main *Tapinoma* clades originated nearly contemporaneously, the first main clade (i.e., that including *T. annandalei*) at 32: 41–25 Ma, and its sister clade at 32: 41–24 Ma. At least one *Tapinoma* lineage – likely a stem group – occurred in the Palearctic prior to the emergence of these major clades, based on the total-clade member †*Tapinoma electrinum* from Rovno amber (34–38 Ma). The second main clade including the Holarctic species is weakly recovered as Indomalayan in both Bayesian models (BDEC:0.50; BDECJ:0.71) while BALJ is equivocal between Indomalayan (0.36 PP), Nearctic (0.33 PP) and Palearctic ranges (0.32 PP). The young Holarctic clade (11: 16–6 Ma) may be ancestrally Holarctic (BDEC:0.65) or Palearctic (BDECJ:0.46) suggesting the importance of an early Oligocene NALB connection and a single westward dispersal. Alternately, the origin may be Nearctic (BALJ:0.52), suggesting an initial Beringian route followed by an eastward NALB dispersal.

The biogeography of the main clade of *Tapinoma* including *T. annandalei* is somewhat speculative and is certainly biased by undersampling. All models support an Indomalayan origin (BALJ:0.85; BDEC:0.72; BDECJ:091), with the MRCA of the extant Indomalayan and Afrotropical species, 15: 21–9 Ma, being poorly to unsupported but potentially either Indomalayan (BALJ:0.40; BDECJ:0.59) or present in both regions (BDEC:0.41). Dispersal over land or ocean to Africa is plausible for both the stem and daughter intervals. Prior to the 'terminal Tethyan event' (Adams et al., 1983) in the late Eocene to early Oligocene (Scotese, 2021; Warners-Ruckstuhl et al., 2013), dispersing ants would have had to traverse the Eastern Neotethys Seaway between Arabia and Asia, or the Mediterranean Tethys; an oceanic route across the predecessor of the Arabian Sea would be hypothetically possible, but would occur over deeper water and a longer distance (Scotese, 2021). While dispersal across the Gibraltar Strait is possible, especially given the intermittent occurrence of full land bridges, the Atlas Mountains would have been a potential barrier to southward range expansion. The possibility of trans-Tethyan rafting is supported by the presence of Bartonian and Priabonian mangroves and silicified driftwood along the shores of the Neotethys in what is now the Egyptian Wadi Al-Hitan Lagerstätte (El-Saadawi et al., 2018). Conversely, a dispersal event in the late Oligocene or more recently would be impeded by the collisional uplift of the Zagros mountains and Makran accretion in present-day central-southern Iran, Iraq, Türkiye and Pakistan (Agard et al., 2011; Allen & Armstrong, 2008; Leturmy & Robin, 2010; Mouthereau et al., 2012; Warners-Ruckstuhl et al., 2013), along with cooling climate and the continuing southward retreat of the African Equatorial Wet Zone (Crowley, 2012).

The route taken by the ancestor of the Neotropical *T. opacum* and *T. litorale* in the middle Oligocene to early Miocene interval is less clear and seems to either imply a long-distance trans-Pacific scenario from the inferred Indomalayan origin, or a stepwise series of dispersals through Australia and Antarctica. The latter route would be implied to have taken place either in the earliest or latest parts of the interval (van den Ende et al., 2017). The presence of *Tapinoma* fossils in Dominican amber (20.45–13.82 Ma) and Serravallian Amazonian amber (13.82–11.63 Ma) supports the establishment of the Neotropical clade over a broad area by the inferred origin time but cannot inform the manner of dispersal. However, the Indian Ocean species *T. annandalei* is sister to the remaining, apparently amphi-Pacific species, speculatively supporting the hypothesis of a trans-Atlantic dispersal to the Neotropics which is obfuscated by missing signal from unsampled Afrotropical and Neotropical lineages. Further investigation of *Tapinoma* internal phylogeny is strongly indicated.

*Technomyrmex genus group*.—The *Technomyrmex* genus group, 49: 58–40 Ma, is weakly inferred to have an Indomalayan origin (BALJ:056; BDEC:0.50; BDECJ:0.50). *Axinidris* has an inferred Afrotropical origin 21: 31–13 Ma (BALJ:1.0; BDEC:0.89; BALJ:0.99). Given

13653113, 2026, 4, Downloaded from https://resjournals.onlinelibrary.wiley.com/doi/10.1111/syen.70073 by Readcube (Labtiva Inc.), Wiley Online Library on [06/11/2026]. See the Terms and Conditions (https://onlinelibrary.wiley.com/terms-and-conditions) on Wiley Online Library for rules of use; OA articles are governed by the applicable Creative Commons License

the fragmentation of the Indomalayan and eastern Afrotropical regions from the late Palaeocene to the Eocene, and the long stem subtending the extant species, a number of scenarios may be plausible. It may not be possible to exclude including vicariance, island-hopping or trans-Tethyan rafting without further sampling, as for the Afrotropical *Tapinoma* discussed above.

*Technomyrmex*, 33: 41–26 Ma, is inferred to have an Indomalayan origin (BALJ: 0.85; BDEC: 0.70; BDECJ: 0.64). The earliest-branching extant lineage, *T. pratensis*, persisted in Indomalaya, while members of the other two main clades show multiple transitions between the ancestral range and the Afrotropics between the Oligocene and the end of the Miocene. The MRCA of both clades, 29: 37–22 Ma, is recovered as Indomalayan with poor support (BALJ: 0.69; BDEC: 0.65; BDECJ: 0.60). A single Indomalayan range for each individual clade was inferred by BALJ (0.66 and 0.70 PP) and BDECJ (0.54 and 0.64 PP), while under BDEC the first main clade was Afrotropical and Indomalayan (0.50 PP) and the second Indomalayan (0.70 PP). The presence of †*Technomyrmex svojtkai* in Ethiopian amber demonstrates that at least one lineage had established in the Afrotropics by the early to middle Miocene (23–16 Ma). While multiple transoceanic dispersals in both westwards and eastwards directions in the mid- to late Miocene may explain the distribution of *Technomyrmex* subclades, it seems plausible that the ancestral range of at least some *Technomyrmex* lineages included the Palearctic, favouring overland dispersals. Although †*Technomyrmex deletus* Emery is from young Sicilian amber (12–5 Ma), its provenance indicates the former presence of a Mediterranean fauna, potentially acting as a source for dispersal to either the Afrotropics, Indomalaya or both. It seems very likely that undersampling has also affected our inferences as in some groups of *Tapinoma*, especially for young clades with apparently wide disjunctions, such as the Afrotropical *T. difficilis* + Australasian *T. cheesmanae*, 9: 12–6 Ma. For this clade, which is sister to two Indomalayan species, only BDEC infers a range encompassing both the Afrotropics and Australasia, with the parent node recovered as also including Indomalaya.

The existence of two Neotropical *Technomyrmex* species, one of which was sampled, also requires explanation. Two fossil species from Dominican amber were formerly considered evidence for the timing and ubiquity of the Neotropical radiation (Brandão et al., 1999; Guerrero, 2019), but our reevaluation places these species in †*Schismiscapus*, *incertae sedis* in the Leptomyrmecini (†*S. caritatis* (Brandão & Baroni Urbani) **comb. nov.**; †*S. hispaniolae* (Wilson) **comb. nov.**); see *Systematic Palaeontology*. The Neotropical *T. gorgona* Fernández & Guerrero is sister to a clade including Afrotropical and Indomalayan-Australasian species, the MRCA of which is inferred to be 14: 18–9 Ma, and to have originated in Indomalaya (BALJ:0.77; BDECJ:0.72) or in a range encompassing the Neotropics and Australasia (BDEC:0.64). By the inferred interval, Australia and South America were separated, the Drake Passage and Tasman Strait having been open since the Late Eocene to the Oligocene (Lawver & Gahagan, 2003; Scher & Martin, 2006). Potential island-hopping combined with an Antarctic terrestrial route could be hypothesized, since parts of the Antarctic coasts may have been partially deglaciated during the mid-Miocene Thermal Maximum (Gasson et al., 2016), and sparse angiosperm pollen and insect remains are known from the western Olympus Range ca. 14 Ma. However, the Antarctic climate is inferred to have rapidly cooled thereafter to conditions unsuitable for insect life (Lewis et al., 2008), and even deglaciated regions would have had harsh alpine conditions. The island-hopping scenario is also contraindicated by the requirement for over-water dispersal against the predominant polar currents in the middle Miocene (Lawver & Gahagan, 2003).

*Dolichoderini and Leptomyrmecini*.—The Dolichoderini and Leptomyrmecini are nearly contemporaneous, arising 51: 57–47 Ma and 52: 62–45 Ma respectively, soon after their MRCA 58: 66–51 Ma. All models infer a Neotropical origin for the total clade and both tribes with high support (0.88–1.0 PP). This suggests that this clade either first dispersed to North America following an eastward route from Indomalaya across Beringia; or westward across a NALB, either via the De Geer route in the early to mid-Palaeocene, or the Thulean route ca. 57 Ma (Brikiatis, 2014). Eight extinct dolichoderine species from Lutetian Sakhalin amber (48–41 Ma) might provide evidence for the Beringian route, but these species cannot be assigned to any less inclusive clade, so cannot be confidently adduced in favour of this hypothesis. Ypresian and Lutetian North American fossils from the Hat Creek amber (southern British Colombia) and the Green River and Kishenehn formations (present-day Colorado, Wyoming, Utah, Montana), including several species of *Dolichoderus*, may be representatives of stem lineages that remained in North America while crown members dispersed to South America. These lineages may have been impeded by the belt of arid latitudes dominating Central America preceding and during the Palaeocene-Eocene Thermal Maximum (Crowley, 2012). The presence of stem dolichoderines during this interval is potentially supported by the persistence of the probable stem genus †*Yantaromyrmex* in Priabonian Bitterfeld amber. Alternately, these North American fossils may be examples of early crown groups redispersing to Eurasia.

*Dolichoderini*.—The 'HoNTIM' clade, 44: 49–40 Ma, is slightly younger than its sister 'AuNT', which arose 49: 55–44 Ma. The basal topology of both clades, with depauperate sister lineages, suggests that extinction played a significant role in the phylogeny. This inference may be supported by the richness of fossil species, especially in Priabonian Palearctic ambers (38–34 Ma). However, most of these fossil species cannot yet be confidently associated with extant clades.

'HoNTIM' is inferred to have originated in the Neotropics alone (BALJ:0.94, BDECJ:0.90) or in a Neotropical-Indomalayan range (BDEC:0.74). In either scenario, but especially the latter, the true range might have included the Nearctic, given the presence of Nearctic Ypresian and Lutetian *Dolichoderus* fossils. The 'HoIM' subclade of Holarctic and Indomalayan species is inferred to have experienced a single dispersal to Eurasia by 39: 42–36 Ma. *Dolichoderus taschenbergi*, representing the Holarctic *D. quadripunctatus* clade, shares a MRCA with the Indomalayan *D. patens* (*sulcaticeps* clade) only about 4 Ma younger than 'HoIM', 35: 38–33 Ma. This timing is supported by the definitive presence of *D. quadripunctatus* (Linnaeus) group members in Baltic and Rovno amber 38–34 Ma (†*D. polonicus*; †*D. tertiarius*, †*D. zherichini* and possibly others). Other unplaced fossil *Dolichoderus*

13653113, 2026, 4, Downloaded from https://resjournals.onlinelibrary.wiley.com/doi/10.1111/syen.70073 by Readcube (Labtiva Inc.), Wiley Online Library on [06/11/2026]. See the Terms and Conditions (https://onlinelibrary.wiley.com/terms-and-conditions) on Wiley Online Library for rules of use; OA articles are governed by the applicable Creative Commons License

from Baltic and Rovno ambers may also be 'HoIM' species. The ca. 39–44 Ma interval between 'HoNTIM' and 'HoIM' suggests that the Old World species followed a westward Beringian route from the New World. Therefore, the extant distribution of the *D. quadripunctatus* clade may be due to diversification while the clade was distributed in both the Nearctic and Indomalaya. Further sampling of the *D. quadripunctatus* group, including putative members such as the Chinese species *D. sagmanotus* Xu, will clarify the relationships among the Nearctic and Palearctic members of the clade and its biogeographic history.

The Neotropical clade of 'core AuNT', 29: 37–23 Ma, is considerably older than its Australasian sister clade, 19: 25–14 Ma. The MRCA of these clades, 41: 48–34 Ma, is inferred to be Neotropical (BALJ:0.94; BDECJ:0.92), but might have encompassed both Neotropical and Australasian regions (BDEC: Neotropical, 0.55 PP; Neotropical and Australasian: 0.42 PP). These ages support an Antarctic dispersal from South America to Australia prior to approximately 35 Ma, when the three landmasses were still contiguous or closely associated (Lawver & Gahagan, 2003). This pattern has been inferred for a variety of animal and plant taxa (Almeida et al., 2012; Duellman et al., 2016; Sanmartín & Ronquist, 2004; Turk et al., 2020; Winterton & Ware, 2015) and is paralleled in Dolichoderinae by *Leptomyrmex* (here; Barden et al., 2017) and the *Iridomyrmex* genus group.

*Leptomyrmex genus group*.—The earliest branch of the Leptomyrmecini (52: 62–45 Ma) is the *Leptomyrmex* genus group, the extant members of which are nevertheless younger than those of their sister clade, at 44: 54–35 Ma, compared with 52: 61–44 Ma. The oldest leptomyrmecine fossils all derive from Mexican Chiapas amber, 23.04–15.98 Ma, while slightly younger Dominican amber fossils are known from several crown clades within the tribe. Like the tribe itself, the *Leptomyrmex* genus group is inferred to have arisen in the Neotropics (BALJ: 0.94; BDECJ: 0.90) or in a Neotropical + Australasian range (BDEC:0.62). The oldest lineage of the genus group is certainly Neotropical: the relictual clade *Anillidris* + *Paranillidris* **gen. nov**., which includes the Dominican amber species †*P. neotropica*, is inferred to be 41: 52–33 Ma, while *Leptomyrmex* is considerably younger, at 33: 43–23 Ma. We consider a terrestrial dispersal over Antarctica to be the likely route for the Australasian *Leptomyrmex*, due to the existence of favourable climatic conditions and contiguous land bridges at the time (see above). Although queens of *Paranillidris* remain unknown, *Anillidris* and the 'micro' clade species *L. burwelli* Smith & Shattuck are winged, suggesting that dispersing ancestors of *Leptomyrmex* were more vagile than the apterous 'macro' clade, which contains most of the species richness (21 of 27 species). The latter group arose only 16: 21–12 Ma.

*Azteca genus group*.—The strictly Neotropical *Azteca* genus group has an inferred age of 45: 55–36 Ma and is maximally supported as ancestrally Neotropical in all models. The long branch to the relict *Gracilidris pombero* is broken by the Dominican amber †*G. humiloides*. *Azteca*, which is copiously represented in Dominican amber, is about 19: 23–15 Ma.

*Dorymyrmex genus group*.—We recover an age of 40: 50–32 Ma for the genus group. *Forelius* arose around 23: 32–16 Ma, the Southern clade of *Forelius* being slightly younger than the Northern clade, at 8: 11–5 Ma and 11: 16–6 Ma respectively. All models highly support a Neotropical origin for *Forelius* (0.89–0.98 PP) and the Southern clade (1.0 PP). The MRCA of the Northern clade is also inferred to be Neotropical, but with variable support (BALJ:0.91; BDEC:0.66; BDECJ:0.66), with the remaining probability in the Bayesian models supporting a New World range. Within the Northern clade, the clade containing *F. mccooki* (McCook) and the two (non-sister) samples identified as *F. pruinosus* from Arizona and Costa Rica is 3: 2–4 Ma. The ancestral range may have been Neotropical (BALJ:0.86; BDECJ:0.71) or New World (BDEC:0.98). The age of this clade is more or less contemporaneous with traditional estimates for complete closure of the Isthmus of Panama, ca. 3.5 Ma (Coates et al., 1992, 2003; Coates & Stallard, 2013; Haug et al., 2001; Haug & Tiedemann, 1998). However, significant increases in migration rate between the Nearctic and Neotropics are known for various terrestrial taxa at intervals from 6.0 to 5.1 Ma, 10.0 to 7.2 Ma and 26.2 to 19.9 Ma (Bacon et al., 2015), suggesting that interchange could have been plausible along any branch of *Forelius*.

We infer crown *Dorymyrmex* to be 29: 38–19 Ma and to be ancestrally Neotropical (BALJ:1.0; BDEC:0.99; BDECJ:1.0). All *Dorymyrmex* groups are also inferred to be Neotropical, except the MRCA of the Nearctic clade, which was recovered as either New World (BDEC:0.99), Nearctic (BALJ:0.69), or with about half the posterior probability favouring the Nearctic (BDECJ:0.48) or Neotropics (BDECJ:0.45).

*Iridomyrmex genus group*.— The *Iridomyrmex* genus group arose 30: 41–21 Ma in the Neotropics (BALJ:0.94; BDECJ:0.85), or in a range encompassing the Neotropics and Australasia (BDEC:0.76). Extant *Linepithema* diverged in the Upper Miocene, 9: 15–4 Ma, while the Australasian-Indomalayan radiation ('ANDPPTOFI') appeared in the Lower Miocene, 20: 25–6 Ma. As in *Leptomyrmex* and the Australasian *Dolichoderus*, a terrestrial Antarctic dispersal is plausible prior to 35 Ma. This timing suggests that either the MRCA of the genus group was present in Australasia, as inferred by BDEC, or that an alternate dispersal route was taken by the MRCA of the Australasian-Indomalayan clade. All models infer an Australasian origin for each constituent genus of this radiation. *Philidris* is most diverse in New Guinea and Indomalaya but expanded into Indomalaya between 18: 22 and 14 Ma and the present. While three species are known from China, as far northeast as Hubei, only *P. laevigata* (Emery) is widespread beyond mainland Southeast Asia. *Ochetellus* and *Iridomyrmex* are richest in Australia. Among *Ochetellus*, only *O. glaber* is native in Indomalaya beyond the Heilprin-Lydekker Line (Ali & Heaney, 2021; Heilprin, 1887; Lydekker, 1896), but is found from Himachal Pradesh to northern Honshu, establishing this range between 14: 17–11 Ma and the present. Most remarkable is the rapid colonization of Indomalaya by *Iridomyrmex anceps* between 5: 7–4 Ma and the present. In *Iridomyrmex*, the youngest dolichoderine genus at 11: 14–9 Ma, only four species of *Iridomyrmex* have penetrated Indomalaya beyond the Heilprin-Lydekker Line, of which two occur only as far as the Lesser Sunda Islands. *Iridomyrmex angusticeps* is also found in the Philippines, but only *I. anceps* surpasses the Wallace Line (Ali & Heaney, 2021;

13653113, 2026, 4, Downloaded from https://resjournals.onlinelibrary.wiley.com/doi/10.1111/syen.70073 by Readcube (Labtiva Inc.), Wiley Online Library on [06/11/2026]. See the Terms and Conditions (https://onlinelibrary.wiley.com/terms-and-conditions) on Wiley Online Library for rules of use; OA articles are governed by the applicable Creative Commons License

Wallace, 1863), where it ranges from Punjab and Maharashtra in the east to Anhui and Zhejiang in the west.

## Comparison to prior studies

Our results support the tribal circumscriptions of Ward et al. (2010), but we recover a number of significant topological differences at multiple resolutions. While we find a deep bipartition between Bothriomyrmecini + Tapinomini and Dolichoderini + Leptomyrmecini, Ward et al. (2010) inferred a pectinate series (Tapinomini, (Bothriomyrmecini, (Dolichoderini, Leptomyrmecini))). Within the Leptomyrmecini, our finding that the *Leptomyrmex* genus group is sister to the clade (*Azteca* genus group, (*Dorymyrmex* genus group, *Iridomyrmex* genus group)) contrasts with a split between the *Leptomyrmex* and *Dorymyrmex* genus groups on the one hand, and the *Azteca* and *Iridomyrmex* genus groups on the other (Ward et al., 2010). Compared with Ward et al. (2010), we find reversed positions of *Bothriomyrmex* (=*Chronoxenus*) and *Bothriomyrmex* (=*Arnoldius*), albeit on short branches. The positions of *Aptinoma* and *Liometopum* are similarly reversed.

*Dolichoderus indrapurensis* was formerly associated with several Australian species in the erstwhile *Diceratoclinea* Wheeler, or equivalently, the *D. scabridus* group sensu Shattuck and Marsden (2013), based on the presence of paired propodeal spines and impressed surface sculpture. However, the development of both characters is dissimilar in *D. indrapurensis* and the *scabridus* group, and there are numerous further differences in the proportions of the head, mesosoma, petiole and appendages. Therefore, it is not unexpected that these lineages are not closely related. The association of *D. indrapurensis* with the *scabridus* group contributed to the hypothesis that the Australasian *Dolichoderus* fauna is a composite of Indomalayan and South American elements (Shattuck & Marsden, 2013), while our results indicate that the Australasian clade derives from a single dispersal from South America.

Our results in *Leptomyrmex* recapitulate the results of prior molecular studies (Barden et al., 2017; Lucky, 2011), both in terms of a sister relationship between monophyletic 'micro' and 'macro' groups and regarding the internal topology of the 'macro' clade. Where sampling overlaps, our results additionally support the geographical structure of the 'macro' clade inferred by Lucky (2011): a southeastern Australian lineage is sister to a clade containing central-eastern and northeastern Australian and New Guinean clades. The northeastern Australian species form a pectinate series including the New Guinean lineage.

In the *Leptomyrmex* genus group, we obtain similar results to Oberski (2024), with a few notable differences. In *Forelius*, we find the large-eyed species *F. albiventris* and *F. macrops* to form a clade. In *Dorymyrmex*, we find the same arrangement of species groups, and the same relationships within the *pyramicus* group, except for *D. ensifer*, as reported above. The anomalous position of *D. ensifer* could not be attributed to data quality or incorrect data organization. Therefore, it appears the discordance may be at least partially an effect of sampling bias, as we sampled only two species of the *flavescens* and *tener* species groups, while Oberski (2024) included 5 and 15 terminals respectively. Since our alignment contained fewer terminals in *Dorymyrmex* but more terminals outside the genus group, it is expected that the different included sites produced different signals. While many *Dorymyrmex* lineages are characterized by very rapid radiation (Oberski, 2024), the branches subtending and within the *flavescens* and *tener* groups are not especially short, suggesting that accelerated rate of evolution was not a major contributor to our incongruous result.

Although most dolichoderine groups have not received divergence dating and biogeographic modelling beyond Ward et al. (2010), the *Leptomyrmex* genus group was previously investigated by Oberski (2022, 2024) with node-dating, while *Leptomyrmex* was investigated using combined-evidence tip-dating (Barden et al., 2017). Our dating results in the *Leptomyrmex* genus group (44: 54–35 Ma) are generally concordant with those of Barden et al. (2017), whose preferred chronogram inferred *Leptomyrmex* + *P. relicta* to be 44: 54–35 Ma and *Leptomyrmex s.s.* to be 37: 48–28 Ma. Although our results for the crown age of *Dorymyrmex* (29: 38–19 Ma) agree with those of Oberski (2024) (27: 32–22 Ma), the same is not true for the remainder of the genus group. Compared with Oberski (2024), we recover considerably older ages for Leptomyrmecini, the genus group, and *Forelius*. While Oberski (2024) found the genus group to be 33: 35–29 Ma, we recover an age of 40: 50–32 Ma; Oberski (2024) inferred a crown age of 15: 17–13 Ma for *Forelius* while we recover *Forelius* to be 23: 32–16 Ma. These differences are likely attributable to several major differences in model premises. Our chronograms differ in intergeneric relationships: the outer outgroup in Oberski (2024) was *Leptomyrmex*, based on Ward et al. (2010), whereas we find the *Dorymyrmex* genus group to be sister to the *Iridomyrmex* genus group. Our calibration and inferential strategies also differed: besides using different models and calibration densities, Oberski (2024) effectively calibrated the Leptomyrmecini root node (as *Leptomyrmex* + (*Dorymyrmex* + *Forelius*)) using a secondary calibration of 53–44 Ma (Boudinot et al., 2016), and the *Dorymyrmex* genus group using †*Forelius chenpauch* Varela-Hernández et al. from Chiapas amber for a range of 26–15 Ma. We instead calibrated the Leptomyrmecini using the Chiapas amber interval and did not separately calibrate the *Dorymyrmex* genus group; we consider †*F. chenpauch* to be *incertae sedis* in Leptomyrmecini (see *Systematic Palaeontology*). Why these differences did not similarly affect the *Dorymyrmex* crown age remains unclear. Regarding historical biogeography, our erroneous placement of *D. flavescens* may affect inferences for the Nearctic clade, which differed among our models. We suggest that the age and biogeographical inferences of Oberski (2024) are more reliable due to topological confidence, and because Oberski (2024) used a much finer-grained area coding, with two Nearctic, two Central American and four South American areas.

## Morphological implications

Our results enable reconsideration of a number of morphological characters pertinent to the evolution and classification of several clades.

13653113, 2026, 4, Downloaded from https://resjournals.onlinelibrary.wiley.com/doi/10.1111/syen.70073 by Readcube (Labtiva Inc.), Wiley Online Library on [06/11/2026]. See the Terms and Conditions (https://onlinelibrary.wiley.com/terms-and-conditions) on Wiley Online Library for rules of use; OA articles are governed by the applicable Creative Commons License

The topology of Tapinomini suggests that the extreme dorsal reduction or loss of the petiolar node is most parsimoniously plesiomorphic to the tribe, with two reversals (*Axinidris* and *Liometopum*). Conversely, the ancestral state being an unreduced node would imply three independent reductions in *Aptinoma*, *Tapinoma* and *Technomyrmex*. This contrasts with the equally parsimonious scenarios of two reductions or two gains of a node in the results of Ward et al. (2010). However, this is a reductive view in that it treats the reduced or lost state as equivalent in the three taxa in which it occurs, and likewise for the present state. This is almost certainly an oversimplification based on qualitative external morphology; it is likely that these states should be defined independently for each genus.

The musculature of the dolichoderine petiole has not been described in any depth (Hashimoto, 1996), nor have the functional correlates of node reduction been tested biomechanically. However, in other ants and outgroup Hymenoptera, several muscles of the second abdominal segment largely originate on the anterodorsal surfaces of the petiolar node and effect various gastral movements (Hashimoto, 1996; Lieberman et al., 2022). In particular, the node may bear the dorsal orthomedial muscles (2domm) and dorsal ortholateral muscles (2dolm), antagonistic retractors and depressors of the gaster; and the dorsal paramedial muscles (2dpmm), which are also depressors (Hashimoto, 1996; Lieberman et al., 2022). Therefore, the reduced node speculatively reduces the area for attachment of these muscles, possibly suggesting lower importance of gastral depression. It is also likely that the emargination of the helcial tergite plays a functional role which is not yet clear. We encourage future investigation of the anatomy of the petiolar node in Tapinomini and in Dolichoderomorpha more broadly, as skeletomusculature is likely to inform the definition of these characters and states and provide information for a more robust interpretation. Such a study would ideally also include *Ecphorella*, the phylogenetic placement of which will also inform the evolutionary scenario. The reduction of the petiolar node in some leptomyrmecines, such as *Forelius*, likely has different skeletomuscular and functional implications, given that in these species the node is strongly flattened anteroposteriorly, but retains a well-developed anterior surface.

The uniquely derived, monotypic *Anillidris bruchi* has historically stymied classificatory efforts due to its extreme adaptations for subterranean life erasing potential synapomorphies of its parent clade, and leading to a 'large number of autapomorphic characters present in all castes [that] make placement of *Anillidris* within the subfamily difficult' (Shattuck, 1992a, p. 36). A medial hypostomal notch or excavation (Figure 5), previously considered synapomorphic to *Leptomyrmex* (Shattuck, 1992a), had in fact been noted in the description of *Paranillidris relicta* (=*Leptomyrmex relictus*) (Boudinot et al., 2016), but as an unillustrated observation. Given that our phylogenies evinced a close relationship between *Anillidris* and *Leptomyrmex* sensu lato, we reinvestigated type and non-type material of *Anillidris* and found that the excavated hypostoma is present in workers (Figure 5a,d). A recent external morphological study of *Anillidris* alates shows that, in contrast to prior characterizations, both queens and males also have a deeply excavated medial hypostoma (Figure 5b,c) (Cantone & Di Giulio, 2023). The reduction of the medial hypostomal lamina should therefore be considered a synapomorphy of the *Leptomyrmex* genus group (Figure 5a–f).

The reduction of the medial hypostomal lamina also occurs homoplasiously in the Bothriomyrmecini (Figure 5g–i). In *Bothriomyrmex* and *Ravavy* the lamina is basically absent, reduced to a tiny posteromedial strip of cuticle (Figure 10g,i). *Anillidris* has a similar state in queens and males (Figure 5b,c) (Cantone & Di Giulio, 2023), but the worker retains two narrow lateral strips or lobes rather than a medial remnant (Figure 5a,d). In *Loweriella*, *Paranillidris* and *Leptomyrmex*, the medial hypostomal lamina is narrow and has a deep medial notch (Figure 5e,f,h). Presumably in all cases, these reductions permit further extension or manoeuvrability of the mouthparts, as the hypostomal cavity encloses the basal sclerites of the maxillolabial complex, in particular the maxillary cardines and the labial postmentum (Richter et al., 2020). The range of motion of the cardines may be especially affected by hypostomal excavation, as the postmentum has a flexible membranous connection to the head capsule, but the cardines articulate condylically; and in *Leptomyrmex s.l.*, which have a comparatively narrow notch, the cardinal apices are closely approximated and located within the hypostomal notch (Richter & Economo, 2023). The external craniocardinal muscle (0mx1), which inserts at the lateral basal apodeme of the cardo, likely serves to extend the mouthparts anteriorly but may also have a rotatory function (Richter & Economo, 2023), suggesting that extension is not the only movement affected by the hypostomal emargination. Speculatively, the modification of the hypostoma in *Bothriomyrmex* could relate to the reduced number of palpomeres, if, for example, greater extension of the maxillolabial complex compensates for the shortened palps.

The lack of phylogenetic clarity in *Dolichoderus* has both contributed to the interpretation of potential homoplasies as synapomorphies and been a consequence of such interpretations. The absence of obvious synapomorphies has also been problematic, especially in the former wastebasket genus *Hypoclinea*, which we find to be polyphyletic, comprising at least five independent lineages. Further sampling of this species-rich genus will certainly evince more patterns, but our results still illustrate the distribution of some important characters. We find evidence for at least five independent origins of mesosomal spination in:

1. *D. indrapurensis*, which has a pair of elongate propodeal spines, with the dorsal propodeal surface also strongly elevated.
2. *D. magnipastor*, representing the *cuspidatus* clade (Dill et al., 2002), as a pair of propodeal spines or processes. Mesosomal armament in the *cuspidatus* clade is diverse, including a lack of any spines or processes and a wide range of variation in the development of presence of tubercles or spines on the propodeum or the propodeum and mesonotum. Ongoing efforts to sample extensively within this clade will clarify the evolution of this variation.
3. The clade *D. extensispinus* + *D. scabridus*, representing the *doriae* and *scabridus* species groups (Shattuck & Marsden, 2013), which have acute propodeal spines of variable length.

13653113, 2026, 4, Downloaded from https://resjournals.onlinelibrary.wiley.com/doi/10.1111/syen.70073 by Readcube (Labtiva Inc.), Wiley Online Library on [06/11/2026]. See the Terms and Conditions (https://onlinelibrary.wiley.com/terms-and-conditions) on Wiley Online Library for rules of use; OA articles are governed by the applicable Creative Commons License

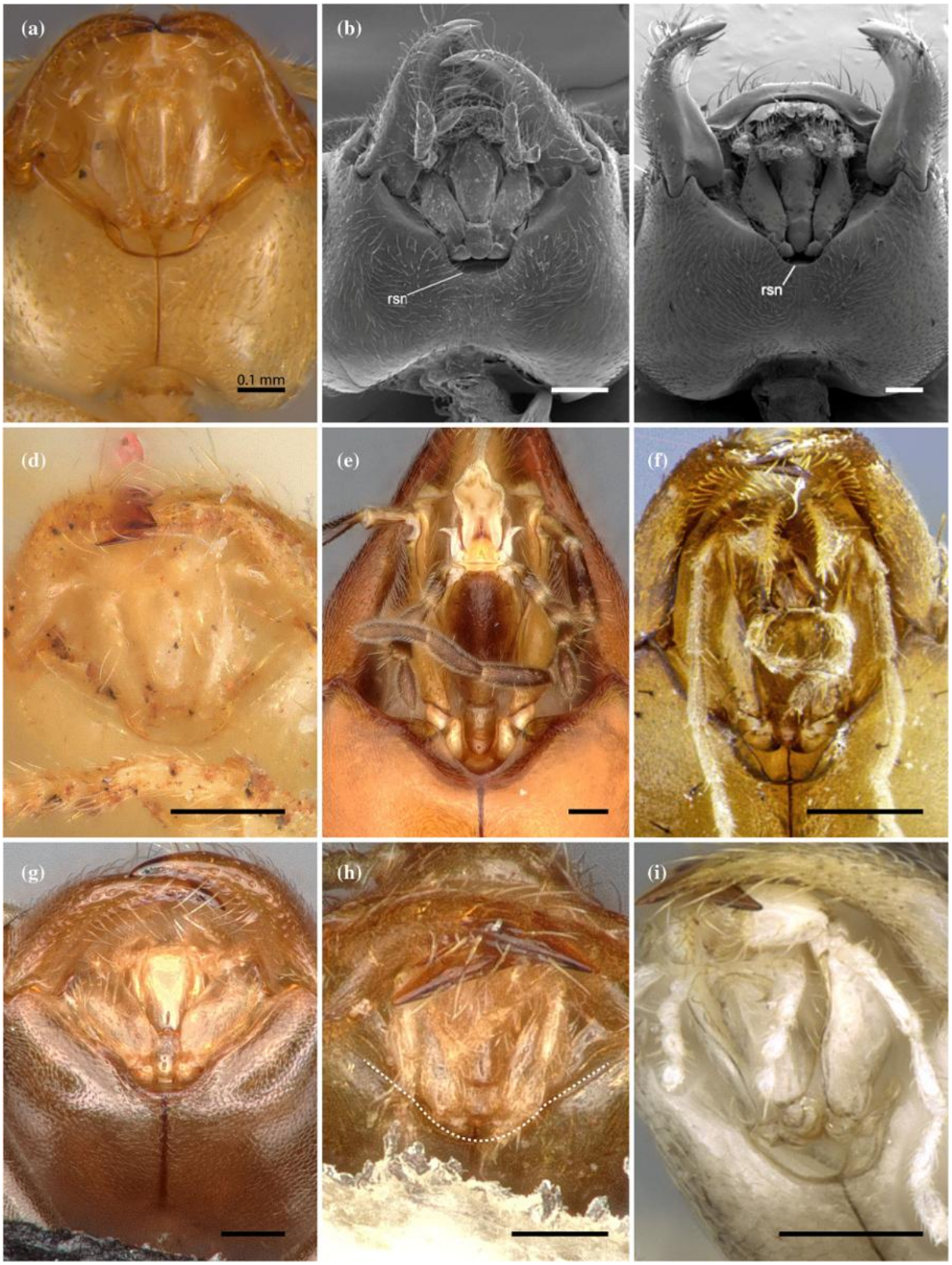



**FIGURE 5** Hypostomal reduction in the *Leptomyrmex* genus group (a–f) and the Bothriomyrmecini (g–i) in ventral view. (a) *Anillidris bruchi* worker, MZSPHYM0144335; (b) *Anillidris bruchi* male; (c) *Anillidris bruchi* queen; (d) *Anillidris bruchi* syntype worker, CASENT0731227; (e) *Leptomyrmex cnemidatus* worker, CASENT0127101; (f) *Paranillidris relicta* worker (g) *Bothriomyrmex wroughtonii javanus* worker, CASENT0758662; (h) *Loweriella boltoni* worker, CASENT0106173; (i) *Ravavy* mg01 worker, CASENT0317901. Image in (a) photographed by Diego Matielo. Image in I from AntWeb (www.antweb.org), photographer Estella Ortega. Images in (b) and (c) reproduced from Figures 2c and 9b in Cantone and Di Giulio (2023) under a Creative Commons attribution licence (CC BY). Image in (f) reproduced from supplementary Figure S2b from Boudinot et al. (2016) under publisher terms and conditions from John Wiley and Sons.

13653113, 2026, 4, Downloaded from https://resjournals.onlinelibrary.wiley.com/doi/10.1111/syen.70073 by Readcube (Labtiva Inc.), Wiley Online Library on [06/11/2026]. See the Terms and Conditions (https://onlinelibrary.wiley.com/terms-and-conditions) on Wiley Online Library for rules of use; OA articles are governed by the applicable Creative Commons License

4. *D. extensispinus*, representing the *doriae* species group (Shattuck & Marsden, 2013), which has acute pronotal spines in addition to the propodeal spines of the parent clade.
5. The clade (*D. schulzi* Emery, (*D. curvilobus*, *D. doloniger*)), representing the *laminatus* and *bispinosus* species groups (Mackay, 1993). This clade also displays significant variation in the development of mesosomal flanges, teeth and spines on the pro- and mesonota and the propodeum. As with the *cuspidatus* clade, more complete sampling, especially including putative clade members like the hexaspinose *D. shattucki* MacKay, will illuminate the nature of the evolutionary dynamics in this heterogeneous group.

Mesosomal spines in *Dolichoderus* may serve a primarily defensive or antipredator role, a common hypothesis which has only rarely been tested directly (Blanchard et al., 2020). However, spines in some ants bear muscles, suggesting an active biomechanical function. For example, in the *Pheidole cervicornis* group, pronotal spine musculature may help support the head (Sarnat et al., 2016). Propodeal spines might include parts of the dorsal orthomedial and dorsal ortholateral propodeal muscles, insert on the anterolateral petiolar condyle and the petiolar levator process respectively. Increased muscle length could therefore effect range of petiolar motion, particularly petiolar elevation, abduction and adduction (Aibekova et al., 2022, 2025; Lieberman et al., 2022; Liu et al., 2019). We further hypothesize that some spines, particularly those of the propodeum, may serve a role in mechanical safety, protecting the propodeopetiolar joint from disarticulation at the extremes of the range of motion.

## Ecomorphology and diversification

It is possible to hypothesize correlations between ecomorphology and rapid diversification in several clades. In *Azteca*, speciation in the last ca. 20 Ma is likely related to arboreality and symbioses with plants (see below). Diversification in the 'macro' clade of *Leptomyrmex* may correlate to the evolution of primarily apterous queens, limiting vagility and encouraging allopatric differentiation, as well as the penetration of new regions of ecomorphospace, for example, highly elongated appendages, highly derived males and replete phenogroups (Boudinot et al., 2016; Lucky & Ward, 2010). It is especially notable that such 'gamergates' or morphologically specialized wingless queens have apparently evolved twice within *Leptomyrmex* (Boudinot et al., 2025; Boudinot et al., 2016).

Novel or pre-existing xerophilic adaptations likely contributed to patterns of accelerated diversification in several clades during the Late Miocene to Early Pliocene, by facilitating persistence, dispersal and rapid colonization in arid zones during cooling, drying climate conditions. In Australia, this pattern is evinced in *Iridomyrmex*. Similar rapid diversification in other xerophilic social insects derived from mesic-tropical ancestors during the 'Hill Gap' period of aridification 10–6 Ma (Hill, 1994) has been demonstrated for *Amitermes* Silvestri (; Heimburger, Schardt, et al., 2022) and is also known in other taxa such as amphibians (Catullo & Scott Keogh, 2014). This pattern also occurs in the *Dorymyrmex* genus group, dramatically so in the Nearctic clade of *Dorymyrmex* (Oberski, 2024), as well as groups including philodromid spiders (Griotti et al., 2023). The recent (i.e., post-Pliocene) diversification of *Dorymyrmex* and insects such as the Australian *Drepanotermes* Silvestri strongly suggests that speciation is ongoing on these groups, implying that continuing anthropogenic climate and habitat changes, for example, aridification, may play a role in their future radiation and biogeography (Heimburger, Maurer, et al., 2022; Oberski, 2024).

## Multiple derivations of myrmecophyty

Our results in *Azteca* support the hypothesis that obligate nesting in *Cecropia* myrmecophytes is independently derived within the genus at least three times, in the *A. aragua* lineage, the *A. coeruleipennis* lineage and the *A. alfari* species group. This convergence was previously hypothesized based on morphological disparity among *Cecropia* nesting species (Benson, 1985; Longino, 1989, 2007). However, it has been repeatedly noted that morphology in *Azteca* is often highly variable (especially in workers) (Longino, 1991, 2007), underscoring the importance of a robust phylogeny for interpreting homoplasy in ecology as well as morphology. One molecular study inferred a similar pattern of convergence as found here, but was based on three mitochondrial fragments and produced both polytomies and several nodes with very low bootstrap support (Ayala et al., 1996). Therefore, the present results are an important test of the previous hypotheses and add insight from divergence dating and succeeding work in other groups.

The first main clade in *Azteca* mostly includes builders of external, often pendant carton nests (*A. chartifex* Forel, *A. schimperi* Emery, *A. trigona* Emery), as well as *A. jelskii* Emery, which may form carton nests or inhabit dead stems (Longino, 2007). In the second main clade, one major lineage comprises the *Cecropia* specialist *A. aragua* Longino, sister to two species nesting in plant cavities, with or without carton (*A. flavigaster* Longino, *A. instabilis* (Smith)) (Longino, 2007). The other lineage is a comb with obligate *Cecropia*-nesters at the earliest branch (*A. coeruleipennis*) and the most deeply nested, the monophyletic *alfari* species group (Longino, 1989) (*A. alfari* Emery, *A. ovaticeps* Forel). The interceding branches are occupied by species nesting in live stems of *Cordia* (*A. pittieri* Forel, *A. cordincola* Forel) or forming carton galleries (*A. forelii* Emery) (Longino, 1996, 2007).

The majority of other unsampled *Cecropia* specialist species are united with *A. aragua* in the morphologically cohesive *A. muelleri* Emery species complex (Longino, 1991), and we hypothesize that sampling these species will validate the monophyly of this complex. The placement of two additional species is less predictable: *A. lattke* Longino may be part of the *muelleri* complex, but differs from all other members in the solid black colouring of the queens (Longino, 1991). The morphology of the unique *A. constructor* Emery is problematic (Longino, 1991), and it may be the case that this species occupies its own branch, separate from other *Cecropia* specialists, analogously to *A. coeruleipennis*. Hence, we suggest that further sampling may reveal one or two additional independent derivations of *Cecropia* mutualism, at least in *A. constructor*, as partially presaged by Longino (1991). *Azteca lattke* and *A. constructor* are therefore especially high-priority targets for future study.

13653113, 2026, 4, Downloaded from https://resjournals.onlinelibrary.wiley.com/doi/10.1111/syen.70073 by Readcube (Labtiva Inc.), Wiley Online Library on [06/11/2026]. See the Terms and Conditions (https://onlinelibrary.wiley.com/terms-and-conditions) on Wiley Online Library for rules of use; OA articles are governed by the applicable Creative Commons License

*Azteca-Cecropia* symbiosis clearly evolved within the *Azteca* crown group, but whether the mutualism initiated with stem or crown *Cecropia* species is unclear. Estimates of *Cecropia* divergence dates suggest that the ancestral myrmecophytes of the *A. muelleri* complex and *A. coeruleipennis* were likely stem lineages (Chomicki & Renner, 2015; Gutiérrez-Valencia et al., 2017). Conversely, the young *A. alfari* species group likely derived symbiosis with crown *Cecropia* (Chomicki & Renner, 2015; Zerega et al., 2005). It may be notable that fossils of *Cecropia* are unknown and that these studies were based on limited plastid or plastid and nuclear gene datasets. We expect future inference of divergence dates in both groups with expanded molecular and morphological data to reveal more details of these coevolutionary dynamics.

The *Azteca-Cecropia* system is analogous to two other recently studied systems, in which obligate ant–plant partnerships arose convergently within genera. The well-known 'acacia ants', *Pseudomyrmex* Lund, evolved symbioses with *Vachellia* Wight & Am. in two non-sister clades, the *P. nigrocinctus* (Emery) and *P. ferrugineus* (Smith) species groups, separated by multiple non-specialist lineages (Ward & Branstetter, 2017). Even more similar to *Azteca* is *Myrmelachista* Roger, which has evolved myrmecophytic partnerships at least three times, again with clades of symbionts separated by a comb of less-specialized, live-stem nesting species (Probst et al., 2024). In *Azteca*, these symbioses are inferred to have originated earlier, and are separated by greater periods of time, than in either *Pseudomyrmex* or *Myrmelachista*. The *Pseudomyrmex ferrugineus* clade has a crown age of only around 5.7 Ma, and the *P. nigrocinctus* clade is only about 3 Ma younger, with a crown age of 2.4 Ma (Ward & Branstetter, 2017). In *Myrmelachista*, the 'devil's garden' symbionts, sister to the Middle American radiation containing the other two specialist clades, is only about 3.8 Ma, and the other mutualisms appeared within less than one Ma. By contrast, the *Azteca coeruleipennis* lineage diverged around 14: 18–11 Ma, *Azteca aragua* (and likely the other *Cecropia* specialists in the *A. muelleri* complex) diverged 13: 17–9 Ma, and the *A. alfari* species group is only 4: 7–2 Ma. This may suggest different sources and strengths of evolutionary pressure leading to the convergence in *Azteca*, the nature of which remain to be clarified. The evolution of mutualisms between *Pseudomyrmex* and *Vachellia* was associated with rapid habitat shifts from closed forest to drier, open habitats with greater pressure from mammalian herbivores (Ward & Branstetter, 2017). In *Myrmelachista*, niche shifts are also implicated, in these cases from high-elevation rainforest and cloud forest to mid- and low elevation environments, where mutualisms may have supported niche partitioning and avoidance of competition from existing, dominant arboreal ants (Probst et al., 2024). A correspondence between niche partitioning and elevation is likely to be a contributor in the *Azteca-Cecropia* system as well, but in contrast to *Myrmelachista*, *Cecropia* specialists are much more abundant and diverse than their congeners at higher elevations, and can be found up to 2000 m (Longino, 1991); it is hypothesized that myrmecophyte microhabitats may help *Azteca* to persist in colder, wetter conditions, while elevation could also help the host trees avoid seasonal drought (Longino, 1991). Because response to disturbance is also suggested to be a significant set of factors in the *Azteca-Cecropia* system (Longino, 1991), a dedicated and expanded study of *Azteca* should include investigation of habitat change and disturbance across the varying climate conditions during the Miocene.

## Divergence dating models

Divergence dating is an often-contentious enterprise due to model limitations and the unavoidability of certain subjective decisions in model specification. These issues have been extensively discussed from a number of statistical, computational, biological and epistemological perspectives (e.g., Barba-Montoya et al., 2019; Klopfstein, 2021; Louca & Pennell, 2020; Morlon et al., 2022; Warnock et al., 2011; Warnock et al., 2015). Limitations in node-dating specifically have partially motivated the development of alternate modelling frameworks (Heath et al., 2014; Stadler et al., 2018; Truman et al., 2025; Zhang et al., 2016; Zhang et al., 2023). Here, we highlight only two particular subjects. First is the well-known difficulty of choosing prior distributions on node ages (i.e., calibration densities). As in most cases, prior information informing parameterization of our calibration densities was limited. Nevertheless, we chose to use informative priors to allow for soft maxima, minimum-age stratigraphic uncertainty and to concentrate prior probability within fossil stratum intervals. While it may be theoretically preferable to use uninformative priors, these are also difficult to design; we reiterate that uniform priors, often described as uninformative, are also informative in that they have expected values and represent a hypothesis about diversification dynamics (that there is equal probability of divergence occurring anywhere in the uniform interval (Warnock et al., 2015)).

An aspect of node-dating which is less frequently considered is the choice of construction of the joint time and birth-death-sampling (BDS) tree process prior. Briefly, the term construction in this context refers to how the model incorporates the time prior with respect to the BDS prior, which differs among software implementations and may have large effects on effective priors, with potential consequences for posterior estimates (Barba-Montoya et al., 2019). In the conditional construction (CC) the joint density of calibration and non-calibration nodes is derived as the product of effective prior on calibration nodes and the density of non-calibration nodes conditioned on calibration ages as specified by the BDS process (Yang & Rannala, 1997). In the multiplicative construction (MC), the time prior is derived as the product of the BDS density for both calibration and non-calibration nodes with calibration densities (Heled & Drummond, 2012, 2015). These approaches have different predicted behaviour regarding the effect of truncation, the correction of imposed calibration densities to satisfy the requirement that parent nodes must be older than their descendants. In both cases, calibrated and effective priors become more dissimilar as truncation increases. CC is expected to produce effective priors that are closer to specified calibration densities. On the other hand, the effects of truncation are apparently also exacerbated for non-calibrated nodes under CC, but not under MC (Barba-Montoya et al., 2019). Unlike many software implementations, PAML provides both constructions (note that prior to version 4.10.7, MCMCtree used CC as the default, while as of version 4.10.8, MC is the default).

13653113, 2026, 4, Downloaded from https://resjournals.onlinelibrary.wiley.com/doi/10.1111/syen.70073 by Readcube (Labtiva Inc.), Wiley Online Library on [06/11/2026]. See the Terms and Conditions (https://onlinelibrary.wiley.com/terms-and-conditions) on Wiley Online Library for rules of use; OA articles are governed by the applicable Creative Commons License

We found that both CC and MC constructions had variable and not obviously predictable behaviour across both calibrated and non-calibrated nodes. Differences in inferred ages varied from negligible (e.g., less than 1 Ma) to substantial (more than 10 Ma). The MC chronogram also differed from the CC chronogram in different ways across the tree, with the root being younger but most internal nodes being older. This suggests that the expected statistical properties of the two constructions may not translate clearly to results, underscoring the value of using both inferential methods when possible. Nevertheless, the choice of chronogram is impeded (here and in general) by a paucity of known constraints, a difficulty often highlighted during parameterization of prior densities, but equally problematic when qualitatively evaluating model realism a posteriori. Our interpretation was that several posterior estimates for major clades under MC were unrealistically young or old, but this conclusion was largely based on comparison to former estimates (Boudinot, Borowiec, & Prebus, 2022; Romiguier et al., 2022; Ward et al., 2010), rather than on definitive palaeontological or palaeogeographic data. It is also possible that we exacerbated the effects of truncation at several nodes due to the overlap and similar modes of the Dominican and Chiapas amber intervals, because these ages were used to calibrate nested clades (Leptomyrmecini, *Leptomyrmex* genus group, *Azteca* genus group). Nevertheless, deviations from our calibration densities and posterior estimates for relevant clades could not be discounted based on known constraints. In sum, further sensitivity testing is desirable here, as in most cases, and newly discovered or interpreted evidence may indicate that the MC chronogram, different prior calibrations or other differences in parameterization produce more reliable results. We encourage the reanalysis of the data published here under different modelling frameworks.

## EXTANT TAXONOMY

A taxonomic synopsis is provided at the tribe, genus group and genus level; for a full taxonomic record, see AntCat (Bolton, 2026). Taxonomic actions and notes are explicated under their relevant taxa. Diagnoses are adapted or expanded from Shattuck (1992a) and Ward et al. (2010). Castes are abbreviated: worker (w), queen (q), male (m). Characters marked with asterisks (*) are apomorphies of groups at the given rank, while those without an asterisk are recognition characters that are likely not synapomorphies; a question mark indicates uncertainty.

**Tribe Bothriomyrmecini Dubovikoff**, 2005.

**Diagnosis**: Posteromedial margin of clypeus not extending between antennal toruli, or only very weakly so (w, q, m; extending further in some queens)*; medial hypostomal lamina absent, notched or strongly reduced to a thin arc (w, q, m)*; forewing 2rs-m absent (q, m)*; basal margin of mandible highly elongate, masticatory margin short (m)*; mandible with no more than three teeth (m)*, with as few as one apical tooth (*Ravavy*) (m)*.

***Loweriella* genus group:**

*Loweriella* Shattuck, 1992; *Ravavy* Fisher, 2009.

**Diagnosis**: Propodeal angle with transverse carinula (w)*; compound eye distant from lateral head margin in frontal view (w)?; scape surpassing posterior head margin (w, q).

**Comments**: The peaked, carinulate propodeum has been described as diagnostic for *Ravavy*, but not previously pointed out for *Loweriella*, in which the carina is somewhat weaker and never elevated as in some morphospecies of *Ravavy*, and may be best seen in dorsal view (Figures 8b and 9b). This character is the only putative synapomorphy so far known that unites this genus group. The eye position and scape length distinguish this genus group from *Bothriomyrmex* but are gestalt characters that have not been morphometrically quantified and which may be plesiomorphic.

The male of *Ravavy* is extremely distinctive, especially with respect to the cephalic morphology, including the proportions of the clypeus and the unusually monodontous mandible (Fisher, 2009). It is conceivable that some of these characters may be shared by *Loweriella*, for which the male is as of yet unknown.

***Bothriomyrmex* genus group:**

*Bothriomyrmex* Emery, 1869. Type species: *Bothriomyrmex costae* Emery, 1869, by monotypy.

= *Arnoldius* Dubovikoff, 2005. Type species: *Bothriomyrmex flavus* Crawley, 1922, by original designation. **syn. nov**.

= *Chronoxenus* Santschi, 1920 (as subgenus of *Bothriomyrmex*). Type species: *Bothriomyrmex myops* Forel, 1895 by subsequent designation of Donisthorpe, 1944:102. **stat. rev**.

**Diagnosis**: Number of maxillary and labial palpomeres reduced: palp formula 4:3, 2:3 or 2:2 (w, q, m)*; compound eye small, usually with 40 or fewer ommatidia (w); scape short, not or only slightly surpassing posterior head margin (w, q)*; propodeum compact; metanotal groove well defined (w, q)*; cupula strongly reduced dorsally and laterally (m)*; digitus (lateropenite) greatly broadened dorsoventrally, but strongly narrowed apically dorsoventrally, apex hooked or bent posterolaterally, barb-like (m)*.

**Comments**: The genus *Bothriomyrmex* was originally described from the Italian species *B. costae* Emery, 1869, and most of the known diversity (including species of the former *Arnoldius* and *Chronoxenus*) was described in the first half of the 20th century. *Chronoxenus* was introduced as a subgenus by Santschi (1919) for the Indomalayan and Australasian species with two, rather than four maxillary palpomeres. Brown Jr. (1973) questioned if *Chronomyrmex* should be considered a junior synonym of *Bothriomyrmex*, but declined to take a formal taxonomic action. Recognizing that *Chronoxenus* was distinguished only by a single reduction apomorphy in a character system already characterized by reduction, Shattuck (1992a) formally synonymized the subgenus under *Bothriomyrmex*. Dubovikoff (2005) reinvestigated the morphology and concluded that there were three separable groups: *Arnoldius* (a newly erected genus), with palp formula 2:2 and the forewing 1m-cu crossvein absent (discoidal cell open); *Bothriomyrmex*, with palp formula 4:3 and 1m-cu present; and *Chronoxenus*, with palp formula 2:3 and 1m-cu present. The species transferred to *Chronoxenus* and *Arnoldius* were particularized by Heterick and Shattuck (2011). The recently discovered *B. paradoxus* Dubovikoff & Longino, 2004, was the first known New World member of the genus complex

13653113, 2026, 4, Downloaded from https://resjournals.onlinelibrary.wiley.com/doi/10.1111/syen.70073 by Readcube (Labtiva Inc.), Wiley Online Library on [06/11/2026]. See the Terms and Conditions (https://onlinelibrary.wiley.com/terms-and-conditions) on Wiley Online Library for rules of use; OA articles are governed by the applicable Creative Commons License

and allied with the Palearctic *Bothriomyrmex s.s.* based on these characters (a single supposed Nearctic species discussed by Santschi (1919) had been combined under *Tapinoma* as *T. dimmocki* (Wheeler) in the revision of Emery (1925)). A second Neotropical species, the Hispañolan *B. enigmaticus*, was placed in *Bothriomyrmex*, despite having a 2:3 palp formula, based on the results of morphometric analyses and in the absence of alate material (Prebus & Lubertazzi, 2016).

We propose that the characters adduced to separate *Arnoldius*, *Bothriomyrmex* and *Chronoxenus* are insufficient to consider these lineages as separate genera. Regarding the wing venation, alates of *Loweriella* are not yet known, but in *Ravavy miafina* Fisher, 2009 and an additional undescribed species (*R.* mg01, CASENT0317900), 1m-cu is present, suggesting the closed discoidal cell is plesiomorphic; the loss of 1m-cu also occurs in various other genera. As pointed out by Shattuck (1992a), reduced palpomere count from a 6:4 dolichoderine groundplan characterizes the entire clade, and based on the conclusions of Prebus and Lubertazzi (2016), this character is also variable within *Bothriomyrmex s.s.* By comparison, most dolichoderine genera retain the groundplan palp formula, but the palps are reduced in several states in *Technomyrmex* (Shattuck, 1992a), and are homoplasiously reduced in *Anillidris* and *Ecphorella*. Therefore, only *Arnoldius* is potentially separable based on autapomorphic states of the palps and wing (palp formula 2:2, 1 m-cu absent), both of which are known to vary within other dolichoderine genera. A case could thus be made for retaining *Arnoldius*. This is, however, untenable, as *Arnoldius* is a derived group nested within an otherwise morphologically homogeneous clade. Specifically, we recover *B.* (=*Chronoxenus*) *wroughtonii javanus* as sister to the clade *B.* (=*Arnoldius*) au1 + *Bothriomyrmex* sensu stricto (*B. saundersi* + *B. paradoxus* nr.). *Chronoxenus* and *Bothriomyrmex* sensu stricto are not differentiable, hence maintaining *Arnoldius* would render *Bothriomyrmex* sensu lato (*Chronoxenus* + *Bothriomyrmex s.s.*) paraphyletic. Additionally, the timing of diversification of the *Bothriomyrmex* lineages is recent and the branches subtending the former genera are very short, being more comparable to species or species groups. This dynamic is paralleled in the subfamily only among members of the *Iridomyrmex* genus group rapid radiation. The latter, however, are clearly diagnosable morphologically. Therefore, we synonymize *Arnoldius* (syn. nov.) and *Chronoxenus* (comb. rev.) into *Bothriomyrmex*, resulting in thirteen changed combinations, of which one is new.

Synapomorphies of *Bothriomyrmex* sensu *latu* do require further discovery and refinement; while the genus is easily separable from *Loweriella* and *Ravavy*, this is mostly due to apomorphies of the latter genera. We note that workers of *Bothriomyrmex s.l.* have the compound eye positioned more laterally, close to the lateral head margin in frontal view, as opposed to the eye situated in a medial (frontal) position in *Loweriella* and *Ravavy*. Two male genitalic synapomorphies are the strong dorsal and lateral reduction of the cupula; and the structure of the digitus (lateropenite), which is strongly narrowed apically dorsoventrally, and is laterally barb-like and hooked. These synapomorphies are shared by *Bothriomyrmex* and *Chronoxenus*; the male of *Arnoldius* is not yet known, but we hypothesize that these characters are present in the entire clade.

Changed and new combinations:

*Bothriomyrmex flavus* Crawley, 1922, **comb. rev.**

*Bothriomyrmex pusillus* (Mayr, 1876) **comb. rev.**

*Bothriomyrmex pusillus aequalis* Forel, 1902 **comb. rev.**

*Bothriomyrmex scissor* Crawley, 1922 **comb. rev.**

*Bothriomyrmex butteli* (Forel, 1913) **comb. nov.**

*Bothriomyrmex dalyi* Forel, 1895 **comb. rev.**

*Bothriomyrmex myops* Forel, 1895 **comb. rev.**

*Bothriomyrmex rossi* Donisthorpe, 1950 **comb. rev.**

*Bothriomyrmex walshi* Forel, 1895 **comb. rev.**

*Bothriomyrmex wroughtonii* Forel, 1895 **comb. rev.**

*Bothriomyrmex wroughtonii formosensis* Forel, 1913 **comb. rev.**

*Bothriomyrmex wroughtonii javanus* Forel, 1909 **comb. rev.**

*Bothriomyrmex wroughtonii victoriae* Forel, 1895 **comb. rev.**

**Tribe Tapinomini Emery**, 1913**: 17.**

= Axinidrini Weber, 1941.

= Liometopini Dlussky & Fedoseeva, 1987.

**Diagnosis**: Petiolar node usually absent or strongly reduced dorsally, anterior face of node absent or very low (w); *if* petiolar node not so reduced, *then either* propodeal spiracle located on dorsal surface of propodeum (*Axinidris*) *or* metanotal groove reduced to a suture, mesonotum and propodeum forming a continuous profile (*Liometopum*).

***Tapinoma* genus group:**

*Aptinoma*, †*Ctenobethylus*, *Ecphorella*, *Liometopum*, *Tapinoma*.

**Diagnosis**: Fifth gastral tergite (seventh abdominal tergite) reflexed beneath fourth tergite, hence fifth tergite not visible in dorsal view and cloacal orifice ventral (w) *or if* seventh abdominal tergite not in this conformation, *then* metanotal grove reduced to a suture, mesonotum and propodeum forming a continuous profile (*Liometopum*) (w)*; workers monomorphic (most *Tapinoma*), polymorphic (*Liometopum*) or dimorphic (*Aptinoma*, some *Tapinoma*); posteromedial corner of gonocoxite produced lateromedially, either lobate (*Liometopum*) or process-like (e.g., digitiform, spiniform, etc.; *Aptinoma*, *Tapinoma*) (m)*.

**Comments**: The genus *Ecphorella* is tentatively placed in this genus group based on the apparent configuration of the gastral tergites. However, the gaster of the single known specimen is somewhat collapsed and is glued by its left side to the card. Acquisition of new material, or new investigative methods applied to the holotype (such as μ-CT scanning) are expected to reveal additional morphological information to characterize *Ecphorella* and its affinities. Within *Tapinoma*, there are potential correlations among distribution, ecology and phylogeny, although our limited sampling means these patterns are provisional. The first main clade of *Tapinoma* comprises tropical arboreal species with the propensity to nest in hollow, attached twigs, often in littoral vegetation. This clade contains an apparently Neotropical lineage, represented by the Caribbean *T. opacum* Wheeler & Mann and *T. litorale* Wheeler and an Old World lineage comprising the Afrotropical *T.* zel_mz01 and Indomalayan *T. indicum* Forel. The other major clade comprises a lineage of Holarctic ground-nesting species (*T. erraticum* (Latreille), (*T. schreiberi* Hamm, *T. sessile* (Say))) and a clade of ecologically diverse Old World species.

***Tapinoma indicum* Forel, 1895 comb. rev.**

*Tapinoma indicum* Forel, 1895.

13653113, 2026, 4, Downloaded from https://resjournals.onlinelibrary.wiley.com/doi/10.1111/syen.70073 by Readcube (Labtiva Inc.), Wiley Online Library on [06/11/2026]. See the Terms and Conditions (https://onlinelibrary.wiley.com/terms-and-conditions) on Wiley Online Library for rules of use; OA articles are governed by the applicable Creative Commons License

**Comment**: This species was associated with *Ravavy* based on an interpretation of cephalic characters as seen in the type images on AntWeb (Seifert, 2025). Although the taxonomic comment *T. indicum* by Seifert (2025) could be construed as notes, rather than a formal act, AntCat (Bolton, 2026) treats it as a combination; hence, we formalize the revised combination.

*Tapinoma indicum* has none of the cephalic apomorphies that delimit Bothriomyrmecini or *Ravavy*; and while the lateral view of the type is obscured by the legs, the dorsal image of the mesosoma is sufficient to rule out the *Loweriella* genus group as well. This species was previously recovered within *Tapinoma* in phylogenomic analysis by Pérez-Flores et al. (2025). We also sampled *T. indicum* and found that it is unambiguously nested within *Tapinoma*, hence we restore the original combination. Explicitly, the type images of *T. indicum* show that it is differentiated from the Bothriomyrmecini by the posterior margin of the clypeus, which extends between the toruli (vs. not extending between toruli in Bothriomyrmecini); and further differs from *Ravavy* in the development of the anterior clypeal margin, which is not produced and emarginate; the short scape, which does not surpass the posterior head margin; and the lack of a transverse carina on the propodeal angle.

***Technomyrmex* genus group**:

*Axinidris*, *Technomyrmex*.

**Diagnosis**: Fifth gastral tergite (seventh abdominal tergite) either vertical, gastral apex poorly defined as either dorsal or ventral (w)* (*Axinidris*), or fifth gastral tergite dorsal, not reflexed beneath fourth tergite, hence cloacal orifice apical (w)* (*Technomyrmex*); petiolar node absent or strongly reduced dorsally (w)* (*Technomyrmex*); propodeal spiracle located on dorsal propodeal surface (w)* (*Axinidris*); propodeum with paired processes or spines and usually with unpaired carina or plate (w)* (*Axinidris*); anterior ventromedial margin of gonostylus produced or broadened (m)*; mandible with more than 17 teeth (m)?; scape shorter than funicular segments 2 + 3 (m)?

**Comments**: The paraphyly of the *bicolor* and *textor* groups sensu Bolton (2007) assorts sampled species along biogeographic lines, suggesting implications for the species not sampled here. The Afrotropical *T. andrei* (*bicolor* group) is sister to two other Afrotropical or Malagasy species, *T. camerunensis* Emery (*camerunensis* group) and *T. voeltzkowi* (Forel) (*textor* group). The sister species *T. impressus* Bolton and *T. lisae* Forel (*bicolor* group) are together sister to the Indomalayan-Australasian *T. dubius* Bolton (*textor* group). Therefore, it is possible that both *bicolor* and *textor* groups may be subdivided into Afrotropical and Indomalayan clades. In the *bicolor* group, the unsampled Afrotropical species are *T. metandrei* Bolton and *T. parandrei* Bolton, which are mutually distinguished largely by colouration (Bolton, 2007) and likely constitute an '*andrei* species group'. All other *bicolor* group species are Indomalayan and may be a monophyletic 'true *bicolor*' group. Among unsampled species in the *textor* group, only *T. textor* and *T. gilvus* are also Indomalayan and may be part of a 'true *textor* group', with the Afrotropical-Malagasy species hypothetically constituting a 'voeltzkowi group'.

***Technomyrmex epinotalis* (Karavaiev, 1935) comb. nov.**

=*Tapinoma epinotale* Karavaiev, 1935.

**Comments**: Unlike all Indomalayan *Tapinoma*, the propodeum of this species is clearly differentiated from the mesonotum, the metanotal groove being impressed and the dorsal propodeal surface not following the mesonotal slope. Additionally, standing hairs are present on the pronotum, mesonotum and propodeum; the posterior head margin is broad and somewhat concave; and the anterior clypeal margin has a broad medial notch. These characters clearly associate *T. epinotalis* with the *albipes* group of *Technomyrmex* (Bolton, 2007). The closest species are *T. modiglianii* Emery and *T. elatior* Forel. As in *T. elatior* but not *T. modiglianii*, *T. epinotalis* appears to lack standing hairs on the head posterad the eye, although such setae are only present in large workers of *T. modiglianii* (Bolton, 2007). On the other hand, standing hairs on the gastral tergites are longer than in *T. elatior*, albeit in the type image somewhat shorter and less numerous than in *T. modiglianii*. Both *T. epinotalis* and *T. elatior* occur in Thailand, and a worker resembling *T. epinotalis* was identified as *T. elatior* by Jaitrong and Yamane (2024), Figure 13. As with the other species transferred to *Technomyrmex* here, it is plausible that future reinvestigation will result in synonymy of *T. epinotalis*, but we choose to only make the new combination, for which the type images provide sufficient evidence.

***Technomyrmex flavidus* (André, 1892) comb. nov.**

= *Tapinoma flavidum* André, 1892.

**Comments**: *Technomyrmex flavidus* was described from Bornean material and placed in *Tapinoma* due to the supposed configuration of the fifth gastral tergite (André, 1892). However, André (1892) also observed that the long, sloping mesonotum and very distinct propodeum, with the convex dorsal surface subequal in length to the posterior surface, were discordant with placement in *Tapinoma*, instead matching *Technomyrmex*. Besides these characters, the very broad, cordate head with small compound eyes well separated from the lateral margins in frontal view and the deep incision of the anteromedial clypeus confidently place this species among the *bicolor* species group of *Technomyrmex* (Bolton, 2007).

The type images of *Technomyrmex flavidus* strongly resemble *T. lisae* Forel in all respects. The only other species that approaches these species is *T. horrens* Bolton, but the latter has a less concave posterior head margin, a much weaker clypeal incision and lacks setae on the third gastral tergite (Bolton, 2007). It seems probable that future direct examination will result in synonymization of *T. lisae* under *T. flavidus*. However, while type images doubtlessly associate *T. flavidus* with *Technomyrmex*, we are not confident in synonymizing the species, especially given the variability of *T. lisae* (Bolton, 2007). Both *T. lisae* and *T. horrens* are polymorphic, but it is unknown if *T. flavidus* is monomorphic or polymorphic, which will be an important character in future investigation.

***Technomyrmex incisus* (Stitz, 1932) comb. nov.**

=*Anonychomyrma incisa* (Stitz, 1932).

=*Iridomyrmex incisus* Stitz, 1932.

**Comments**: This species was described as *Iridomyrmex incisus* by Stitz (1932) from Sumatran material and was later transferred from *Iridomyrmex* to *Anonychomyrma* by Shattuck (1992c), based on the description (S. Shattuck, pers. comm.). While Stitz describes the

13653113, 2026, 4, Downloaded from https://resjournals.onlinelibrary.wiley.com/doi/10.1111/syen.70073 by Readcube (Labtiva Inc.), Wiley Online Library on [06/11/2026]. See the Terms and Conditions (https://onlinelibrary.wiley.com/terms-and-conditions) on Wiley Online Library for rules of use; OA articles are governed by the applicable Creative Commons License

petiolar node as 'strongly anteriorly inclined, the cuneate margin rounded' (Stitz, 1932, p. 734), the reduction of the petiolar node is extreme and doubtlessly is in the tapinomine condition. Although the configuration of the gastral tergites cannot be ascertained from type images, the elongate mesosomal profile, with a distinct metanotal groove and dorsal propodeal surface, the broad head and the deep U-shaped incision of the anteromedial clypeal margin distinguish this species from all Indomalayan *Tapinoma*, instead indicating a solid relationship with the Malesian members of the *Technomyrmex bicolor* species group (Bolton, 2007). The syntype workers key to *T. lisae*, which Bolton (2007) also notes is morphologically variable. Identification of *T. lisae* in Bolton (2007) relies partly on the absence of setae on the second gastral tergite. Despite the rather poor condition of the syntypes of *T. incisus*, which could suggest that the apparent absence of setae is due to abrasion, there are no conspicuous sockets representing setal insertions, and the setae on the third gastral tergite are well-preserved. While the differences in colouration and the precise shape of the clypeal notch fall within expected intraspecific variation, we did not examine *T. incisus* directly, so we leave possible synonymization to future investigation, as with *T. flavidus*.

**Tribe Dolichoderini Forel**, 1878.

= Hypoclineini Emery, 1877.

***Dolichoderus* genus group**:

†*Damzenomyrmex*, *Dolichoderus*.

**Diagnosis**: Hypostoma with anterolateral tooth or flange (sometimes weakly developed) (w, q, m)*; anterior mesopectal flange convex, prolonged anteriorly (w, q)*; cuticle thick, often heavily sculptured (w, q, m)*; posterior surface of propodeum usually concave, sometimes sloped or less often flat (w, q, some m)*.

**Tribe Leptomyrmecini Emery**, 1913.

= Anonychomyrmini Donisthorpe, 1947.

= Iridomyrmecini Dubovikoff, 2005.

**Diagnosis**: Penial sclerites (penisvalvae) with proximodorsal sclerotic bridge (m)*; propodeal spiracle located laterally or posterodorsally (w, q, m); metanotal sulcus well developed (w); without diagnostic traits of Bothriomyrmecini, Dolichoderini or Tapinomini: posteromedial clypeal margin extending between antennal toruli (w, q, m), hypostoma without anterolateral tooth (w, q, m), petiolar node present and usually not strongly reduced (w, q, m).

**Remarks**: The tribe is diverse and heterogeneous, making it difficult to diagnose except by exclusion from other tribes, although the male genitalic character is synapomorphic and appears reliable. As far as is known, all members of the tribe are Neotropical or Australasian, with a few species of otherwise Australasian genera ranging into Indomalaya.

***Leptomyrmex* genus group**:

*Anillidris*, *Leptomyrmex*, *Paranillidris* Lieberman, Oberski & Boudinot **gen. nov**.

**Diagnosis**: Medial hypostomal lamina reduced, either notched (*Leptomyrmex*, *Paranillidris*) or absent medially, reduced to narrow lobes laterally (*Anillidris*) (w, q, m)*; appendages often highly elongate (w, q, m)*; queens often primarily apterous (*Leptomyrmex* 'macro' clade); basivolsellar process dorsoventrally aligned with digitus (lateropenite), or absent (m)*; cuspis (distal lobe of the parossiculus) highly reduced or absent (m)*.

**Comments**: The *Leptomyrmex* genus group is a well-supported clade both molecularly and morphologically, despite the numerous autapomorphies of *Anillidris*. The sister relationship of *Anillidris* and the Neotropical species formerly included in *Leptomyrmex* implies that to retain monophyly, either *Anillidris* be subsumed under *Leptomyrmex*, the Neotropical species be synonymized under *Anillidris*, or these species be provided their own genus. We think that the latter approach best represents the morphological, phylogenetic and geographical distinctions among the three lineages.

***Leptomyrmex* Mayr, 1862**.

**Type species**: *Formica erythrocephala* Fabricius, 1775.

**Constituent species**:

*Leptomyrmex aitchisonoi* Smith & Shattuck, 2009
*Leptomyrmex burwelli* Smith & Shattuck, 2009
*Leptomyrmex cnemidatus* Wheeler, 1915
*Leptomyrmex darlingtoni* Wheeler, 1934
*Leptomyrmex dolichoscapus* Smith & Shattuck, 2009
*Leptomyrmex erythrocephala* Fabricius, 1775
*Leptomyrmex flavitarsus* (Smith, 1859)
*Leptomyrmex fragilis* (Smith, 1859)
*Leptomyrmex garretii* Smith & Shattuck, 2009
*Leptomyrmex geniculatus* Emery, 1914
*Leptomyrmex melanoticus* Wheeler, 1934
*Leptomyrmex mjobergi* Forel, 1915
*Leptomyrmex niger* Emery, 1900
*Leptomyrmex nigriceps* Emery, 1914
*Leptomyrmex nigriventris* (Guérin-Méneville, 1831)
*Leptomyrmex pallens* Emery, 1883
*Leptomyrmex pilosus* Smith & Shattuck, 2009
*Leptomyrmex puberulus* Wheeler, 1934
*Leptomyrmex rothneyi* Forel, 1902
*Leptomyrmex ramorniensis* Smith & Shattuck, 2009
*Leptomyrmex ruficeps* Emery, 1895
*Leptomyrmex rufipes* Emery, 1895
*Leptomyrmex rufithorax* Forel, 1915
*Leptomyrmex tibialis* Emery, 1895
*Leptomyrmex unicolor* Emery, 1895
*Leptomyrmex varians* Emery, 1895
*Leptomyrmex wiburdi* Wheeler, 1915

**Diagnosis**: Head, mesosoma and legs without stout erect hairs (vs. present in *Paranillidris* gen. nov.); (w); antennal toruli contacting epistomal line (vs. separated in *Paranillidris* gen. nov.); (w); mandible without concavity proximad subapical tooth (vs. present in *Paranillidris* gen. nov.); (w); anterior clypeal margin convex or concave (w); gyne wingless ('macro' clade; also in *Paranillidris* gen. nov.; winged in 'micro' clade) (q); male forewing with pterostigmal appendage (vs. absent in other *Leptomyrmex* genus group taxa) (m)*.

***Paranillidris* Lieberman, Oberski & Boudinot gen. nov**.

https://zoobank.org/urn:lsid:zoobank.org:act:682524B1-67DB-4A7D-AFA1-838AF8DA4B28

**Type species**: *Leptomyrmex relictus* Boudinot et al., 2016.

13653113, 2026, 4, Downloaded from https://resjournals.onlinelibrary.wiley.com/doi/10.1111/syen.70073 by Readcube (Labtiva Inc.), Wiley Online Library on [06/11/2026]. See the Terms and Conditions (https://onlinelibrary.wiley.com/terms-and-conditions) on Wiley Online Library for rules of use; OA articles are governed by the applicable Creative Commons License

**Constituent species**:

*Paranillidris relicta* Boudinot et al., 2016 **comb. nov**.

†*Paranillidris neotropica* Baroni Urbani, 1980 **comb. nov**.

=†*Leptomyrmex neotropicus*

**Etymology**: From Ancient Greek παρα- (*para*-) 'beside, near' + *Anillidris*, indicating the sister relationship and shared range of the two genera. Feminine

**Diagnosis**: Extant species: head, mesosoma and legs with stout erect hairs (w, m)*; antennal toruli separated from epistomal line (w)*; mandible with concavity proximad subapical tooth (w)*; anterior mesonotal region not hump-like in appearance (w); petiole wedge-shaped in profile view, with a low node and elongated posteriorly (w). Extant and fossil species: Anterior clypeal margin convex (w); basivolsellar process highly reduced or absent (m); digitus (lateropenite) strongly falcate, ventral margin curving dorsally before arcing apicoventrally (m).

**Comments**: The state of the antennal toruli, which do not contact the epistomal line, is uncertain for †*P. neotropica*.

***Azteca* genus group**:

*Azteca*, *Gracilidris*.

**Diagnosis**: Funicular antennomeres submoniliform (m); scape and pedicel subequal in length (m); mandibles strap-shaped to spiniform (m); petiole squamiform, not elongated posteriorly, very broadly attached to abdominal segment III (m); digitus (lateropenite) styliform (m). No characters are yet known that unite workers and queens morphologically.

***Dorymyrmex* genus group**:

*Dorymyrmex*, *Forelius*.

**Diagnosis**: Anterior clypeal margin with long, decurved hairs which reach or surpass the length of the closed mandibles (w, most q)*; ventromedial margin of genital capsule with subrectangular process projecting posteromedially (m)*; sclerotic bridge of penial sclerites (penisvalvae) roughly oblong, especially anteriorly, and prolonged anteroposteriorly (m); antennomere three kinked (m)*; forewing Rs + M, Rsf2 and Mf2+ spectral or absent (m)*; forewing marginal cell open (m)*.

***Iridomyrmex* genus group**:

*Linepithema*, *Anonychomyrma*, *Nebothriomyrmex*, *Doleromyrma*, *Papyrius*, *Philidris*, *Turneria*, *Ochetellus*, *Froggattella*, *Iridomyrmex*.

**Diagnosis**: Propodeum rounded, or with paired tubercles (w; *Turneria*)* or spinose processes (w; *Froggattella*)*; posterior propodeal surface sometimes concave (w; *Ochetellus*, *Froggattella*, *Turneria*)*;

**Comment**: Analogously to the tribe, this clade is morphologically very diverse and heterogeneous, hence no synapomorphies are known for the entire group. Other than the Neotropical *Linepithema*, all genera are Australasian-Indomalayan. *Anonychomyrma*, formerly considered Indomalayan-Australasian, is strictly Australasian given the removal of the species *Iridomyrmex anceps* (=*Anonychomyrma glabrata* syn. nov.) and *Technomyrmex incisus* (=*Anonychomyrma incisa* comb. nov.) here.

***Iridomyrmex anceps* (Roger, 1863)**.

= *Anonychomyrma glabrata* (Smith, 1857) **syn. nov**.

= *Tapinoma glabrata* Smith, 1857.

**Comment**: This species was described as *Tapinoma glabrata* Smith, 1857, despite having a well-developed, albeit anteriorly inclined petiolar node, as noted in the description (Smith, 1857). Partially on this basis, Mayr (1886) transferred the species to *Iridomyrmex*, from which Shattuck (1992c) combined it under *Anonychomyrma* along with a number of other species, based on the description (S. Shattuck, pers. comm.). Identity with *Iridomyrmex*, rather than *Anonychomyrma*, is apparent due to the sinuate profile of the anterior clypeal margin, which has a 'shoulder' delimiting the lateral and medial regions, and the medial region bearing a projection; the posterior placement of eyes; and the lack of standing hairs on the mesosoma and appendages. The syntype worker of *glabrata* on AntWeb from Malacca, peninsular Malaysia (CASENT0901920) matches the key and redescription of *I. anceps* in Heterick and Shattuck (2011). Additionally, *I. anceps* is the only member of the genus that occurs east of the Lesser Sunda Islands, although it should be noted that *I. anceps* has been suggested to be a species complex (Hoffmann et al., 2011).

***Ochetellus democles* (Walker, 1839) comb. nov**.

= *Eucharis democles* Walker, 1839.

**Comment**: This species, described from a male, was considered a chalcidoid wasp in the genus *Eucharis* for almost a century and a half, until Bouček (1988) excluded it from Eucharitidae, suggesting it was a formicine based on an identification by Barry Bolton, but without a formal action. Reconsiderations by B. L. Fisher (unpublished) and S. Shattuck (unpublished), with which we agree, instead identify this male as *Ochetellus*. AntCat.org already treats *Ochetellus democles* as a valid combination, but lacks an available citation. Here, we formalize the combination, recognizing the contributions of Drs Fisher and Shattuck in pointing out the problem.

A pressing question of synonymy remains. The type of *O. democles* and male syntypes of *O. glaber* are highly similar morphologically and share a type locality in Sydney, New South Wales, Australia. However, the stated similarity is due to examination of images on AntWeb.org, and we were unable to access material directly. Therefore, we are not confident in proposing a synonymy. It must be noted, however, that if these specimens are conspecific, that *O. democles* would be a senior synonym, despite the wide usage of *O. glaber*.

## KEY TO EXTANT GENERA OF DOLICHODERINAE (WORKERS)

Note: Key expanded and adapted from Shattuck (1992a), who also provides keys to queens and males; and from Bolton (1994). Characters for *Linepithema* and *Gracilidris* adapted from Wild & Cuezzo (2006) and Wild (2007). *Ecphorella* is known only from the holotype worker.

**1 (1)** Posteromedial margin of clypeus not extending posteriorly between frontal carinae, or only scarcely so (Figure 6a–c). **(2)** Medial hypostomal lamina usually reduced to a thin arc, notched or absent (Figures 5g–i and 7b).....**2**

13653113, 2026, 4, Downloaded from https://resjournals.onlinelibrary.wiley.com/doi/10.1111/syen.70073 by Readcube (Labtiva Inc.), Wiley Online Library on [06/11/2026]. See the Terms and Conditions (https://onlinelibrary.wiley.com/terms-and-conditions) on Wiley Online Library for rules of use; OA articles are governed by the applicable Creative Commons License

1′**(1)** Posteromedial margin of clypeus extending posteriorly between frontal carinae (Figure 6d). **(2)** Medial hypostomal lamina variable, but usually complete (as in Figure 7a).....**5**

**2 [1] (1)** Medial hypostomal lamina complete (Figure 7a). **(2)** Palp formula 6:4. **(R)** Western Australia.....***Nebothriomyrmex*** (Leptomyrmecini, *Iridomyrmex* genus group)

2′ **(1)** Medial hypostomal lamina reduced to a thin arc, notched or absent (Figures 5g–i and 7b). **(2)** Palp formula 6:4 or reduced. **(R)** Global except Nearctic and South America.....**3** (Bothriomyrmecini)

**3 [2′] (1)** Palp formula 4:3, 2:3 or 2:2. **(2)** Scape short, not surpassing posterior head margin, or only slightly so (Figure 6a). **(3)** Propodeal angle without carinula (Figure 8a). **(R)** Neotropics, Palearctic, Indomalaya, Australasia.....***Bothriomyrmex***

3′ **(1)** Palp formula 6:4. **(2)** Scape surpassing posterior head margin (Figure 6b,c). **(3)** Propodeal angle with transverse carinula (Figures 8b,c and 9). **(R)** Afrotropics, Madagascar, Indomalaya.....**4** (*Loweriella* genus group)

**4 [3′] (1)** Head much longer than wide, usually widest anteriorly (Figure 6c). **(2)** Anteromedial clypeal margin emarginate (Figure 6c). **(3)** Without overall hairy habitus: mesosomal setation mostly limited to dilute, appressed pubescence (Figures 6c and 9a). **(R)** Afrotropics, Madagascar, Indomalaya.....***Ravavy***

4′ **(1)** Head slightly longer than wide, slightly wider anteriorly (Figure 6b). **(2)** Anteromedial clypeal margin transverse to convex (Figure 6b). **(3)** With overall hairy habitus: head, mesosoma and gaster with numerous standing setae (Figures 6b and 9b). **(R)** Indomalaya (Borneo).....***Loweriella***

**5 [1′] (1)** Petiolar node absent (Figures 10a, 11c and 13c), or node strongly reduced dorsally, with very low anterior surface (Figures 11a,b and 13a), and overhung by gaster (Figure 10a); **OR** if node present, then setae on anterior clypeal margin not reaching or surpassing apex of closed mandible in frontal view.....**6** (Tapinomini, *part*)

5′ **(1)** Petiolar node present, well-developed dorsally (Figure 10b); **OR** if node dorsally reduced and overhung by gaster, then anterior clypeal margin with recurved setae reaching or surpassing apex of closed mandible in frontal view (some *Dorymyrmex* genus group).....**10**

**6 [5] (1)** Propodeum armed: with paired processes, denticles, tubercles, or acute angles; and/or propodeal angle carinate (Figure 11a,b). **(2)** Propodeal spiracle located on dorsal surface of propodeum (Figure 11a,b). **(3)** Petiolar node present, but very low (Figure 11a,b). **(4)** Anterior clypeal margin with distinct notch. **(R)** Afrotropics.....***Axinidris***

6′ **(1)** Propodeum unarmed: without processes or carinae (Figures 10a and 11c). **(2)** Propodeal spiracle located on lateral surface of propodeum (Figures 10a and 11c). **(3)** Petiolar node absent (Figures 10a and 11c). **(4)** Anterior clypeal margin variable: notched, convex, transverse, or emarginate.....**7**

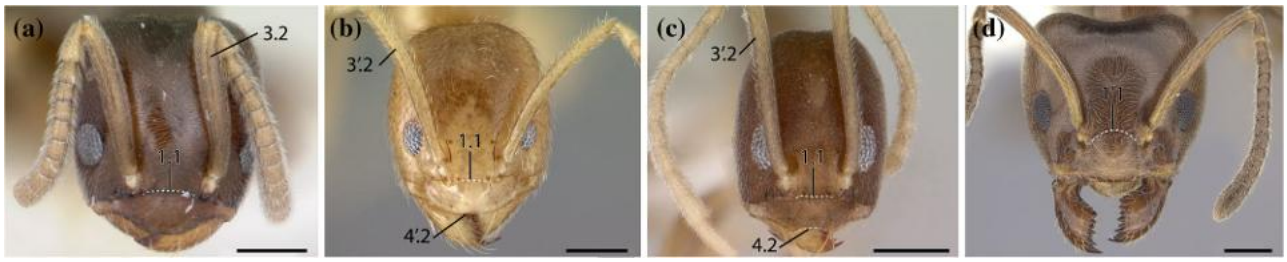



**FIGURE 6** Selected characters from key couplets 1, 3 and 4. Labels are in the format <couplet>. <character>; an apostrophe indicates the second lug of the couplet. All scale bars = 0.2 mm. (a) *Bothriomyrmex paradoxus* CASENT0103277. (b) *Loweriella boltoni* CASENT0009998. (c) *Ravavy miafina* CASENT0439855. (d) *Azteca chartifex* CASENT0249593. All images from AntWeb (www.antweb.org), photographers April Nobile (a, c), Erin Prado (b) and Will Ericson (d).

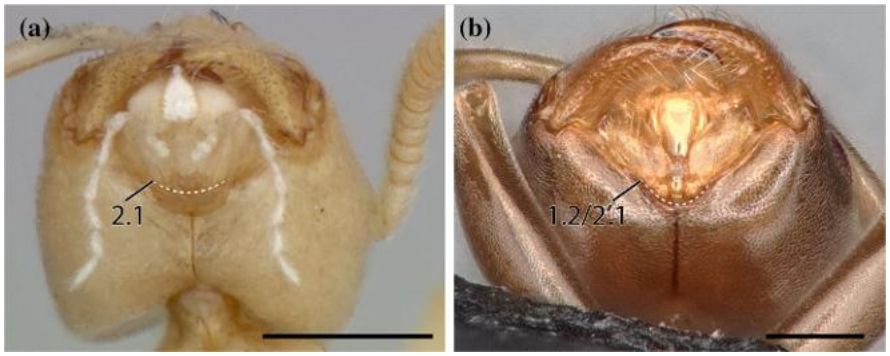



**FIGURE 7** Selected characters from key couplets 1 and 2. Labels are in the format <couplet>. <character>; an apostrophe indicates the second lug of the couplet. Ventral views. All scale bars = 0.2 mm. (a) *Nebothriomyrmex majeri* CASENT0009951. (b) *Bothriomyrmex wroughtonii javanus* CASENT0758662. Image in A from AntWeb (www.antweb.org), photographer April Nobile.

13653113, 2026, 4, Downloaded from https://resjournals.onlinelibrary.wiley.com/doi/10.1111/syen.70073 by Readcube (Labtiva Inc.), Wiley Online Library on [06/11/2026]. See the Terms and Conditions (https://onlinelibrary.wiley.com/terms-and-conditions) on Wiley Online Library for rules of use; OA articles are governed by the applicable Creative Commons License

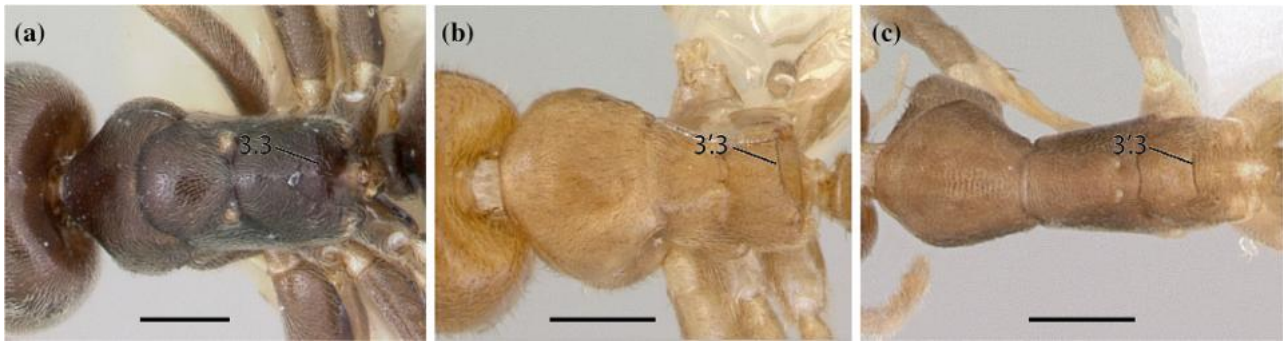



**FIGURE 8** Selected characters from key couplet 3. Labels are in the format <couplet>. <character>; an apostrophe indicates the second lug of the couplet. All scale bars = 0.2 mm. (a) *Bothriomyrmex paradoxus* CASENT0103277. (b) *Loweriella boltoni* CASENT0172291. (c) *Ravavy miafina* CASENT0439855. All images from AntWeb (www.antweb.org), photographer April Nobile.




**FIGURE 9** Selected characters from key couplet 3. Labels are in the format <couplet>. <character>; an apostrophe indicates the second lug of the couplet. All scale bars = 0.5 mm. (a) *Ravavy miafina* CASENT0439855. (b) *Loweriella boltoni* CASENT0009998. All images from AntWeb (www.antweb.org), photographers April Nobile (a, c) and Erin Prado (b).




**FIGURE 10** Selected characters from key couplets 5 and 6. Labels are in the format <couplet>. <character>. An apostrophe indicates the second lug of the couplet. All scale bars = 0.5 mm. (a) *Technomyrmex gorgona* CASENT0173586. (b) *Linepithema anathema* CASENT0104904. All images from AntWeb (www.antweb.org), photographer April Nobile.

**7 [6′] (1)** Fifth gastral tergite (abdominal tergite 7) located dorsally, not reflexed beneath fourth tergite, hence fifth tergite visible in dorsal view and cloacal orifice apical (Figure 12a–d). **(2)** Pronotum generally with two or more erect hairs (Figure 12d). **(R)** Afrotropics, Indomalaya, Australasia, rare in Central America .....***Technomyrmex***

7′ **(1)** Fifth gastral tergite reflexed beneath fourth tergite, hence fifth tergite not visible in dorsal view and cloacal orifice ventral (Figure 12e–h). **(2)** Pronotum usually erect hairs (Figure 12h) .....**8** (*Tapinoma* genus group, *part*)

**8 [7′] (1)** Pronotum with erect hairs (Figure 13a). **(2)** Mandible with larger teeth but no denticles (Figure 13b). **(R)** Afrotropical (Angola) .....***Ecphorella***

8′ **(1)** Pronotum almost always without erect hairs (Figure 13c). **(2)** Mandible with 2–15 denticles (Figure 13d).....**9**

**9 [8′] (1)** Palp formula 6:3 (Figure 14a). **(2)** Workers dimorphic, major workers not phragmotic (Figure 14b). **(3)** Anterior clypeal margin transverse or shallowly and broadly emarginate (Figure 14b). **(R)** Madagascar.....***Aptinoma***

13653113, 2026, 4, Downloaded from https://resjournals.onlinelibrary.wiley.com/doi/10.1111/syen.70073 by Readcube (Labtiva Inc.), Wiley Online Library on [06/11/2026]. See the Terms and Conditions (https://onlinelibrary.wiley.com/terms-and-conditions) on Wiley Online Library for rules of use; OA articles are governed by the applicable Creative Commons License

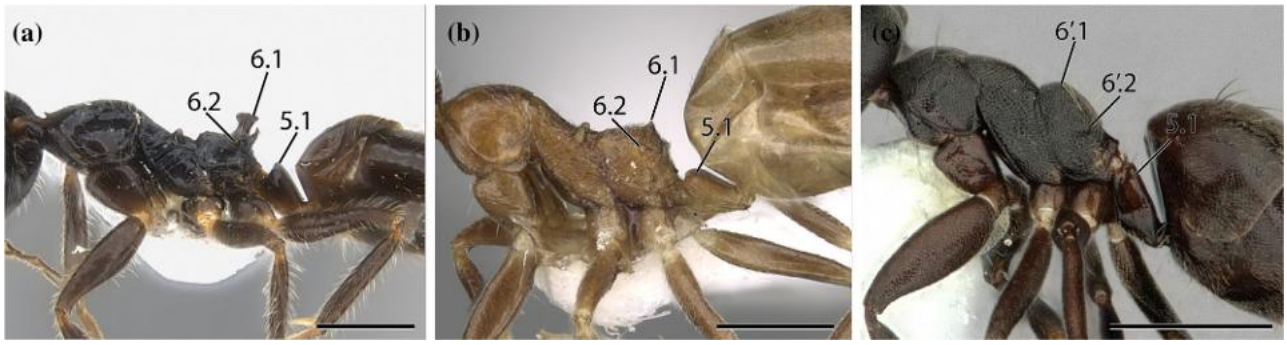



**FIGURE 11** Selected characters from key couplets 5 and 6. Labels are in the format <couplet>. <character>. An apostrophe indicates the second lug of the couplet. Profile views. All scale bars = 0.5 mm. (a) *Axinidris acholii* CASENT0217121. (b) *Axinidris tridens* CASENT0281999. (c) *Technomyrmex albicoxis* CASENT0886048. Images in a and b from AntWeb (www.antweb.org), photographers Erin Prado (a) and Shannon Hartman (b).

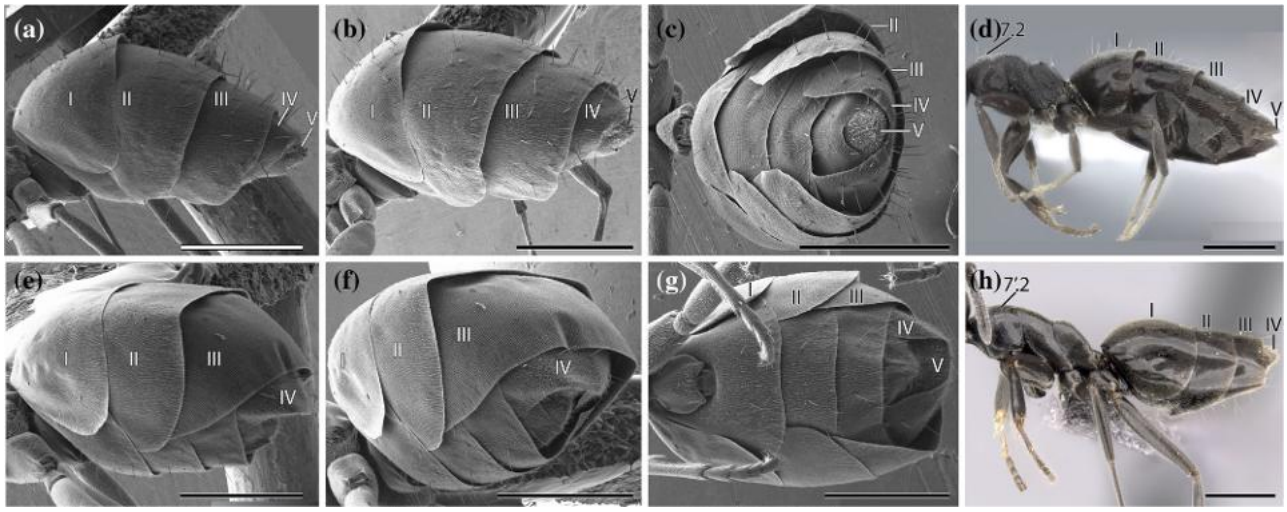



**FIGURE 12** Selected characters from key couplet 7. Labels are in the format <couplet>. <character>; an apostrophe indicates the second lug of the couplet; or Roman numerals indicate numeration of gastral tergites referred to in 7.1 and 7′.1 (a–c, e–g) scanning electron micrographs; (d, h) photomicrographs. All scale bars = 0.5 mm. (a–c) *Technomyrmex albipes* ANTWEB1008594. (d) *Technomyrmex albipes* CASENT0246603. (e–g) *Tapinoma simrothi* ANTWEB1008592. (h) *Tapinoma simrothi* CASENT0263927. All images from AntWeb (www.antweb.org), imagers Roberto Keller (a–c, e–g), Andrea Walker (d), Estella Ortega (h).

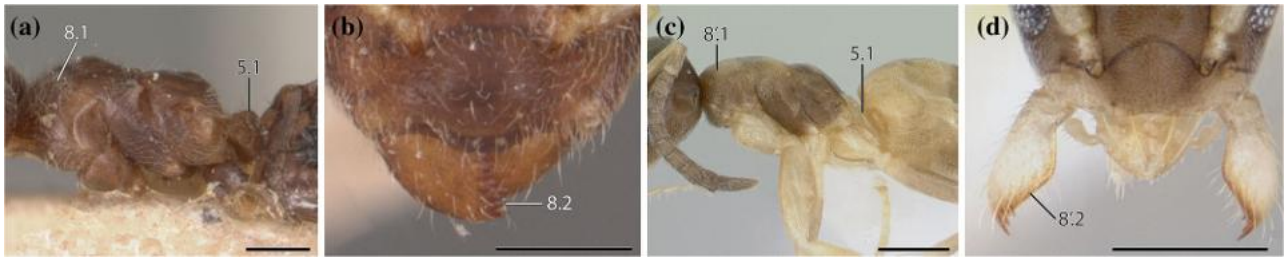



**FIGURE 13** Selected characters from key couplets 5 and 7. Labels are in the format <couplet>. <character>; an apostrophe indicates the second lug of the couplet. All scale bars = 0.2 mm. (a, b): *Ecphorella wellmani* CASENT0102456. (c, d) *Tapinoma melanocephalum* CASENT0103323. All images from AntWeb (www.antweb.org), photographer April Nobile.

9′ **(1)** Palp formula 6:4 (Figure 14c). **(2)** Workers almost always monomorphic; if workers dimorphic, then majors phragmotic (Figure 14d). **(3)** Anterior clypeal margin variable, sometimes with deep medial notch or incision. **(R)** Global.....***Tapinoma***

**10 [5′] (1)** Anterolateral hypostoma dentate or flanged (sometimes weakly developed) (Figure 15a). **(2)** Cuticle thick, often heavily sculptured (Figure 15b–d). **(3a)** Posterior surface of propodeum usually concave (Figure 15b,c), **(3b)** sometimes sloped, or less often

13653113, 2026, 4, Downloaded from https://resjournals.onlinelibrary.wiley.com/doi/10.1111/syen.70073 by Readcube (Labtiva Inc.), Wiley Online Library on [06/11/2026]. See the Terms and Conditions (https://onlinelibrary.wiley.com/terms-and-conditions) on Wiley Online Library for rules of use; OA articles are governed by the applicable Creative Commons License

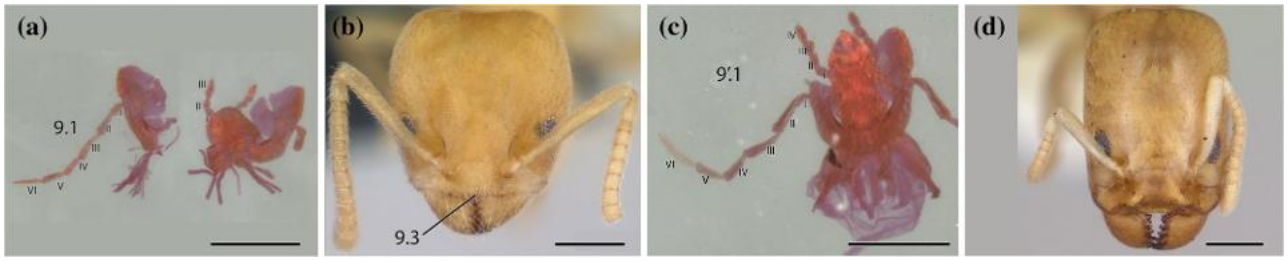



**FIGURE 14** Selected characters from key couplet 9. Labels are in the format <couplet>. <character>; an apostrophe indicates the second lug of the couplet. (a, c) dissected maxilla and labium. (b, d). All scale bars = 0.2 mm. Roman numerals enumerate palpomeres. (a) *Aptinoma mangabe* CASENT0345098. (b) *Aptinoma mangabe* CASENT0130146. (c) *Tapinoma* mg07 CASENT0345106. (d) *Tapinoma annandalei* major worker CASENT0172851. All images from AntWeb (www.antweb.org), photographers Brett Morgan (a, c) and April Nobile (b, d).

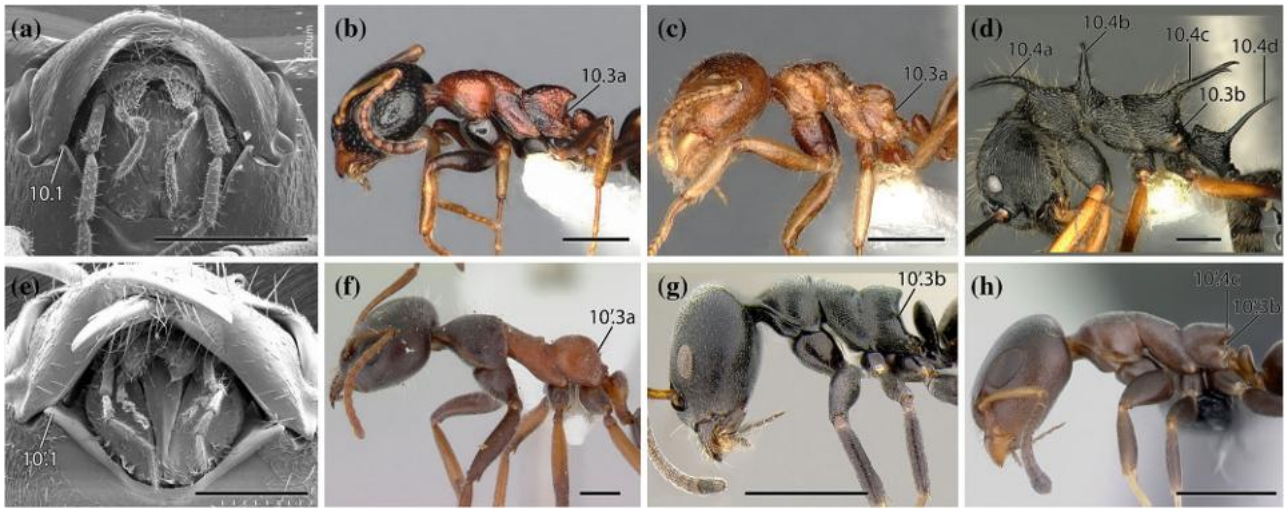



**FIGURE 15** Selected characters from key couplet 10. Labels are in the format <couplet>. <character>; an apostrophe indicates the second lug of the couplet. (a, e) ventral view of hypostoma, scanning electron micrographs. (b–d, f–h) photomicrographs. All scale bars = 0.5 mm. (a) *Dolichoderus laminatus* ANTWEB1008520. (b) *Dolichoderus quadripunctatus* SMFHYM0008908. (c) *Dolichoderus* tap03 SMFHYM0008939. (d) *Dolichoderus shattucki* CASENT0632946. (e) *Iridomyrmex purpureus* ANTWEB1008536. (f) *Iridomyrmex anteroinclinus* CASENT0172045. (g) *Ochetellus sororis* CASENT0171060. (h) *Turneria bidentata* CASENT0069974. Images in a, e–h from AntWeb (www.antweb.org), imagers Roberto Keller (a, e, h), April Nobile (f), Eli Sarnat.

flat to convex (Figure 15d). **(4)** Body often with spines or processes, one or more of: **(4a)** pronotum with paired spines, denticles or tubercles (Figure 15d); **(4b)** mesonotum with paired spines, tubercles or subdentate flanges (Figure 15d); **(4c)** propodeum with paired spines, tubercles or a median spine (Figure 15d); **(4d)** petiolar node with a single median spine or bidentate (Figure 15d). **(5)** Anterior margin of mesosternal region (i.e., the anterior mesopectal flange) convex. **(R)** Global, except Afrotropics..... .....***Dolichoderus*** (Dolichoderini)

10′ **(1)** Anterolateral hypostoma without teeth or flanges (Figure 15e). **(2)** Cuticle almost always thin and weakly sculptured (Figure 15f–h). **(3a)** Posterior surface of propodeum usually convex (Figure 15f), **(3b)** rarely sloped or concave (Figure 15g). **(4)** Body rarely with spines and processes: **(4a)** pronotum always without paired spines, tubercles or denticles (Figure 15f–h); **(4b)** mesonotum always without paired spines, tubercles or flanges (Figure 15f–h); **(4c)** propodeum rarely with paired spinose processes or tubercles (Figure 15h); **(4d)** petiolar node without spine or teeth (Figure 15f–h). **(6)** Anterior margin of mesosternal region (i.e., the anterior mesopectal flange) transverse, not convex.....**11**

**11 [10′] (1)** Medial hypostomal lamina notched or very deeply emarginate (Figure 5a–f). **(2)** Appendages often extremely elongate. **(R)** Neotropics, Australasia, Indomalaya ..... ..... **12** (Leptomyrmecini: *Leptomyrmex* genus group)

11′ **(1)** Medial hypostomal lamina complete, unreduced (as in Figure 7a). **(2)** Appendages not extremely elongate.....**14**

**12 [11] (1)** Compound eye absent (Figure 16a,g). **(2)** Palp formula 2:3. **(3)** Appendages short (Figure 16g). **(R)** Neotropics ..... .....***Anillidris***

12′ **(1)** Compound eye present (Figure 16b,c,e,j). **(2)** Palp formula 6:4 or 5:4. **(3)** Appendages not shortened, often extremely elongate (Figure 16j).....**13**

**13 [12′] (1)** Head, mesosoma, metasoma and legs with stout erect hairs (Figure 16c,d,i). **(2)** Torulus separated from epistomal line (Figure 16c). **(3)** Anterior clypeal margin convex (Figure 16c,d). **(4)**

13653113, 2026, 4, Downloaded from https://resjournals.onlinelibrary.wiley.com/doi/10.1111/syen.70073 by Readcube (Labtiva Inc.), Wiley Online Library on [06/11/2026]. See the Terms and Conditions (https://onlinelibrary.wiley.com/terms-and-conditions) on Wiley Online Library for rules of use; OA articles are governed by the applicable Creative Commons License

Mandible emarginate-concave proximad subapical tooth (Figure 16c,d). **(R)** Neotropics.....***Paranillidris*** gen. nov.

13′ **(1)** Erect hairs limited to clypeus, coxae and gastral sternites (Figure 16b,e–f,h,j). **(2)** Torulus contacting epistomal line (Figure 16b,e). **(3)** Anterior clypeal margin transverse to shallowly concave (Figure 16b,e,f). **(4)** Mandible without concavity proximad subapical tooth (Figure 16e,f). **(R)** Indomalaya, Australasia.....***Leptomyrmex***

**14 [11′] (1)** Anterior clypeal margin with long decurved setae which reach or surpass the apex of the closed mandible in frontal view (Figure 17a,b). **(R)** New World.....

.....**15** (Leptomyrmecini: *Dorymyrmex* genus group)

14′ **(1)** Anterior clypeal margin with usually straight setae which usually do not reach or surpass the apex of the closed mandible in frontal view and are often much shorter (Figure 17c,d).....**16**

**15 [14] (1)** Propodeum with unpaired medial cone, tooth or spine (Figure 18a–c). **(2)** Third maxillary palpomere elongate, longer than palpomeres 4 + 5 + 6 together (Figure 18a,b). **(3)** Apical mandibular tooth much longer than subapical tooth (Figure 17a). **(4)** Psammophore present (sometimes short or weakly developed) (Figure 18a,b,d).....***Dorymyrmex***

15′ **(1)** Propodeum without tooth or spine. **(2)** Third maxillary palpomere not elongate, subequal in length to palpomere 4 (Figure 18d). **(3)** Apical mandibular tooth subequal to or only slightly longer than subapical tooth (Figure 17b). **(4)** Psammophore absent (Figure 18d) .....***Forelius***

**16 [14′] (1)** Metanotal groove reduced to a suture (Figure 19a,d), therefore **(2)** Mesonotum and propodeum forming a continuous, convex profile in lateral view (Figure 19a). **(3)** Metanotal spiracle located laterally, not within dorsal region of metanotal suture or abutting it anteriorly (Figure 19d) **(R)** Holarctic.....

.....***Liometopum*** (Tapinomini: *Tapinoma* genus group, *part*)

16′ **(1)** Metanotal groove not so reduced, either forming a groove or angle (Figure 18 B-C, E-F); therefore **(2)** Mesonotum and propodeum divided, not forming a continuous, uninterrupted profile in lateral view (Figure 18b,c). **(3)** Metanotal spiracle located dorsally, within metanotal groove (Figure 19e) or abutting it anteriorly (Figure 19f). **(R)**

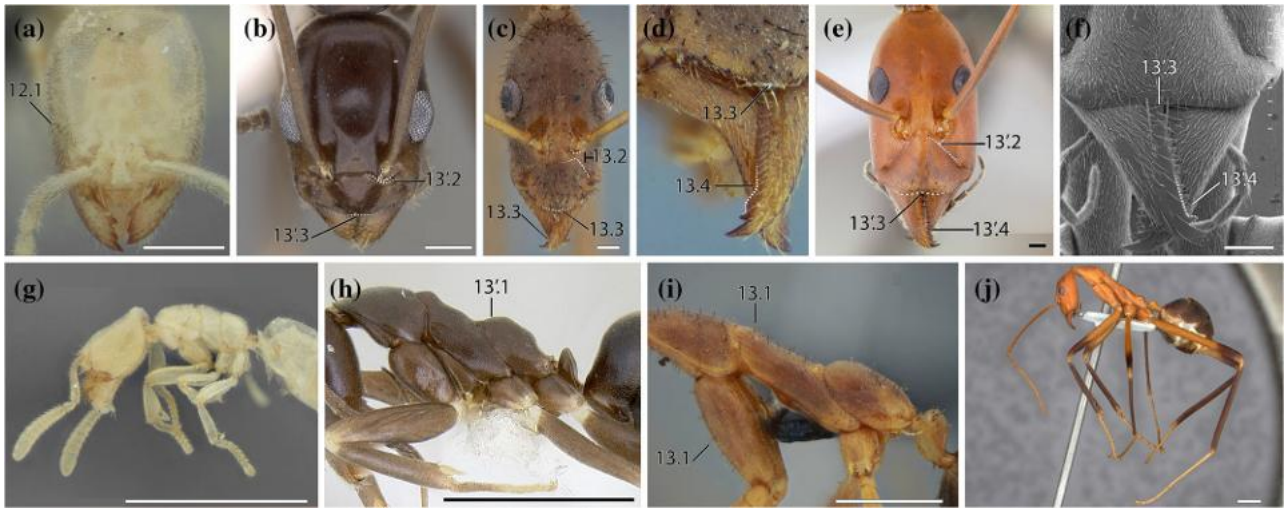



**FIGURE 16** Selected characters from key couplet 13. Labels are in the format <couplet>. <character>; an apostrophe indicates the second lug of the couplet. (f) scanning electron micrograph; (a–e, g–j) photomicrographs. Scale bars in (a–f) = 0.2 mm. Scale bars in (g–j) = 1.0 mm. (a, g) *Anillidris bruchi* UFV-LABECOL-004260. (b) *Leptomyrmex aitchisoni* CASENT0012033. (c, d, i) *Paranillidris relicta* ANTWEB1032698. (e) *Leptomyrmex erythrocephalus* CASENT0106077. (f) *Leptomyrmex pallens* ANTWEB1008544. (h) *Leptomyrmex burwelli* CASENT0106001. (j) *Leptomyrmex cnemidatus* CASENT0841233. All images from AntWeb (www.antweb.org), imagers Julio Chaul (a, c–e, i), Estella Ortega (b), Michael Branstetter (e, h), Roberto Keller (f), Ziv Lieberman (j).

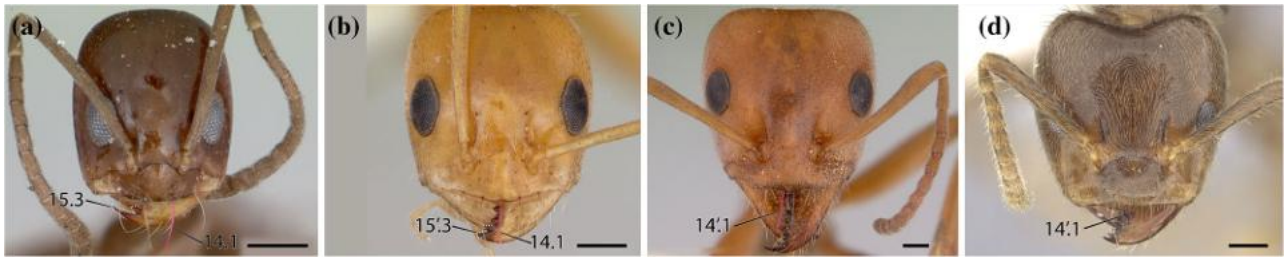



**FIGURE 17** Selected characters from key couplets 14 and 15. Labels are in the format <couplet>. <character>; an apostrophe indicates the second lug of the couplet. All scale bars = 0.2 mm. (a) *Forelius brasiliensis* CASENT0173737. (b) *Dorymyrmex wheeleri* CASENT0173018. (c) *Iridomyrmex rufoinclinus* CASENT0172060. (d) *Azteca australis* CASENT0249534. All images from AntWeb (www.antweb.org), photographers April Nobile (a–c) and Shannon Hartman (d).

13653113, 2026, 4, Downloaded from https://resjournals.onlinelibrary.wiley.com/doi/10.1111/syen.70073 by Readcube (Labtiva Inc.), Wiley Online Library on [06/11/2026]. See the Terms and Conditions (https://onlinelibrary.wiley.com/terms-and-conditions) on Wiley Online Library for rules of use; OA articles are governed by the applicable Creative Commons License

Neotropics, Australasia.....
.....**17** (Leptomyrmecini: *Iridomyrmex* genus group, *part*.)

**17 [16′] (1)** Posterior face of propodeum concave (Figure 20a–c). **(2)** Propodeal angle sometimes with tubercles or spinose process (Figure 20b,c).....**18**

17′ **(1)** Posterior face of propodeum convex, sloped or flat, not concave (Figure 20d). **(2)** Propodeum always without tubercles or processes (Figure 20d).....**20**

**18 [17] (1)** Anteromedial clypeal margin emarginate (Figure 20e). **(2)** Propodeum almost always without tubercles or processes (Figure 20a). **(3)** Propodeal spiracle located on lateral propodeal surface, well-separated from dorsal propodeal surface in lateral view (Figure 20a). **(R)** Palearctic, Indomalaya, Australasia.....***Ochetellus***

18′ **(1)** Anteromedial clypeal margin convex, not emarginate (Figure 20f,g). **(2)** Propodeum always with distinct tubercles or spinose processes (Figure 20b,c). **(3)** Propodeal spiracle located near or on the dorsal propodeal surface or a process thereof in lateral view (Figure 20b,c).....**19**

**19 [18′] (1)** Propodeum with posteriorly directed spinose processes (Figure 20b). **(2)** Propodeal spiracle located prebasally on spine, that is, just distad the spine base (Figure 20b) **(3)** Standing hairs abundant on head, mesosoma, appendages and gaster (Figure 20b); **(4)** Eye of moderate size, elliptical, inner margins not converging in frontal view (Figure 20f). **(R)** Australia.....***Froggattella***

19′ **(1)** Propodeum with blunt tubercles (Figure 20c). **(2)** Propodeal spiracle located apicoventrally on tubercle (Figure 20c). **(3)** Standing hairs




**FIGURE 18** Selected characters from key couplets 14 and 15. Labels are in the format <couplet>. <character>; an apostrophe indicates the second lug of the couplet. All scale bars = 0.5 mm. (a) *Dorymyrmex ensifer* CASENT0249686. (b) *Dorymyrmex tener* CASENT0841205. (c) *Dorymyrmex lipan* CASENT0103440. (d) *Forelius brasiliensis* CASENT0173737. All images from AntWeb (www.antweb.org), photographers Ryan Perry (a), Jill Oberski (b) and April Nobile (c–d).




**FIGURE 19** Selected characters from key couplets 14 and 15. Labels are in the format <couplet>. <character>; an apostrophe indicates the second lug of the couplet. All scale bars = 0.5 mm. (a) *Liometopum occidentale* CASENT0884397. (b, e) *Azteca beltii* JTLC000009501. (c, f) *Linepithema neotropicum* CASENT0104903. (d) *Liometopum microcephalum* CASENT0885473. All images from AntWeb (www.antweb.org), photographers Ziv Lieberman (a, d), Shannon Hartman (b, e) and April Nobile (c, f).

13653113, 2026, 4, Downloaded from https://resjournals.onlinelibrary.wiley.com/doi/10.1111/syen.70073 by Readcube (Labtiva Inc.), Wiley Online Library on [06/11/2026]. See the Terms and Conditions (https://onlinelibrary.wiley.com/terms-and-conditions) on Wiley Online Library for rules of use; OA articles are governed by the applicable Creative Commons License

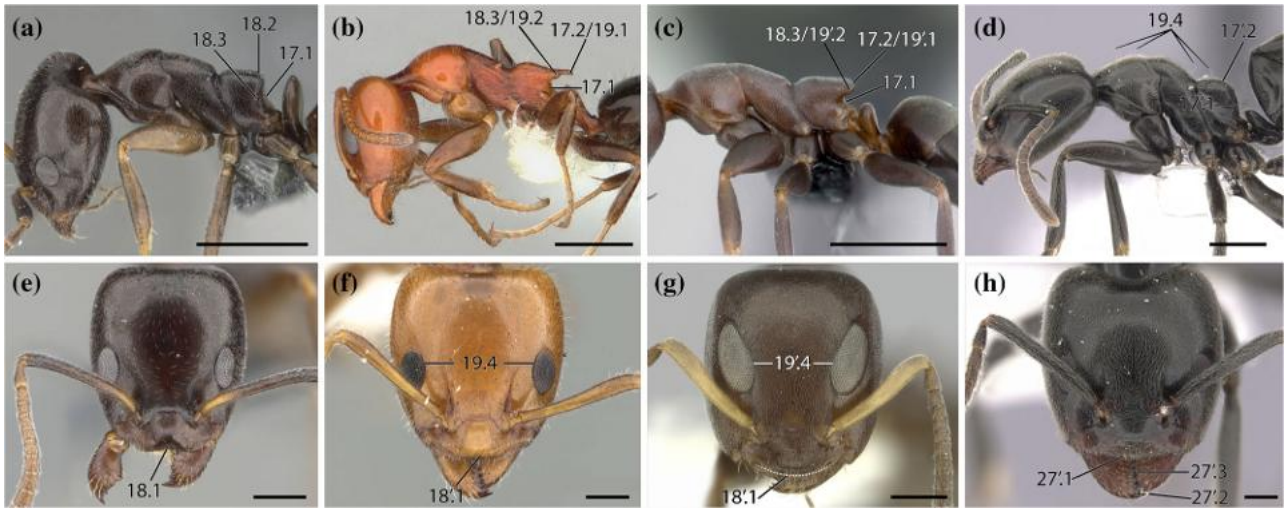



**FIGURE 20** Selected characters from key couplets 17–19 and 27. Labels are in the format <couplet>. <character>; an apostrophe indicates the second lug of the couplet. Scale bars in (a–c) = 0.5 mm. Scale bars in (d–h) = 0.2 mm. (a, e) *Ochetellus glaber* CASENT0275747. (b) *Froggattella kirbii* CASENT0886007. (c) *Turneria bidentata* CASENT0069974. (d, h) *Anonychomyrma biconvexa* CASENT0249516. (f) *Froggattella kirbii* CASENT0249701. (g) *Turneria arbusta* CASENT0249807. All images from AntWeb (www.antweb.org), photographers Michele Esposito (a, e), Ziv Lieberman (b), April Nobile (c), Will Ericson (d, h), Ryan Perry (f) and Shannon Hartman (g).

absent on head, mesosoma, appendages and gaster (Figure 20c,g). **(4)** Eye large, elongate, inner margins converging in frontal view (Figure 2g). **(R)** Australasia.....***Turneria***

**20 [17′] (R)** Neotropical (one species of *Linepithema* introduced globally).....**21**

20′ **(R)** Indomalayan or Australasian (one Neotropical species of *Linepithema* introduced globally and included in both lugs of the couplet) .....**23**

**21 [20] (1)** Apical mandibular tooth usually subequal in length to subapical tooth (longer than subapical tooth in 5 species, *aurita* group) (Figure 21a). **(2)** Pronotum, mesonotum and propodeal dorsum usually with at least a few suberect to erect hairs, often many (Figure 21d). **(3)** Petiolar node low, rounded-cuneate (Figure 21d). **(4)** Workers polymorphic. **(5)** Major workers often with ocelli. ..... ***Azteca***

21′ **(1)** Apical mandibular tooth elongate, much longer than subapical tooth (Figure 21b,c). **(2)** Pronotum and mesonotum almost always without standing hairs or with at most a few pairs of erect hairs on pronotum (Figure 21e,f) (1 species with >8 hairs, *Linepithema hirsutum*). **(3)** Petiolar node squamiform (Figure 21e,f). **(4)** Workers monomorphic. **(5)** Ocelli absent.....**22**

**22 [21′] (1)** Anteromedial clypeal margin emarginate (Figure 21b). **(2)** Eye variable in size, comprising 17–110 ommatidia. (3) Eye situated medially, separated from lateral head margin in frontal view (Figure 21b). (4) Eye located anterior to longitudinal midpoint of head in frontal view (Figure 21b). (5) Petiolar node not apically curved posteriorly (Figure 21e).....***Linepithema***

22′ **(1)** Anteromedial clypeal margin convex (Figure 21c). **(2)** Eye large, comprising 130–150 ommatidia. **(3)** Eye situated laterally, not separated from lateral head margin in frontal view (Figure 21c). **(4)** Eye located around the longitudinal midpoint of head in frontal view (Figure 21c). (5) Petiolar node apically curved posteriorly (Figure 21f)... .....***Gracilidris***

**23 [22′] (1)** Palp formula 5:3. **(2)** Propodeum with distinct subvertical anterior surface (Figure 22e). **(3)** Anterior clypeal margin with 8–20 very short setae which scarcely surpass the anterior clypeal margin (Figure 22a). **(4)** Mandible with ~11–14 teeth of similar size (Figure 22a). **(R)** Australasia.....***Papyrius***

23′ **(1)** Palp formula 6:4. **(2)** Metanotal groove variably developed, but propodeum only very rarely with distinct anterior surface (Figure 22f–h). **(3)** Anterior clypeal margin with ~2–16 setae which distinctly surpass the anterior clypeal margin (Figure 22b–d). **(4)** Mandible with 5–12 teeth and usually several denticles (Figure 22c). **(R)** Neotropics, Indomalaya, Australasia.....**24**

**24 [23′] (1)** Anterior clypeal margin sinuate, clypeus shouldered, that is, with head in full-face view, anterolateral clypeal margin separated from anteromedial region by a projection or angle (Figure 22b,c). **(2)** Anteromedial clypeal margin often with a medial projection (sometimes weakly developed) (Figure 22c).....**25**

24′ **(1)** Anterior clypeal margin not sinuate, clypeus unshouldered, that is, with head in full-face view, anterolateral clypeal margin not separated from anteromedial region by a projection or angle (Figure 22d). **(2)** Anteromedial clypeal margin without a projection (Figure 22d).....**26**

**25 [24] (1)** Posterior head usually margin distinctly and broadly emarginate, hence head often cordate or subcordate in frontal view (Figure 22b). **(2)** Eye located largely anterior to longitudinal midpoint of head in frontal view (Figure 22b). **(3)** Medial clypeal projection generally weakly developed (Figure 22b). **(4)** Petiolar node cuneate, strongly inclined anteriorly (Figure 22f). **(5)** Body and appendages

13653113, 2026, 4, Downloaded from https://resjournals.onlinelibrary.wiley.com/doi/10.1111/syen.70073 by Readcube (Labtiva Inc.), Wiley Online Library on [06/11/2026]. See the Terms and Conditions (https://onlinelibrary.wiley.com/terms-and-conditions) on Wiley Online Library for rules of use; OA articles are governed by the applicable Creative Commons License

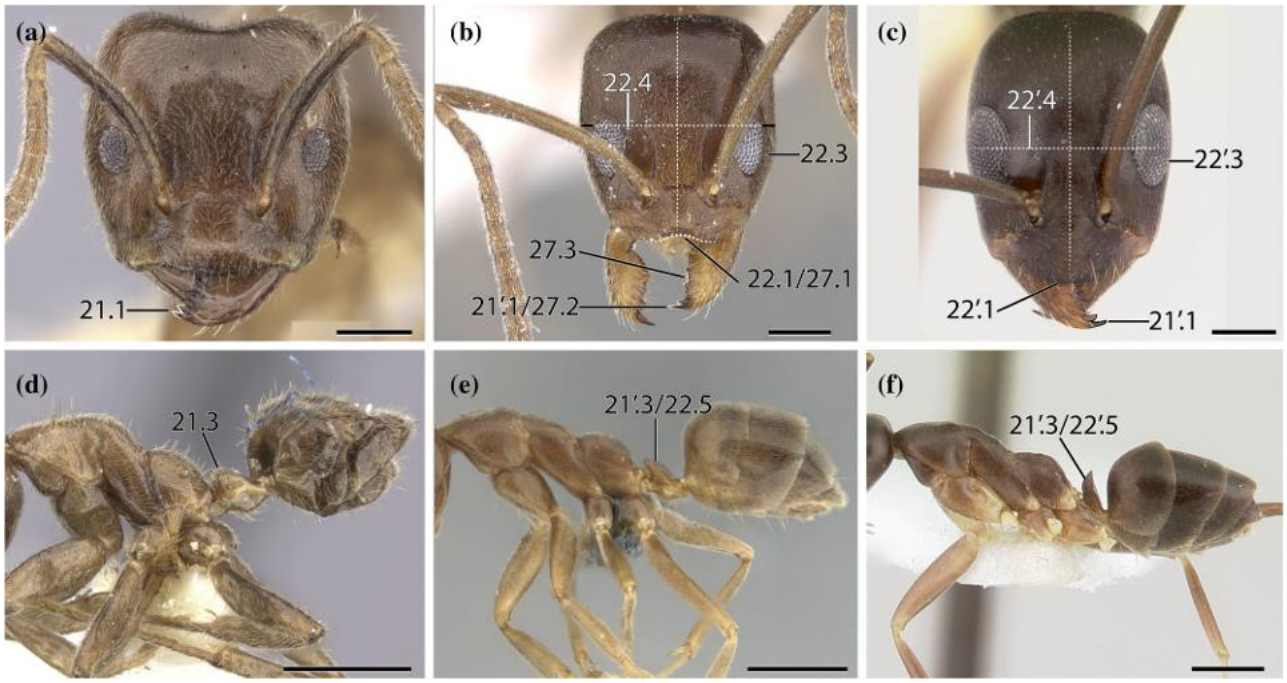



**FIGURE 21** Selected characters from key couplets 21–22 and 27. Labels are in the format <couplet>. <character>; an apostrophe indicates the second lug of the couplet. Scale bars in (a–c)= 0.2 mm. Scale bars in (d–f) = 0.5 mm. (a, d) *Azteca lattke* CASENT0619158. (b, e) *Linepithema humile* CASENT0813010. (c, f) *Gracilidris pombero* CASENT0179539. All images from AntWeb (www.antweb.org), photographers Will Ericson (a, d), Bradley Reynolds (b, e) and Erin Prado (c, f).

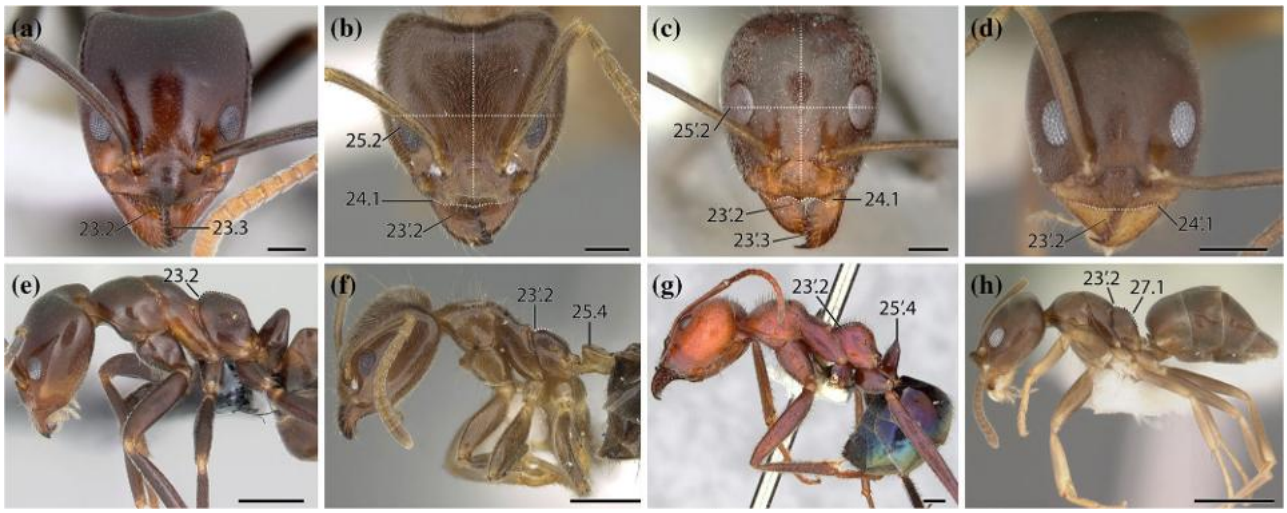



**FIGURE 22** Selected characters from key couplets 23–26. Labels are in the format <couplet>. <character>; an apostrophe indicates the second lug of the couplet. Scale bars in a–d = 0.2 mm. Scale bars in E–H = 0.5 mm. (a) *Papyrius nitidus* CASENT0106012. (b, f) *Philidris myrmecodiae* CASENT0919859. (c) *Iridomyrmex anceps* CASENT0886057. (d, h) *Doleromyrma* sp. CASENT0010854. (e) *Papyrius nitidus* CASENT0070200. (g) *Iridomyrmex purpureus*. All images from AntWeb (www.antweb.org), photographers Michael Branstetter (a), Michele Esposito (b, f), Ziv Lieberman (c, g) and April Nobile (d, e, h).

occasionally strongly reflective, but never iridescent (Figure 22b,f) .....***Philidris***

25′ **(1)** Posterior head margin convex, transverse or less often weakly emarginate in frontal view (Figure 22c). **(2)** Eye located around or posterior to longitudinal midpoint of head in frontal view (Figure 22c). **(3)** Medial clypeal projection variable, sometimes strongly developed (Figure 22c). **(4)** Petiolar node variable, cuneate to squamiform, somewhat inclined anteriorly to vertical (Figure 22g) **(5)** Body and appendages sometimes iridescent, either subtly or strongly so (Figure 22g) .....***Iridomyrmex***

**26 [24′] (1)** Dorsal propodeal surface distinctly shorter than posterior surface (Figure 22h). **(2)** Mandible with 4 or 5 teeth and 4 or

13653113, 2026, 4, Downloaded from https://resjournals.onlinelibrary.wiley.com/doi/10.1111/syen.70073 by Readcube (Labtiva Inc.), Wiley Online Library on [06/11/2026]. See the Terms and Conditions (https://onlinelibrary.wiley.com/terms-and-conditions) on Wiley Online Library for rules of use; OA articles are governed by the applicable Creative Commons License

5 denticles. **(3)** Fourth gastral sternite flat posteriorly. **(4)** Standing hairs absent on scape, mesosomal dorsum and legs.....***Doleromyrma***

26′ **(1)** Dorsal propodeal surface usually subequal in length to posterior surface or longer. **(2)** Mandible with 5–10 teeth and 0–13 denticles. **(3)** Fourth gastral sternite keel-shaped posteriorly. **(4)** Standing hairs usually present on at least one of scape, mesosomal dorsum or legs.....**27**

**27 [26′] (1)** Anteromedial clypeal margin broadly emarginate (Figure 21b). **(2)** Apical mandibular tooth much longer than subapical tooth (Figure 21b). **(3)** Mandibular teeth separated by distinctly shorter denticles (fig. 26B). **(4)** Standing hairs absent on scape, mesosomal dorsum and legs (Figure 21b,e).....

.....***Linepithema*** (one introduced species, *L. humile*)

27′ **(1)** Anteromedial clypeal margin transverse to convex (Figure 20h). **(2)** Apical mandibular tooth subequal in length to subapical tooth (Figure 20h). **(3)** Mandibular teeth somewhat varying in size, but without distinctly shorter denticles (Figure 20h). **(4)** Standing hairs almost always present on at least one of scape, mesosomal dorsum or legs (Figure 20d).....***Anonychomyrma***

## SYSTEMATIC PALAEONTOLOGY

**Note**: Castes for which material is known for a given taxon are listed after taxon names in square brackets. Where applicable, type species are indicated with asterisks (*). Abbreviations: m = male, q = queen, w = worker.

*Incertae sedis* in Leptomyrmecini:

1. '*Forelius* Emery, 1888'.

1.1. †*Forelius chenpauch* Varela-Hernández et al., 2023 [w]. – Chiapas.

2. †*Schismiscapus* Varela-Hernández et al., 2022 [w].

†*Forelius chenpauch* Varela-Hernández et al., 2023.

This species was described from Miocene Chiapas amber (Mexico) and was placed in *Forelius* due to the supposed presence of two long, curved setae on the anterior clypeal margin, the mandibular dentition and partially visible characters of the petiolar node and first gastral tergite. We agree that the presence of a dorsally developed petiolar node and the differentiation between the basal and masticatory mandibular margins reasonably exclude the species from *Tapinoma* and further agree that exclusion from *Liometopum* is reasonable based on the mesosomal profile and biogeographic setting. However, the clypeal setae are not visible in any of the figures, and the diagnostic length of long recurved setae in the *Dorymyrmex* genus group is generally considered by comparison to the length of the apex of the closed mandible, while in †*F. chenpauch*, the mandible is open, and the setal length was considered by reaching the external mandibular margin. Therefore, this condition is uncertain. Additionally, *Forelius* generally have four or more clypeal setae, although we acknowledge that fewer setae could be due to extinct variation or taphonomy. Varela-Hernández et al. (2023) discuss the presence and ubiquity of *Azteca* species in Chiapas and Dominican ambers relative to the paucity of *Forelius*, but do not consider that †*F. chenpauch* may itself belong to *Azteca*. From the figures, it appears that the anterior clypeal margin is basically transverse, as in many *Azteca*, rather than convex as in all *Forelius*. The overall habitus of the head and mesosoma also evoke the *Azteca* gestalt. In sum, while we do not transfer †*F. chenpauch* to *Azteca* or any other genus at this time, we also consider the evidence as presented to be insufficient for confident placement in *Forelius*, and encourage further study, or at least dissemination of more informative figures.

†*Schismiscapus* Varela-Hernández et al., 2022.

Type species: †*Schismiscapus exstinctum* by original designation.

Constituent species:

†*Schismiscapus caritatis* (Brandão et al., 1999) **comb. nov.** [w] – Dominican.

=†*Technomyrmex caritatis* Brandão et al., 1999.

†*Schismiscapus hispaniolae* (Wilson, 1985) **comb. nov.** [w] – Dominican.

=†*Iridomyrmex hispaniolae* Wilson, 1985.

†*Schismiscapus exstinctum* Varela-Hernández et al., 2022 [w] – Chiapas.

This distinctive genus was placed in Leptomyrmecini and considered near to *Leptomyrmex* based on the presence of a medial hypostomal notch. Based on the paratype photographs, it is unclear to us if the hypostoma is in fact notched or laminar; the entire medial hypostomal area has a similar appearance which is distinct from the surrounding head capsule, with no distinguishable excavation, and the medial hypostomal lamina is generally translucent when present in Dolichoderinae. If the hypostoma is indeed reduced, it is likely that †*Schismiscapus* is a stem lineage of the *Leptomyrmex* genus group, based on the number of observed differences to *Paranillidris* and *Leptomyrmex*. Varela-Hernández et al. (2022) also examined two Dominican amber species attributed to *Technomyrmex*, †*T. caritatis* and *T. hispaniolae*, which are highly similar in appearance, but determined that these similarities were homoplasies based on the results of a 15-taxon, 29-character matrix presumably analysed under parsimony (no inferential information is specified). However, this matrix apparently lacks signal, as the phylogeny produced differs from ours at all extant nodes, except sister relationships between certain pairs of *Dolichoderus* and *Dorymyrmex* species. Similarly, the cladistic analysis of Brandão et al. (1999), while recovering a few natural groups, overall produced a broadly discordant topology relative to our results.

As previously noted, the two Dominican '*Technomyrmex*' are highly similar to one another but lack characters of the petiole and gaster diagnostic for the *Technomyrmex*. Specifically, the petiolar node is present and dorsally well developed, and the first gastral tergite lacks a medial groove and does not overhang the petiole. The most pertinent characters allying †*T. caritatis* and †*T. hispaniolae* to *Technomyrmex* are the reported five visible gastral tergites and the larval morphology of *T. caritatis*, most obviously the terminal, posterodorsal knob, which most closely resembles the 'specialized' larvae of the former *Engramma* (=*Technomyrmex*) (Brandão et al., 1999; Wheeler & Wheeler, 1951). This seemingly contradictory combination of characters led Bolton (2007) to treat these species as *incertae sedis* in

13653113, 2026, 4, Downloaded from https://resjournals.onlinelibrary.wiley.com/doi/10.1111/syen.70073 by Readcube (Labtiva Inc.), Wiley Online Library on [06/11/2026]. See the Terms and Conditions (https://onlinelibrary.wiley.com/terms-and-conditions) on Wiley Online Library for rules of use; OA articles are governed by the applicable Creative Commons License

*Technomyrmex*, having not examined primary material. As we also were unable to access physical material in the context of this study, we could not confirm the state of the gastral tergites directly and acknowledge that it is an important character to re-evaluate, preferably with advanced imaging techniques. These latter characters notwithstanding, we consider the similarities among the three fossil species to be compelling enough to transfer the Dominican *Technomyrmex* to †*Schismiscapus*, allowing that future examination of these fossils may falsify our hypothesis.

**Diagnosis** (putatively strongest synapomorphies italicized):

1. *Head longer than broad, broadest posteriorly, posterior margin emarginate, posterolateral corners rounded.*
2. Eye located anteriorly on head.
3. Frontal carina extending to half the frontal eye length or greater.
4. Frontal carina sinuate, with lateral extension at antennal insertion.
5. *Scape long, surpassing posterior head margin by 1.3–2 times its length.*
6. *Flagellomeres elongate, 2 to 4 times as long as broad.*
7. Anterior margin of clypeus emarginate medially.
8. *Clypeal disc with a pair of long paramedial setae*
9. *Basal angle of mandible rounded but marked by a tooth*
10. Apical mandibular tooth slightly longer than subapical tooth.
11. *Masticatory margin of mandible with 5–7 teeth and 9 denticles, in similar pattern of apical-subapical-2 denticles-tooth-5 denticles-one or two teeth-two denticles-basal margin tooth.*
12. *Basal margin of mandible dentate with three denticles or teeth decreasing in size proximally.*
13. Palp formula 6:4.
14. Maxillary palps elongate, approximately reaching backwards halfway as long as the ventral head surface.
15. *Mesosoma gracile, elongate and narrow, with sinuous profile.*
16. *Pronotum without standing hairs, or a single pair of erect hairs present.*
17. *Pronotum somewhat bell-shaped, narrow dorsoventrally anteriorly, ventrolateral margin expanding posteroventrally.*
18. *Mesothorax very long, mesonotum initially sloping posteriorly at a steep angle, then with a longer, shallower angle.*
19. *Mesopleural area pinched dorsoventrally at point where mesonotal slope changes.*
20. Posterior margin of mesonotum somewhat raised anterad metanotal groove.
21. *Metanotal groove strongly impressed and long, with or without striate sculpture.*
22. *Propodeum subcuboidal: dorsal surface plane to slightly convex, propodeal angle rounded to angular, but forming a nearly right angle; posterior propodeal surface subvertical or slightly concave, with additional shallow concavity just dorsad metapleural gland bulla.*
23. Propodeal spiracle located posteriorly on lateral surface of propodeum near the dorsal surface.
24. *Petiole elongate, pedunculate.*
25. *Petiolar node with distinct, subvertical anterior face and inclined posterior face.*
26. *Petiole behind node long, subcylindrical.*
27. *Legs very elongate.*
28. Gaster relatively small, compact and round, not compressed.
29. First gastral tergite without longitudinal impression and apparently not overhanging petiole.

## CONCLUSION

We here perform the first phylogenomic inferences of the evolution of the Dolichoderinae at the subfamily scale, including divergence dating and biogeographic analyses. Our results from a variety of alignment and modelling strategies substantiate the monophyly of tribes and most genera, while revealing novel relationships among tribes and groups of genera. Our inferences provide the first molecular scaffolds of the species-rich and morphologically diverse genera *Dolichoderus*, *Iridomyrmex* and *Technomyrmex*, while supporting previous investigations in *Azteca*, *Dorymyrmex*, *Forelius* and *Leptomyrmex* sensu stricto (Ayala et al., 1996; Barden et al., 2017; Lucky, 2011; Oberski, 2024). We explore connections between phylogeny, morphology and ecology in and among several genera.

For the first time, we place the unique genus *Anillidris* among the newly defined *Leptomyrmex* genus group, based on the agreement of phylogeny and morphology. The sister relationship of the eyeless, short-limbed subterranean *Anillidris* and the large-eyed, long-limbed *Paranillidris* **gen. nov**. suggests striking adaptive pressure towards dissimilar foraging and nesting strategies in these depauperate lineages, stimulating future investigation into the life history of *P. relicta* and the ancestral morphology and ecology of the genus group. That the synapomorphic hypostomal notch is retained throughout the genus group, despite striking biological differences between these genera, as well as morphological divergence in the 'micro' and 'macro' clades of *Leptomyrmex*, invigorates further inquiry into the functional correlations between cephalic morphology and trophic or social ecology.

Our phylogeny leads to the synonymization of the genera *Arnoldius* and *Chronoxenus* under *Bothriomyrmex*, emphasizing the misleading nature of characters showing strong meristic and structural reduction. Variable molecular support for morphology-based hypotheses in this genus group and across the dolichoderine tree indicates a need for character exploration, refinement and redefinition. The convergent evolution of a modified hypostoma in the *Leptomyrmex* genus group and in the tribe Bothriomyrmecini especially stimulates new character quantification and ecomorphological study. Our topological results in the Tapinomini also motivate a reconsideration of character interpretation in the reduction of the petiolar node, for which skeletomusculature will play an important role. Such research may also illuminate the function of other abdominal dolichoderine synapomorphies such as the emarginate helcial tergite. The finding that mesosomal spines are derived multiple times in *Dolichoderus* has implications for the taxonomy of species

13653113, 2026, 4, Downloaded from https://resjournals.onlinelibrary.wiley.com/doi/10.1111/syen.70073 by Readcube (Labtiva Inc.), Wiley Online Library on [06/11/2026]. See the Terms and Conditions (https://onlinelibrary.wiley.com/terms-and-conditions) on Wiley Online Library for rules of use; OA articles are governed by the applicable Creative Commons License

groups therein and encourages study into the genetic basis of homoplasy in this and other highly derived lineages.

Connections between phylogeny and ecomorphology are apparent in the arid-adapted *Dorymyrmex*, *Forelius* and *Iridomyrmex*. Myrmecophyty is also a probable contributor to species diversity, appearing in many dolichoderine groups and with numerous plant partners. Although we discuss hypotheses about convergence in the *Azteca-Cecropia* system, these findings form a basis for similar study into the timing and phylogenetic distribution of ant–plant symbioses in other taxa.

We infer the Dolichoderinae + Aneuretinae to have evolved in the Upper Cretaceous and the crown Dolichoderinae soon after the K-Pg boundary, with major suprageneric clades arising largely in the Palaeogene and many genera between the Oligocene and Miocene. While many groups will require further sampling to clarify biogeographic details, especially in taxa with diverse extant distributions, we find several cases of recurring dispersal patterns among lineages. A trans-Antarctic dispersal route is likely in at least the *Iridomyrmex* genus group, the Australasian clade of *Dolichoderus*, and *Leptomyrmex s.s.*; dispersal between Eurasia and the New World via Beringia or North Atlantic Land Bridges is potentially implicated in the *Tapinoma*, the *Technomyrmex* genus group, *Liometopum*, the clade Dolichoderini + Leptomyrmecini and certain clades of *Dolichoderus*.

Our model comparisons highlight properties of node-dating models which are infrequently explicitly explored. Most pertinently, we infer chronograms under alternate constructions of the joint time and birth-death-sampling tree process prior, computational approaches which are rarely directly compared in empirical studies. We find that model behaviour is not obviously predictable from premises, arguing for wider adoption of such comparisons to better understand how statistical assumptions interact with model parameterization and prior information.

In sum, the present study constitutes a robust framework for understanding the relationships and diversity of the Dolichoderinae, in terms of species richness, morphology and ecology. While many questions remain, our findings provide a strong foundation for future quantitative investigation of character evolution, especially the nature and occurrence of convergence and symplesiomorphy across the tree.

## AUTHOR CONTRIBUTIONS

**Ziv E. Lieberman:** Conceptualization; data curation; formal analysis; funding acquisition; investigation; methodology; project administration; writing – original draft; writing – review and editing; validation; visualization. **Jill T. Oberski:** Formal analysis; investigation; methodology; writing – original draft; writing – review and editing; visualization. **Brendon E. Boudinot:** Conceptualization; investigation; supervision; writing – original draft; writing – review and editing.

## ACKNOWLEDGEMENTS

For provision of specimens from personal research collections, we would like to thank John Longino, Jim Wetterer and Philip Ward. We also thank Brian Fisher for providing access to material from CAS and further acknowledge Brian Fisher, Michele Esposito and Bradley Reynolds for their roles in maintaining AntWeb and AntCat. We thank Sarah Mueller for providing access to *Anillidris* type specimens for imaging, as well as Diego Matielo for taking additional images of *Anillidris* workers. Michael Branstetter was instrumental in bioinformatic data processing (see Table S2). We are grateful to Chao Zhang for assistance with ASTER; to Sishuo Wang and Sandra Álvarez-Carretero for crucial help with PAML; to Nick Matzke for detailed help with BioGeoBEARS; to David Cerny and Benjamin Redelings for guidance with RevBayes; and to Mark Miller for very timely help with CIPRES. For high-performance computing, JTO thanks Ted Schultz and Jovana Jasso for access and support at the SI/HPC and Christoph Sinai likewise at SGN TBG. We are also grateful to the curation staff for BioSample at the National Center for Biotechnology Information for their support with data management and availability. ZEL thanks Philip Ward, Marek Borowiec and Jason Bond for advising and Zachary Griebenow for discussion. Barry Bolton provided valuable insight into *Technomyrmex* and the subject of collective groups; Steve Shattuck and Jonghyun Park likewise on *Anonychomyrma*, *Iridomyrmex* and *Technomyrmex*. Gwen Payne provided useful perspectives on Mediterranean palaeoenvironments in the context of historical biogeography. We thank the editor and three anonymous reviewers for their time and expertise providing extensive and incisive comments which greatly improved the manuscript.

## FUNDING INFORMATION

This work was supported by a United States National Science Foundation grant DEB-1932062 to Philip Ward; and by the University of California, Davis, through a UC Davis Jastro-Shields and a UC Davis Duffy-Dingle research award to ZEL.

## CONFLICT OF INTEREST STATEMENT

The authors declare no competing interests.

## DATA AVAILABILITY STATEMENT

All newly generated sequence data are available under the NCBI (https://www.ncbi.nlm.nih.gov/) BioProject PRJNA1281292; BioSample and Sequence Read Archive accessions are provided in Table S2. All the original data and scripts necessary to reproduce the analyses reported in this study, along with associated outputs and additional files, can be accessed at https://doi.org/10.5281/zenodo.18752606. Voucher data and images are accessible at AntWeb (www.antweb.org).

## ORCID

*Ziv E. Lieberman* https://orcid.org/0000-0001-6352-327X
*Jill T. Oberski* https://orcid.org/0000-0002-4904-4464
*Brendon E. Boudinot* https://orcid.org/0000-0002-4588-0430

## REFERENCES

Aberer, A.J., Kobert, K. & Stamatakis, A. (2014) ExaBayes: massively parallel Bayesian tree inference for the whole-genome era. *Molecular Biology and Evolution*, 31(10), 2553–2556. Available from: https://doi.org/10.1093/molbev/msu236

Adams, C.G., Gentry, A.W. & Whybrow, P.J. (1983) Dating the terminal Tethyan event. *Utrecht Micropaleontological Bulletin*, 30, 273–298.

13653113, 2026, 4, Downloaded from https://resjournals.onlinelibrary.wiley.com/doi/10.1111/syen.70073 by Readcube (Labtiva Inc.), Wiley Online Library on [06/11/2026]. See the Terms and Conditions (https://onlinelibrary.wiley.com/terms-and-conditions) on Wiley Online Library for rules of use; OA articles are governed by the applicable Creative Commons License

Agard, P., Omrani, J., Jolivet, L., Whitechurch, H., Vrielynck, B., Spakman, W. et al. (2011) Zagros orogeny: a subduction-dominated process. *Geological Magazine*, 148(5–6), 692–725. Available from: https://doi.org/10.1017/S001675681100046X

Aibekova, L., Boudinot, B.E., Georg Beutel, R., Richter, A., Keller, R.A., Hita-Garcia, F. et al. (2022) The skeletomuscular system of the mesosoma of *Formica rufa* workers (Hymenoptera: Formicidae). *Insect Systematics and Diversity*, 6(2), 1–26. Available from: https://doi.org/10.1093/isd/ixac002

Aibekova, L., Richter, A., Beutel, R.G., van de Kamp, T., Economo, E.P., Griebenow, Z. et al. (2025) The mesosoma of *Protanilla* (Leptanillinae) and the groundplan of the Formicidae (Hymenoptera). *Journal of Morphology*, 286(7), e70064. Available from: https://doi.org/10.1002/jmor.70064

Ali, J.R. & Heaney, L.R. (2021) Wallace's line, Wallacea, and associated divides and areas: history of a tortuous tangle of ideas and labels. *Biological Reviews*, 96(3), 922–942. Available from: https://doi.org/10.1111/brv.12683

Allen, M.B. & Armstrong, H.A. (2008) Arabia–Eurasia collision and the forcing of mid-Cenozoic global cooling. *Palaeogeography, Palaeoclimatology, Palaeoecology*, 265(1), 52–58. Available from: https://doi.org/10.1016/j.palaeo.2008.04.021

Almeida, E.A.B., Pie, M.R., Brady, S.G. & Danforth, B.N. (2012) Biogeography and diversification of colletid bees (Hymenoptera: Colletidae): emerging patterns from the southern end of the world. *Journal of Biogeography*, 39(3), 526–544. Available from: https://doi.org/10.1111/j.1365-2699.2011.02624.x

Andersen, A.N. (1995) A classification of Australian ant communities, based on functional groups which parallel plant life-forms in relation to stress and disturbance. *Journal of Biogeography*, 22(1), 15–29. Available from: https://doi.org/10.2307/2846070

André, E. (1892) Voyage de M. Chaper à Bornéo. Catalogue des fourmis et description des espèces nouvelles. *Mémoires de la Société Zoologique de France*, 5, 46–55.

Anisimova, M., Gil, M., Dufayard, J.F., Dessimoz, C. & Gascuel, O. (2011) Survey of branch support methods demonstrates accuracy, power, and robustness of fast likelihood-based approximation schemes. *Systematic Biology*, 60(5), 685–699. Available from: https://doi.org/10.1093/sysbio/syr041

Archibald, S.B., Rasnitsyn, A.P., Brothers, D.J. & Mathewes, R.W. (2018) Modernisation of the Hymenoptera: ants, bees, wasps, and sawflies of the early Eocene Okanagan highlands of western North America. *The Canadian Entomologist*, 150(2), 205–257. Available from: https://doi.org/10.4039/tce.2017.59

Ayala, F.J., Wetterer, J.K., Longino, J.T. & Hartl, D.L. (1996) Molecular phylogeny of *Azteca* ants (Hymenoptera: Formicidae) and the colonization of *Cecropia* trees. *Molecular Phylogenetics and Evolution*, 5(2), 423–428. Available from: https://doi.org/10.1006/mpev.1996.0037

Bacon, C.D., Silvestro, D., Jaramillo, C., Smith, B.T., Chakrabarty, P. & Antonelli, A. (2015) Biological evidence supports an early and complex emergence of the isthmus of Panama. *Proceedings of the National Academy of Sciences*, 112(19), 6110–6115. Available from: https://doi.org/10.1073/pnas.1423853112

Bankevich, A., Nurk, S., Antipov, D., Gurevich, A.A., Dvorkin, M., Kulikov, A.S. et al. (2012) SPAdes: a new genome assembly algorithm and its applications to single-cell sequencing. *Journal of Computational Biology*, 19(5), 455–477. Available from: https://doi.org/10.1089/cmb.2012.0021

Barba-Montoya, J., dos Reis, M. & Yang, Z. (2019) Comparison of different strategies for using fossil calibrations to generate the time prior in Bayesian molecular clock dating. *Molecular Phylogenetics and Evolution*, 114, 386–400. Available from: https://doi.org/10.1016/j.ympev.2017.07.005

Barden, P., Boudinot, B.E. & Lucky, A. (2017) Where fossils dare and males matter: combined morphological and molecular analysis untangles the evolutionary history of the spider ant genus *Leptomyrmex* Mayr (Hymenoptera: Dolichoderinae). *Invertebrate Systematics*, 31(6), 765–780. Available from: https://doi.org/10.1071/IS16067

Battistuzzi, F.U., Billing-Ross, P., Paliwal, A. & Kumar, S. (2011) Fast and slow implementations of relaxed-clock methods show similar patterns of accuracy in estimating divergence times. *Molecular Biology and Evolution*, 28(9), 2439–2442. Available from: https://doi.org/10.1093/molbev/msr100

Benson, W.W. (1985) Amazon ant-plants. In: Prance, G.T. & Lovejoy, T.E. (Eds.) *Key environments. Amazonia*. Oxford: Pergamon Press, pp. 239–266.

Bequaert, J. (1922) IV. Ants in their diverse relations to the plant world. *Bulletin of the American Museum of Natural History*, 45, 333–583.

Billen, J. (1986) Morphology and ultrastructure of the abdominal glands in dolichoderine ants (Hymenoptera, Formicidae). *Insectes Sociaux*, 33(3), 278–295. Available from: https://doi.org/10.1007/BF02224246

Billen, J. (1994) Morphology and classification of the exocrine glands in ants. *Ari*, 18, 1–4.

Billen, J. (2009) Diversity and morphology of exocrine glands in ants. In: *Proceedings XIX Simpósio Mirmecologia*. Ouro Preto, Brazil: XIX Simpósio de Mirmecologia, Vol. 17, pp. 21–27.

Blaimer, B.B., Brady, S.G., Schultz, T.R., Lloyd, M.W., Fisher, B.L. & Ward, P.S. (2015) Phylogenomic methods outperform traditional multi-locus approaches in resolving deep evolutionary history: a case study of formicine ants. *BMC Evolutionary Biology*, 15(1), 271. Available from: https://doi.org/10.1186/s12862-015-0552-5

Blaimer, B.B., Ward, P.S., Schultz, T.R., Fisher, B.L. & Brady, S.G. (2018) Paleotropical diversification dominates the evolution of the hyperdiverse ant tribe Crematogastrini (Hymenoptera: Formicidae). *Insect Systematics and Diversity*, 2(5), 1–14. Available from: https://doi.org/10.1093/isd/ixy013

Blanchard, B.D., Nakamura, A., Cao, M., Chen, S.T. & Moreau, C.S. (2020) Spine and dine: a key defensive trait promotes ecological success in spiny ants. *Ecology and Evolution*, 10(12), 5852–5863. Available from: https://doi.org/10.1002/ece3.6322

Bolger, A.M., Lohse, M. & Usadel, B. (2014) Trimmomatic: a flexible trimmer for Illumina sequence data. *Bioinformatics*, 30(15), 2114–2120. Available from: https://doi.org/10.1093/bioinformatics/btu170

Bolton, B. (1994) *Identification guide to the ant genera of the world*. Cambridge, Mass.: Harvard University Press.

Bolton, B. (2007) Taxonomy of the dolichoderine ant genus *Technomyrmex* Mayr (Hymenoptera: Formicidae) based on the worker caste. *Contributions of the American Entomological Institute*, 35(1), 1–150.

Bolton, B. (2026) *An online catalog of the ants of the world*. https://antcat.org/

Borgmeier, T. (1937) Formigas novas ou pouco conhecidas da América do Sul e Central, principalmente do Brasil (Hym. Formicidae). *Archivos do Instituto de Biologia Vegetal (Rio de Janeiro)*, 3, 217–255.

Borowiec, M.L. (2016) AMAS: a fast tool for alignment manipulation and computing of summary statistics. *PeerJ*, 4, e1660. Available from: https://doi.org/10.7717/peerj.1660

Borowiec, M.L. (2019) Convergent evolution of the army ant syndrome and congruence in big-data phylogenetics. *Systematic Biology*, 68(4), 642–656. Available from: https://doi.org/10.1093/sysbio/syy088

Borowiec, M.L., Rabeling, C., Brady, S.G., Fisher, B.L., Schultz, T.R. & Ward, P.S. (2019) Compositional heterogeneity and outgroup choice influence the internal phylogeny of the ants. *Molecular Phylogenetics and Evolution*, 134, 111–121. Available from: https://doi.org/10.1016/j.ympev.2019.01.024

Borowiec, M.L. et al. (2025) Evaluating UCE data adequacy and integrating uncertainty in a comprehensive phylogeny of ants. *Systematic Biology*, 74(5), 700–722. Available from: https://doi.org/10.1093/sysbio/syaf001

13653113, 2026, 4, Downloaded from https://resjournals.onlinelibrary.wiley.com/doi/10.1111/syen.70073 by Readcube (Labtiva Inc.), Wiley Online Library on [06/11/2026]. See the Terms and Conditions (https://onlinelibrary.wiley.com/terms-and-conditions) on Wiley Online Library for rules of use; OA articles are governed by the applicable Creative Commons License

Bouček, Z. (1988) *Australasian Chalcidoidea (Hymenoptera). A biosystematic revision of genera of fourteen families, with a reclassification of species*. Wallingford, Oxon, U.K.: CAB International.

Bouckaert, R., Heled, J., Kühnert, D., Vaughan, T., Wu, C.H., Xie, D. et al. (2014) BEAST 2: a software platform for Bayesian evolutionary analysis. *PLoS Computational Biology*, 10(4), e1003537. Available from: https://doi.org/10.1371/journal.pcbi.1003537

Boudinot, B.E. (2013) The male genitalia of ants: musculature, homology, and functional morphology (Hymenoptera, Aculeata, Formicidae). *Journal of Hymenoptera Research*, 30, 29–49. Available from: https://doi.org/10.3897/jhr.30.3535

Boudinot, B.E. (2015) Contributions to the knowledge of Formicidae (Hymenoptera, Aculeata): a new diagnosis of the family, the first global male-based key to subfamilies, and a treatment of early branching lineages. *European Journal of Taxonomy*, 120, 1–62. Available from: https://doi.org/10.5852/ejt.2015.120

Boudinot, B.E. (2025) Ecomorphology of ants. In: Betz, O. (Ed.) *Insect Ecomorphology: linking functional insect morphology to ecology and evolution*. London: Elsevier Academic Press, pp. 469–524.

Boudinot, B.E., Bock, B.L., Tröger, D., Weingardt, M., Hammel, J.U., Grabe, V. et al. (2026) Discovery of Goethe's amber ant: its phylogenetic and evolutionary implications. *Scientific Reports*, 16(1), 2880. Available from: https://doi.org/10.1038/s41598-026-36004-4

Boudinot, B.E., Borowiec, M.L. & Prebus, M.M. (2022) Phylogeny, evolution, and classification of the ant genus *Lasius*, the tribe Lasiini and the subfamily Formicinae (Hymenoptera: Formicidae). *Systematic Entomology*, 47(1), 113–151. Available from: https://doi.org/10.1111/syen.12522

Boudinot, B.E., Probst, R.O., Brandão, C.A., Feitosa, R. & Ward, P.S. (2016) Out of the Neotropics: newly discovered relictual species sheds light on the biogeographical history of spider ants (*Leptomyrmex*, Dolichoderinae, Formicidae). *Systematic Entomology*, 41(3), 658–671. Available from: https://doi.org/10.1111/syen.12181

Boudinot, B.E., van de Kamp, T., Peters, P. & Knöllinger, K. (2024) Male genitalia, hierarchical homology, and the anatomy of the bullet ant (*Paraponera clavata*; Hymenoptera, Formicidae). *Journal of Morphology*, 285(9), e21757. Available from: https://doi.org/10.1002/jmor.21757

Bouju, V. & Perrichot, V. (2020) A review of amber and copal occurrences in Africa and their paleontological significance. *BSGF Earth Sciences Bulletin*, 191, 17. Available from: https://doi.org/10.1051/bsgf/2020018

Brandão, C.R.F., Wagensberg, J., Baroni Urbani, C. & Yamamoto, C.I. (1999) New *Technomyrmex* in Dominican amber (Hymenoptera: Formicidae), with a reappraisal of Dolichoderinae phylogeny. *Entomologica Scandinavica*, 29(4), 411–428.

Branstetter, M.G., Longino, J.T., Ward, P.S. & Faircloth, B.C. (2017) Enriching the ant tree of life: enhanced UCE bait set for genome-scale phylogenetics of ants and other Hymenoptera. *Methods in Ecology and Evolution*, 8(6), 768–776. Available from: https://doi.org/10.1111/2041-210X.12742

Brikiatis, L. (2014) The De Geer, Thulean and Beringia routes: key concepts for understanding early Cenozoic biogeography. *Journal of Biogeography*, 41(6), 1036–1054. Available from: https://doi.org/10.1111/jbi.12310

Brown, W.L., Jr. (1973) A comparison of the Hylean and Congo-west African rain forest ant faunas. In: Meggers, B.J., Ayensu, E.S. & Duckworth, W.D. (Eds.) *Tropical forest ecosystems in Africa and South America: a comparative review*. Washington, D. C.: Smithsonian Institution Press, pp. 161–185.

Camacho, G.P., Franco, W., Branstetter, M.G., Pie, M.R., Longino, J.T., Schultz, T.R. et al. (2022) UCE phylogenomics resolves major relationships among Ectaheteromorph ants (Hymenoptera: Formicidae: Ectatomminae, Heteroponerinae): a new classification for the subfamilies and the description of a new genus. *Insect Systematics and Diversity*, 6(1), 5. Available from: https://doi.org/10.1093/isd/ixab026

Cantone, S. & di Giulio, A. (2023) A fine morphological study of the rare *Anillidris bruchi* Santschi (Hymenoptera: Formicidae: Dolichoderinae) male and queen. *Insects*, 14(9), 723. Available from: https://doi.org/10.3390/insects14090723

Castresana, J. (2000) Selection of conserved blocks from multiple alignments for their use in phylogenetic analysis. *Molecular Biology and Evolution*, 17(4), 540–552. Available from: https://doi.org/10.1093/oxfordjournals.molbev.a026334

Catullo, R.A. & Scott Keogh, J. (2014) Aridification drove repeated episodes of diversification between Australian biomes: evidence from a multi-locus phylogeny of Australian toadlets (*Uperoleia*: Myobatrachidae). *Molecular Phylogenetics and Evolution*, 79, 106–117. Available from: https://doi.org/10.1016/j.ympev.2014.06.012

Chomicki, G. & Renner, S.S. (2015) Phylogenetics and molecular clocks reveal the repeated evolution of ant-plants after the late Miocene in Africa and the early Miocene in Australasia and the Neotropics. *New Phytologist*, 207(2), 411–424. Available from: https://doi.org/10.1111/nph.13271

Coates, A.G., Aubry, M.P., Berggren, W.A., Collins, L.S. & Kunk, M. (2003) Early Neogene history of the central American arc from Bocas del Toro, western Panama. *GSA Bulletin*, 115(3), 271–287. Available from: https://doi.org/10.1130/0016-7606(2003)115%3C0271:ENHOTC%3E2.0.CO;2

Coates, A.G., Jackson, J.B., Collins, L.S., Cronin, T.M., Dowsett, H.J., Bybell, L.M. et al. (1992) Closure of the isthmus of Panama: the near-shore marine record of Costa Rica and western Panama. *GSA Bulletin*, 104(7), 814–828. Available from: https://doi.org/10.1130/0016-7606(1992)104%3C0814:COTIOP%3E2.3.CO;2

Coates, A.G. & Stallard, R.F. (2013) How old is the isthmus of Panama? *Bulletin of Marine Science*, 89(4), 801–813. Available from: https://doi.org/10.5343/bms.2012.1076

Cohen, K.M., Finney, S.C., Gibbard, P.L. & Fan, J.X. (2013) The ICS international chronostratigraphic chart v2024/12. *Episodes*, 36, 199–204.

Cox, B. (2001) The biogeographic regions reconsidered. *Journal of Biogeography*, 28(4), 511–523. Available from: https://doi.org/10.1046/j.1365-2699.2001.00566.x

Crowley, C.W. (2012) *An atlas of Cenozoic climate zones*. Arlington, TX, USA: University of Texas at Arlington.

dal Pos, D., Mikó, I., Talamas, E.J., Vilhelmsen, L. & Sharanowski, B.J. (2023) A revised terminology for male genitalia in Hymenoptera (Insecta), with a special emphasis on Ichneumonoidea. *PeerJ*, 11, e15874. Available from: https://doi.org/10.7717/peerj.15874

Dejean, A. & Djieto-Lordon, C. (1996) Ecological studies on the relationships between ants (Hymenoptera, Formicidae) and the myrmecophyte *Scaphopetalum thonneri*. *Sociobiology*, 28(1), 91–102.

del Toro, I., Pacheco, J.A. & Mackay, W. (2009) Revision of the ant genus *Liometopum* (Hymenoptera: Formicidae). *Sociobiology*, 53(2A), 296–369.

di Franco, A. et al. (2019) Evaluating the usefulness of alignment filtering methods to reduce the impact of errors on evolutionary inferences. *BMC Evolutionary Biology*, 19(1), 21. Available from: https://doi.org/10.1186/s12862-019-1350-2

Dill, M., Williams, D.J. & Maschwitz, U. (2002) Herdsmen ants and their mealybug partners. *Abhandlungen der Senckenbergischen Naturforschenden Gesellschaft*, 557, 1–373.

Dlussky, G.M. (1997) Genera of ants (Hymenoptera: Formicidae) from Baltic amber. *Paleontologicheskii Zhurnal*, 1997(6), 50–62.

Dlussky, G.M. & Perkovsky, E.E. (2002) Ants (Hymenoptera, Formicidae) from the Rovno Amber. *Vestnik Zoologii*, 36(5), 3–20.

Dlussky, G.M. & Rasnitsyn, A.P. (2003) Ants (Hymenoptera: Formicidae) of formation Green River and some other middle Eocene deposits of North America. *Russian Entomological Journal*, 11(4), 411–436.

Doré, M. et al. (2025) Evolutionary history of ponerine ants highlights how the timing of dispersal events shapes modern biodiversity. *Nature*

13653113, 2026, 4, Downloaded from https://resjournals.onlinelibrary.wiley.com/doi/10.1111/syen.70073 by Readcube (Labtiva Inc.), Wiley Online Library on [06/11/2026]. See the Terms and Conditions (https://onlinelibrary.wiley.com/terms-and-conditions) on Wiley Online Library for rules of use; OA articles are governed by the applicable Creative Commons License

*Communications*, 16(8297), 1–17. Available from: https://doi.org/10.1038/s41467-025-63709-3

dos Reis, M., Zhu, T. & Yang, Z. (2014) The impact of the rate prior on Bayesian estimation of divergence times with multiple loci. *Systematic Biology*, 63(4), 555–565. Available from: https://doi.org/10.1093/sysbio/syu020

Dubovikoff, D.A. (2005) The system of taxon *Bothriomyrmex* Emery, 1869 sensu lato (Hymenoptera: Formicidae) and relatives genera. *Caucasian Entomological Bulletin*, 1(1), 89–94.

Duellman, W.E., Marion, A.B. & Hedges, S.B. (2016) Phylogenetics, classification, and biogeography of the treefrogs (Amphibia: Anura: Arboranae). *Zootaxa*, 4104(1), 1–109. Available from: https://doi.org/10.11646/zootaxa.4104.1.1

Eisner, T. (1957) A comparative morphological study of the proventriculus of ants (Hymenoptera: Formicidae). *Bulletin of the Museum of Comparative Zoology*, 116, 437–490.

El-Saadawi, W., Osman, R., El-Faramawi, M., Bkhat, H., El-Din, M.K. & Ziada, N. (2018) On the Eocene mangroves of Wadi Al-Hitan world heritage site, Fayum, Egypt. *The Egyptian Society of Experimental Biology (Botany)*, 14(1), 197–209. Available from: https://doi.org/10.5455/egyjebb.20180515093213

Emery, C. (1913) Hymenoptera. Fam. Formicidae. Subfam. Dolichoderinae. *Genera Insectorum*, 137, 1–50.

Emery, C. (1925) Les espèces européennes et orientales du genre *Bothriomyrmex*. *Bulletin de la Société Vaudoise Des Sciences Naturelles*, 56, 5–22.

Erixon, P. et al. (2003) Reliability of Bayesian posterior probabilities and bootstrap frequencies in phylogenetics. *Systematic Biology*, 52(5), 665–673. Available from: https://doi.org/10.1080/10635150390235485

Faircloth, B.C. (2013) illumiprocessor: a trimmomatic wrapper for parallel adapter and quality trimming. https://doi.org/10.6079/J9ILL

Faircloth, B.C. (2016) PHYLUCE is a software package for the analysis of conserved genomic loci. *Bioinformatics*, 32(5), 786–788. Available from: https://doi.org/10.1093/bioinformatics/btv646

Faircloth, B.C., Branstetter, M.G., White, N.D. & Brady, S.G. (2015) Target enrichment of ultraconserved elements from arthropods provides a genomic perspective on relationships among Hymenoptera. *Molecular Ecology Resources*, 15(3), 489–501. Available from: https://doi.org/10.1111/1755-0998.12328

Faircloth, B.C., McCormack, J.E., Crawford, N.G., Harvey, M.G., Brumfield, R.T. & Glenn, T.C. (2012) Ultraconserved elements anchor thousands of genetic markers spanning multiple evolutionary timescales. *Systematic Biology*, 61(5), 717–726. Available from: https://doi.org/10.1093/sysbio/sys004

Fisher, B.L. (2009) Two new dolichoderine ant genera from Madagascar: *Aptinoma* gen. n. and *Ravavy* gen. n. (Hymenoptera: Formicidae). *Zootaxa*, 2118(1), 37–52. Available from: https://doi.org/10.11646/zootaxa.2118.1.3

Forel, A. (1878) Études myrmécologiques en 1878 (première partie) avec l'anatomie du gésier des fourmis. *Bulletin de la Société Vaudoise Des Sciences Naturelles*, 15, 337–392.

Forel, A. (1909) Fourmis du Musée de Bruxelles. Fourmis de Benguela récoltées par M. Creighton-Wellman, et fourmis du Congo récoltées par MM. Luja, Kohl et Laurent. *Annales de la Société Entomologique de Belgique*, 53, 51–73.

Freitas, F.V., Branstetter, M.G., Franceschini-Santos, V.H., Dorchin, A., Wright, K.W., López-Uribe, M.M. et al. (2023) UCE phylogenomics, biogeography, and classification of long-horned bees (Hymenoptera: Apidae: Eucerini), with insights on using specimens with extremely degraded DNA. *Insect Systematics and Diversity*, 7(4), 3. Available from: https://doi.org/10.1093/isd/ixad012

Gasson, E., DeConto, R.M., Pollard, D. & Levy, R.H. (2016) Dynamic Antarctic ice sheet during the early to mid-Miocene. *Proceedings of the National Academy of Sciences*, 113(13), 3459–3464. Available from: https://doi.org/10.1073/pnas.1516130113

Grabherr, M.G., Haas, B.J., Yassour, M., Levin, J.Z., Thompson, D.A., Amit, I. et al. (2011) Full-length transcriptome assembly from RNA-Seq data without a reference genome. *Nature Biotechnology*, 29(7), 644–652. Available from: https://doi.org/10.1038/nbt.1883

Griebenow, Z.H. et al. (2023) Comparative morphology of male genital skeletomusculature in the Leptanillinae (Hymenoptera: Formicidae), with a standardized muscular terminology for the male genitalia of Hymenoptera. *Arthropod Systematics & Phylogeny*, 81, 945–1018.

Griotti, M., Sara Ceccarelli, F. & Roig-Juñent, S. (2023) Following the aridity: historical biogeography and diversification of the Philodromidae spider genus *Petrichus* in South America. *Molecular Phylogenetics and Evolution*, 180, 107684. Available from: https://doi.org/10.1016/j.ympev.2022.107684

Guerrero, R.J. (2019) Subfamilia Dolichoderinae. Capítulo 24. In: Fernández, F., Guerrero, R.J. & Delsinne, T. (Eds.) *Hormigas de Colombia*. Bogotá: Universidad Naciomal de Colombia, pp. 693–720.

Gullan, P.J., Buckley, R.C. & Ward, P.S. (1993) Ant-tended scale insects (Hemiptera: Coccidae: *Myzolecanium*) within lowland rain forest trees in Papua New Guinea. *Journal of Tropical Ecology*, 9(1), 81–91. Available from: https://doi.org/10.1017/S0266467400006994

Gutiérrez-Valencia, J., Chomicki, G. & Renner, S.S. (2017) Recurrent breakdowns of mutualisms with ants in the neotropical ant-plant genus *Cecropia* (Urticaceae). *Molecular Phylogenetics and Evolution*, 111, 196–205. Available from: https://doi.org/10.1016/j.ympev.2017.04.009

Hashimoto, Y. (1996) Skeletomuscular modifications associated with the formation of an additional petiole on the anterior abdominal segments in aculeate Hymenoptera. *Japanese Journal of Entomology*, 64, 340–356.

Haug, G.H. & Tiedemann, R. (1998) Effect of the formation of the isthmus of Panama on Atlantic Ocean thermohaline circulation. *Nature*, 393(6686), 673–676. Available from: https://doi.org/10.1038/31447

Haug, G.H. et al. (2001) Role of Panama uplift on oceanic freshwater balance. *Geology*, 29(3), 207–210. Available from: https://doi.org/10.1130/0091-7613(2001)029%3C0207:ROPUOO%3E2.0.CO;2

Heath, T.A., Huelsenbeck, J.P. & Stadler, T. (2014) The fossilized birth-death process for coherent calibration of divergence-time estimates. *Proceedings of the National Academy of Sciences*, 111(29), E2957–E2966. Available from: https://doi.org/10.1073/pnas.1319091111

Heilprin, A. (1887) *The geographical and geological distribution of animals*. London: Keegan, Paul, Trench & Co.

Heimburger, B., Maurer, S.S., Schardt, L., Scheu, S. & Hartke, T.R. (2022) Historical and future climate change fosters expansion of Australian harvester termites, *Drepanotermes*. *Evolution*, 76(9), 2145–2161. Available from: https://doi.org/10.1111/evo.14573

Heimburger, B., Schardt, L., Brandt, A., Scheu, S. & Hartke, T.R. (2022) Rapid diversification of the Australian *Amitermes* group during late Cenozoic climate change. *Ecography*, 2022(9), e05944. Available from: https://doi.org/10.1111/ecog.05944

Heled, J. & Drummond, A.J. (2012) Calibrated tree priors for relaxed phylogenetics and divergence time estimation. *Systematic Biology*, 61(1), 138–149. Available from: https://doi.org/10.1093/sysbio/syr087

Heled, J. & Drummond, A.J. (2015) Calibrated birth–death phylogenetic time-tree priors for Bayesian inference. *Systematic Biology*, 64(3), 369–383. Available from: https://doi.org/10.1093/sysbio/syu089

Heterick, B.E. & Shattuck, S.O. (2011) Revision of the ant genus *Iridomyrmex* (Hymenoptera: Formicidae). *Zootaxa*, 2845(1), 1–175. Available from: https://doi.org/10.11646/zootaxa.2845.1.1

Hill, R.S. (1994) The history of selected Australian taxa. In: *History of the Australian vegetation: cretaceous to recent*. Cambridge: Cambridge University Press, pp. 390–419.

Hoang, D.T., Chernomor, O., von Haeseler, A., Minh, B.Q. & Vinh, L.S. (2018) UFBoot2: improving the ultrafast bootstrap approximation. *Molecular Biology and Evolution*, 35(2), 518–522. Available from: https://doi.org/10.1093/molbev/msx281

13653113, 2026, 4, Downloaded from https://resjournals.onlinelibrary.wiley.com/doi/10.1111/syen.70073 by Readcube (Labtiva Inc.), Wiley Online Library on [06/11/2026]. See the Terms and Conditions (https://onlinelibrary.wiley.com/terms-and-conditions) on Wiley Online Library for rules of use; OA articles are governed by the applicable Creative Commons License

Hoffmann, B.D., Andersen, A.N. & Zhang, X. (2011) Taxonomic confusion of two tramp ant species: *Iridomyrmex anceps* and *Ochetellus glaber* are really species complexes. *Current Zoology*, 57(5), 662–667. Available from: https://doi.org/10.1093/czoolo/57.5.662

Höhna, S., Landis, M.J., Heath, T.A., Boussau, B., Lartillot, N., Moore, B.R. et al. (2016) RevBayes: Bayesian phylogenetic inference using graphical models and an interactive model-specification language. *Systematic Biology*, 65(4), 726–736. Available from: https://doi.org/10.1093/sysbio/syw021

Hölldobler, B. & Wilson, E.O. (1990) *The ants*. Berlin: Springer.

Hsu, P.-W., Sosa-Calvo, J., Tseng, S.P., Yamane, S., Hsu, F.C., Wetterer, J.K. et al. (2025) Admixture between lineages of the tramp ant *Technomyrmex albipes* revealed by mitochondrial and ultraconserved element sequencing. *NeoBiota*, 101, 135–159. Available from: https://doi.org/10.3897/neobiota.101.162972

Hughes, A. et al. (2024) A dire need for better standards of data quality, transparency, and reproducibility in IUCN RedList assessments. *EcoEvoRxiv*. Available from: https://doi.org/10.32942/X2KK7D

Hurvich, C.M. & Tsai, C.-L. (1989) Regression and time series model selection in small samples. *Biometrika*, 76(2), 297–307. Available from: https://doi.org/10.1093/biomet/76.2.297

Inoue, J., Donoghue, P.C.J. & Yang, Z. (2010) The impact of the representation of fossil calibrations on Bayesian estimation of species divergence times. *Systematic Biology*, 59(1), 74–89. Available from: https://doi.org/10.1093/sysbio/syp078

Jaitrong, W. & Yamane, S. (2024) A revision of the ant genus *Technomyrmex* Mayr, 1872 (Hymenoptera: Formicidae: Dolichoderinae) in Thailand and Laos. *Natural History Bulletin of the Siam Society*, 66(1), 29–118.

Janzen, D.H. (1974) Epiphytic myrmecophytes in Sarawak: mutualism through the feeding of plants by ants. *Biotropica*, 6(4), 237–259. Available from: https://doi.org/10.2307/2989668

Jeffreys, H. (1961) *The theory of probability*, 3rd edition. Oxford: Clarendon Press.

Johnson, C., Agosti, D., Delabie, J., Dumpert, K., Williams, D.J., von Tschirnhaus, M. et al. (2001) *Acropyga* and *Azteca* ants (Hymenoptera: Formicidae) with scale insects (Sternorrhyncha: Coccoidea): 20 million years of intimate symbiosis. *American Museum Novitates*, 3335, 1–18.

Kalyaanamoorthy, S., Minh, B.Q., Wong, T.K.F., von Haeseler, A. & Jermiin, L.S. (2017) ModelFinder: fast model selection for accurate phylogenetic estimates. *Nature Methods*, 14(6), 587–589. Available from: https://doi.org/10.1038/nmeth.4285

Katoh, K. & Standley, D.M. (2013) MAFFT multiple sequence alignment software version 7: improvements in performance and usability. *Molecular Biology and Evolution*, 30(4), 772–780. Available from: https://doi.org/10.1093/molbev/mst010

Klopfstein, S. (2021) The age of insects and the revival of the minimum age tree. *Austral Entomology*, 60(1), 138–146. Available from: https://doi.org/10.1111/aen.12478

Lanfear, R., Frandsen, P.B., Wright, A.M., Senfeld, T. & Calcott, B. (2017) PartitionFinder 2: new methods for selecting partitioned models of evolution for molecular and morphological phylogenetic analyses. *Molecular Biology and Evolution*, 34(3), 772–773. Available from: https://doi.org/10.1093/molbev/msw260

Lawver, L.A. & Gahagan, L.M. (2003) Evolution of Cenozoic seaways in the circum-Antarctic region. *Palaeogeography, Palaeoclimatology, Palaeoecology*, 198(1–2), 11–37. Available from: https://doi.org/10.1016/S0031-0182(03)00392-4

Leturmy, P. & Robin, C. (2010) Tectonic and stratigraphic evolution of Zagros and Makran during the Mesozoic-Cenozoic: introduction. *Geological Society, London, Special Publications*, 330(1), 1–4. Available from: https://doi.org/10.1144/sp330.1

Lewis, A.R., Marchant, D.R., Ashworth, A.C., Hedenäs, L., Hemming, S.R., Johnson, J.V. et al. (2008) Mid-Miocene cooling and the extinction of tundra in continental Antarctica. *Proceedings of the National Academy of Sciences*, 105(31), 10676–10680. Available from: https://doi.org/10.1073/pnas.0802501105

Lieberman, Z.E., Billen, J., van de Kamp, T. & Boudinot, B.E. (2022) The ant abdomen: the skeletomuscular and soft tissue anatomy of *Amblyopone australis* workers (Hymenoptera: Formicidae). *Journal of Morphology*, 283(6), 693–770. Available from: https://doi.org/10.1002/jmor.21471

Liu, S.-P. et al. (2019) The mesosomal anatomy of *Myrmecia nigrocincta* workers and evolutionary transformations in Formicidae (Hymenoptera). *Arthropod Systematics & Phylogeny*, 77(1), 1–19. Available from: https://doi.org/10.26049/ASP77-1-2019-01

Longino, J.T. (1989) Taxonomy of the *Cecropia*-inhabiting ants in the *Azteca alfari* species group (Hymenoptera: Formicidae): evidence for two broadly sympatric species. *Contributions in Science*, 412, 1–16.

Longino, J.T. (1991) Taxonomy of the *Cecropia*-inhabiting *Azteca* ants. *Journal of Natural History*, 25, 1571–1602.

Longino, J.T. (1996) Taxonomic characterization of some live-stem inhabiting *Azteca* (Hymenoptera: Formicidae) in Costa Rica, with special reference to the ants of *Cordia* (Boraginaceae) and *Triplaris* (Polygonaceae). *Journal of Hymenoptera Research*, 5, 131–156.

Longino, J.T. (2007) A taxonomic review of the genus *Azteca* (Hymenoptera: Formicidae) in Costa Rica and a global revision of the aurita group. *Zootaxa*, 1491(1), 1–63. Available from: https://doi.org/10.11646/zootaxa.1491.1.1

Louca, S. & Pennell, M.W. (2020) Extant timetrees are consistent with a myriad of diversification histories. *Nature*, 580(7804), 502–505. Available from: https://doi.org/10.1038/s41586-020-2176-1

Lowe, S. et al. (2019) *100 of the world's worst invasive alien species: a selection from the global invasive species database*. Auckland: The Invasive Species Specialist Group. Available from: https://doi.org/10.1525/9780520948433-159

Lucky, A. (2011) Molecular phylogeny and biogeography of the spider ants, genus *Leptomyrmex* Mayr (Hymenoptera: Formicidae). *Molecular Phylogenetics and Evolution*, 59(2), 281–292. Available from: https://doi.org/10.1016/j.ympev.2011.03.004

Lucky, A. & Ward, P.S. (2010) Taxonomic revision of the ant genus *Leptomyrmex* Mayr (Hymenoptera: Formicidae). *Zootaxa*, 2688(1), 1–67. Available from: https://doi.org/10.11646/zootaxa.2688.1.1

Lydekker, R. (1896) *A geographical history of mammals*. Cambridge: Cambridge University Press.

Mackay, W. (1993) A review of the New World ants of the genus *Dolichoderus* (Hymenoptera: Formicidae). *Sociobiology*, 22(1), 1–148.

Matte, A., Guénard, B., Gautam, S., Azuma, F., Katzke, J., Hita Garcia, F. et al. (2025) The evolution of cheaper workers facilitated larger societies and accelerated diversification in ants. *Science Advances*, 11(51), eadx8068. Available from: https://doi.org/10.1126/sciadv.adx8068

Matzke, N.J. (2018) BioGeoBEARS: BioGeography with Bayesian (and likelihood) Evolutionary Analysis with R Scripts. https://doi.org/10.5281/zenodo.1478250

Mayr, E. (1944) Wallace's line in the light of recent zoogeographic studies. *The Quarterly Review of Biology*, 19(1), 1–14.

Mayr, G. (1868) Die Ameisen des baltischen Bernsteins. *Beiträge Zur Naturkunde Preussens*, 1, 1–102.

Mayr, G. (1886) Notizen über die Formiciden-Sammlung des British Museum in London. *Verhandlungen der Kaiserlich-Königlichen Zoologisch-Botanischen Gesellschaft in Wien*, 36, 353–368.

Minh, B.Q., Nguyen, M.A.T. & von Haeseler, A. (2013) Ultrafast approximation for phylogenetic bootstrap. *Molecular Biology and Evolution*, 30(5), 1188–1195. Available from: https://doi.org/10.1093/molbev/mst024

Minh, B.Q., Schmidt, H.A., Chernomor, O., Schrempf, D. & Woodhams, M.D. (2020) IQ-TREE 2: new models and efficient methods for phylogenetic inference in the genomic era. *Molecular Biology and Evolution*, 37(5), 1530–1534. Available from: https://doi.org/10.1093/molbev/msaa015

13653113, 2026, 4, Downloaded from https://resjournals.onlinelibrary.wiley.com/doi/10.1111/syen.70073 by Readcube (Labtiva Inc.), Wiley Online Library on [06/11/2026]. See the Terms and Conditions (https://onlinelibrary.wiley.com/terms-and-conditions) on Wiley Online Library for rules of use; OA articles are governed by the applicable Creative Commons License

Morlon, H., Robin, S. & Hartig, F. (2022) Studying speciation and extinction dynamics from phylogenies: addressing identifiability issues. *Trends in Ecology & Evolution*, 37(6), 497–506. Available from: https://doi.org/10.1016/j.tree.2022.02.004

Mouthereau, F., Lacombe, O. & Vergés, J. (2012) Building the Zagros collisional orogen: timing, strain distribution and the dynamics of Arabia/Eurasia plate convergence. *Tectonophysics*, 532–535, 27–60. Available from: https://doi.org/10.1016/j.tecto.2012.01.022

Naser-Khdour, S., Minh, B.Q., Zhang, W., Stone, E.A. & Lanfear, R. (2019) The prevalence and impact of model violations in phylogenetic analysis. *Genome Biology and Evolution*, 11(12), 3341–3352. Available from: https://doi.org/10.1093/gbe/evz193

Nguyen, L.-T., von Haeseler, A. & Minh, B.Q. (2018) Complex models of sequence evolution require accurate estimators as exemplified with the invariable site plus gamma model. *Systematic Biology*, 67(3), 552–558. Available from: https://doi.org/10.1093/sysbio/syx092

Oberski, J.T. (2022) First phylogenomic assessment of the amphitropical New World ant genus *Dorymyrmex* (Hymenoptera: Formicidae), a longstanding taxonomic puzzle. *Insect Systematics and Diversity*, 6(1), 8. Available from: https://doi.org/10.1093/isd/ixab022

Oberski, J.T. (2024) Ultraconserved element (UCE) phylogenomics illuminates the evolutionary history and biogeography of *Dorymyrmex* pyramid ants. *Systematic Entomology*, 50(2), 1–24. Available from: https://doi.org/10.1111/syen.12658

Oberski, J.T., Griebenow, Z.H., Adams, R.M.M., Andersen, A., Andrade-Silva, J., Barden, P. et al. (2025) Ant systematics: past, present, and future. *Insect Systematics and Diversity*, 9(4), 11. Available from: https://doi.org/10.1093/isd/ixaf025

Pan, Q., Darras, H. & Keller, L. (2024) LncRNA gene ANTSR coordinates complementary sex determination in the Argentine ant. *Science Advances*, 10(22), eadp1532. Available from: https://doi.org/10.1126/sciadv.adp1532

Parham, J.F., Donoghue, P.C.J., Bell, C.J., Calway, T.D., Head, J.J., Holroyd, P.A. et al. (2012) Best practices for justifying fossil calibrations. *Systematic Biology*, 61(2), 346–359. Available from: https://doi.org/10.1093/sysbio/syr107

Pavan, M. (1955) Studi sui Formicidae. I. Contributo alla conoscenza degli organi gastrali dei Dolichoderinae. *Natura (Milano)*, 46, 135–145.

Peeters, C. & Wiwatwitaya, D. (2014) *Philidris* ants living inside *Dischidia* epiphytes from Thailand. *Asian Myrmecology*, 6, 49–61.

Pérez-Flores, O., Branstetter, M.G., Longino, J.T., Matos-Maraví, P., Borovanska, M. & Janda, M. (2025) A phylogenomic overview of the ant genus *Tapinoma* Foerster, 1850 (Formicidae: Dolichoderinae), with the phylogeographic history of the ghost ant *Tapinoma melanocephalum*. *Insect Systematics and Diversity*, 9(5), ixaf035. Available from: https://doi.org/10.1093/isd/ixaf035

Perrichot, V., Boudinot, B.E., Engel, M.S., Xu, C., Bojarski, B. & Szwedo, J. (2022) Ants (Hymenoptera: Formicidae) from Miocene Ethiopian amber: filling gaps in the geological record of African terrestrial biota. *Zoological Journal of the Linnean Society*, 196(2), 775–791. Available from: https://doi.org/10.1093/zoolinnean/zlac053

Perrichot, V., Boudinot, B.F. & Chény, C. (2018) The age and paleobiota of Ethiopian amber revisited. In: *5th International Paleontological Congress*. Paris, France: 5th International paleontological Congress, p. 23.

Poinar, G., Archibald, B. & Brown, A. (1999) New amber deposit provides evidence of early Paleogene extinctions, paleoclimates, and past distributions. *The Canadian Entomologist*, 131(2), 171–177. Available from: https://doi.org/10.4039/Ent131171-2

Prebus, M.M. & Lubertazzi, D. (2016) A new species of the ant genus *Bothriomyrmex* Emery, 1869 (Hymenoptera: Formicidae) from the Caribbean region. *European Journal of Taxonomy*, 211, 1–12. Available from: https://doi.org/10.5852/ejt.2016.211

Prebus, M.M. & Rabeling, C. (2025) Phylogenomics resolve the systematics and biogeography of the ant tribe Myrmicini and tribal relationships within the hyperdiverse ant subfamily Myrmicinae. *Systematic Biology*, 74(4), 526–544. Available from: https://doi.org/10.1093/sysbio/syaf022

Probst, R.S., Longino, J.T. & Branstetter, M.G. (2024) Evolutionary déjà vu? A case of convergent evolution in an ant–plant association. *Proceedings of the Royal Society B: Biological Sciences*, 291(2026), 20241214. Available from: https://doi.org/10.1098/rspb.2024.1214

Puttick, M.N. (2019) MCMCtreeR: functions to prepare MCMCtree analyses and visualize posterior ages on trees. *Bioinformatics*, 35(24), 5321–5322. Available from: https://doi.org/10.1093/bioinformatics/btz554

Puttick, M.N. & Title, P. (2019) MCMCtreeR.

QGIS Association. (2026) QGIS. https://doi.org/10.5281/zenodo.6139224

R Core Team. (2023) *R: a language and environment for statistical computing*. Vienna, Austria: R Foundation for Statistical Computing.

Rambaut, A. (2018) FigTree.

Rambaut, A., Drummond, A.J., Xie, D., Baele, G. & Suchard, M.A. (2018) Posterior summarization in Bayesian phylogenetics using tracer 1.7. *Systematic Biology*, 67(5), 901–904. Available from: https://doi.org/10.1093/sysbio/syy032

Ranwez, V., Douzery, E.J.P., Cambon, C., Chantret, N. & Delsuc, F. (2018) MACSE v2: toolkit for the alignment of coding sequences accounting for frameshifts and stop codons. *Molecular Biology and Evolution*, 35(10), 2582–2584. Available from: https://doi.org/10.1093/molbev/msy159

Richter, A. & Economo, E.P. (2023) The feeding apparatus of ants: an overview of structure and function. *Philosophical Transactions of the Royal Society, B: Biological Sciences*, 378(1891), 20220556. Available from: https://doi.org/10.1098/rstb.2022.0556

Richter, A. et al. (2020) Comparative analysis of worker head anatomy of *Formica* and *Brachyponera* (Hymenoptera: Formicidae). *Arthropod Systematics & Phylogeny*, 78(1), 133–170. Available from: https://doi.org/10.26049/ASP78-1-2020-06

Romiguier, J., Borowiec, M.L., Weyna, A., Helleu, Q., Loire, E., la Mendola, C. et al. (2022) Ant phylogenomics reveals a natural selection hotspot preceding the origin of complex eusociality. *Current Biology*, 32(13), 2942–2947.e4. Available from: https://doi.org/10.1016/j.cub.2022.05.001

Sanmartín, I. & Ronquist, F. (2004) Southern hemisphere biogeography inferred by event-based models: plant versus animal patterns. *Systematic Biology*, 53(2), 278–298. Available from: https://doi.org/10.1080/10635150490423430

Santschi, F. (1919) Fourmis du genre *Bothriomyrmex* Emery. (Systématique et moeurs). *Revue Zoologique Africaine*, 7, 201–224.

Santschi, F. (1936) Fourmis nouvelles ou intéressantes de la République Argentine. *Revista de Entomologia*, 6, 402–421.

Santschi, F. (1937) Les sexués du genre *Anillidris* Santschi. *Bulletin de la Société Entomologique de France*, 42, 68–70.

Sarnat, E.M., Fischer, G. & Economo, E.P. (2016) Inordinate spinescence: taxonomic revision and microtomography of the *Pheidole cervicornis* species group (Hymenoptera, Formicidae). *PLoS One*, 11(7), e0156709. Available from: https://doi.org/10.1371/journal.pone.0156709

Scher, H.D. & Martin, E.E. (2006) Timing and climatic consequences of the opening of Drake Passage. *Science*, 312(5772), 428–430. Available from: https://doi.org/10.1126/science.1120044

Schmidt, F.A. et al. (2013) News on the enigmatic ant genus *Anillidris* (Hymenoptera: Formicidae: Dolichoderinae: Leptomyrmecini). Austria: The Austrian Society of Entomofaunistics, Myrmecological News, 19, 25–30.

Scotese, C.R. (2021) An atlas of Phanerozoic paleogeographic maps: the seas come in and the seas go out. *Annual Review of Earth and Planetary Sciences*, 49, 679–728. Available from: https://doi.org/10.1146/annurev-earth-081320-064052

Seifert, B. (2025) Treachery pigmentation pattern leads to misidentification: *Tapinoma melanocephalum* (Fabricius), *Tapinoma pygmaeum* (Dufour) and *Tapinoma jandai* sp. nov. (Hymenoptera, Formicidae).

13653113, 2026, 4, Downloaded from https://resjournals.onlinelibrary.wiley.com/doi/10.1111/syen.70073 by Readcube (Labtiva Inc.), Wiley Online Library on [06/11/2026]. See the Terms and Conditions (https://onlinelibrary.wiley.com/terms-and-conditions) on Wiley Online Library for rules of use; OA articles are governed by the applicable Creative Commons License

*Contributions to Entomology*, 75(2), 245–252. Available from: https://doi.org/10.3897/contrib.entomol.75.e154879

Seifert, B. et al. (2017) Four species within the supercolonial ants of the *Tapinoma nigerrimum* complex revealed by integrative taxonomy (Hymenoptera: Formicidae). *Myrmecological News*, 24, 123–144.

Shattuck, S.O. (1992a) Generic revision of the ant subfamily Dolichoderinae (Hymenoptera: Formicidae). *Sociobiology*, 21, 1–181.

Shattuck, S.O. (1992b) Higher classification of the ant subfamilies Aneuretinae, Dolichoderinae and Formicinae (Hymenoptera: Formicidae). *Systematic Entomology*, 17(2), 199–206. Available from: https://doi.org/10.1111/j.1365-3113.1992.tb00332.x

Shattuck, S.O. (1992c) Review of the dolichoderine ant genus *Iridomyrmex* Mayr with descriptions of three new genera (Hymenoptera: Formicidae). *Journal of the Australian Entomological Society*, 31, 13–18.

Shattuck, S.O. & Marsden, S. (2013) Australian species of the ant genus *Dolichoderus* (Hymenoptera: Formicidae). *Zootaxa*, 3716(2), 101–143. Available from: https://doi.org/10.11646/zootaxa.3716.2.1

Shimodaira, H. & Hasegawa, M. (1999) Multiple comparisons of log-likelihoods with applications to phylogenetic inference. *Molecular Biology and Evolution*, 16(8), 1114–1116. Available from: https://doi.org/10.1093/oxfordjournals.molbev.a026201

Smith, D.J. & Shattuck, S.O. (2009) Six new, unusually small ants of the genus *Leptomyrmex* (Hymenoptera: Formicidae). *Zootaxa*, 2142(1), 57–68. Available from: https://doi.org/10.11646/zootaxa.2142.1.5

Smith, F. (1857) Catalogue of the hymenopterous insects collected at Sarawak, Borneo; Mount Ophir, Malacca; and at Singapore, by A. R. Wallace. [part]. *Journal of the Proceedings of the Linnean Society of London. Zoology*, 2, 42–88.

Stadler, T., Gavryushkina, A., Warnock, R.C.M., Drummond, A.J. & Heath, T.A. (2018) The fossilized birth-death model for the analysis of stratigraphic range data under different speciation modes. *Journal of Theoretical Biology*, 447, 41–55. Available from: https://doi.org/10.1016/j.jtbi.2018.03.005

Stitz, H. (1932) Formicidae der Deutschen Limnologischen Sunda-Expedition. *Archiv Fur Hydrobiologie Suppl.-Bd. 9* (Tropische Binnengewässer 2), 19, 733–737.

Talavera, G. & Castresana, J. (2007) Improvement of phylogenies after removing divergent and ambiguously aligned blocks from protein sequence alignments. *Systematic Biology*, 56(4), 564–577. Available from: https://doi.org/10.1080/10635150701472164

Tribble, C. et al. (2023) RevGadgets: Visualization and post-processing of 'RevBayes' analyses. https://CRAN.R-project.org/package=RevGadgets

Truman, K., Vaughan, T.G., Gavryushkin, A. & Gavryushkina, A.".S.". (2025) The fossilized birth–death model is identifiable. *Systematic Biology*, 74(1), 112–123. Available from: https://doi.org/10.1093/sysbio/syae058

Turk, E., Čandek, K., Kralj-Fišer, S. & Kuntner, M. (2020) Biogeographical history of golden orbweavers: chronology of a global conquest. *Journal of Biogeography*, 47(6), 1333–1344. Available from: https://doi.org/10.1111/jbi.13838

van Dam, M.H. et al. (2021) Genomic characterization and curation of UCEs improves species tree reconstruction. *Systematic Biology*, 70(2), 307–321. Available from: https://doi.org/10.1093/sysbio/syaa063

van den Ende, C., White, L.T. & van Welzen, P.C. (2017) The existence and break-up of the Antarctic land bridge as indicated by both amphi-Pacific distributions and tectonics. *Gondwana Research*, 44, 219–227. Available from: https://doi.org/10.1016/j.gr.2016.12.006

Varela-Hernández, F., Riquelme, F. & Guerrero, R. (2023) A Miocene ant species of the genus *Forelius* Emery, 1888 (Hymenoptera: Formicidae: Dolichoderinae) from Mexico. *Palaeontologia Electronica*, 26(3), a36. Available from: https://doi.org/10.26879/1294

Varela-Hernández, F., Riquelme, F., Guerrero, R.J. & Vázquez-Franco, C.M. (2022) New ant species *Schismiscapus exstinctum* gen. et sp. nov. (Formicidae: Dolichoderinae) from Miocene Mexican amber. *Historical Biology*, 35(7), 1209–1215. Available from: https://doi.org/10.1080/08912963.2022.2085568

Wallace, A.R. (1863) On the physical geography of the Malay archipelago. *The Journal of the Royal Geographical Society of London*, 33, 217–234. Available from: https://doi.org/10.2307/1798448

Wang, T.B. et al. (2010) Natural history observations on the velvety tree ant (*Liometopum occidentale*): unicoloniality and mating flights. *Sociobiology*, 55(3), 787–794.

Ward, P.S., Blaimer, B.B. & Fisher, B.L. (2016) A revised phylogenetic classification of the ant subfamily Formicinae (Hymenoptera: Formicidae), with resurrection of the genera *Colobopsis* and *Dinomyrmex*. *Zootaxa*, 4072(3), 343–357. Available from: https://doi.org/10.11646/zootaxa.4072.3.4

Ward, P.S., Brady, S.G., Fisher, B.L. & Schultz, T.R. (2015) The evolution of myrmicine ants: phylogeny and biogeography of a hyperdiverse ant clade (Hymenoptera: Formicidae). *Systematic Entomology*, 40(1), 61–81. Available from: https://doi.org/10.1111/syen.12090

Ward, P.S., Brady, S.G., Fisher, B.L. & Schultz, T.R. (2010) Phylogeny and biogeography of dolichoderine ants: effects of data partitioning and relict taxa on historical inference. *Systematic Biology*, 59(3), 342–362. Available from: https://doi.org/10.1093/sysbio/syq012

Ward, P.S. & Branstetter, M.G. (2017) The acacia ants revisited: convergent evolution and biogeographic context in an iconic ant/plant mutualism. *Proceedings of the Royal Society B: Biological Sciences*, 284(1850), 20162569. Available from: https://doi.org/10.1098/rspb.2016.2569

Ward, P.S., Fisher, B.L., Wernegreen, J.J. & Blaimer, B.B. (2025) Evolutionary history, novel lineages and symbiont coevolution in the ant tribe Camponotini (Hymenoptera: Formicidae). *Systematic Entomology*, 50(3), 646–676. Available from: https://doi.org/10.1111/syen.12678

Warners-Ruckstuhl, K.N., Govers, R. & Wortel, R. (2013) Tethyan collision forces and the stress field of the Eurasian plate. *Geophysical Journal International*, 195(1), 1–15. Available from: https://doi.org/10.1093/gji/ggt219

Warnock, R.C.M., Parham, J.F., Joyce, W.G., Lyson, T.R. & Donoghue, P.C.J. (2015) Calibration uncertainty in molecular dating analyses: there is no substitute for the prior evaluation of time priors. *Proceedings of the Royal Society B: Biological Sciences*, 282(1798), 20141013. Available from: https://doi.org/10.1098/rspb.2014.1013

Warnock, R.C.M., Yang, Z. & Donoghue, P.C.J. (2011) Exploring uncertainty in the calibration of the molecular clock. *Biology Letters*, 8(1), 156–159. Available from: https://doi.org/10.1098/rsbl.2011.0710

Wheeler, G.C. & Wheeler, J. (1951) The ant larvae of the subfamily Dolichoderinae. *Proceedings of the Entomological Society of Washington*, 53(4), 169–210.

Wheeler, W.M. (1915) The ants of the Baltic Amber. *Schriften der Physikalisch-Ökonomischen Gesellschaft zu Königsberg*, 55, 1–142.

Wheeler, W.M. (1922) Ants of the American Museum Congo expedition. A contribution to the myrmecology of Africa. *Bulletin of the American Museum of Natural History*, 45, 1139 + xl.

Wheeler, W.M. (1942) Studies of Neotropical ant-plants and their ants. *Bulletin of the Museum of Comparative Zoology*, 90(1), 262 + 57.

Wilson, E.O. (1985) Ants of the Dominican amber (Hymenoptera: Formicidae). 3. The subfamily Dolichoderinae. *Psyche (Cambridge)*, 92, 17–37.

Winterton, S.L. & Ware, J.L. (2015) Phylogeny, divergence times and biogeography of window flies (Scenopinidae) and the therevoid clade (Diptera: Asiloidea). *Systematic Entomology*, 40(3), 491–519. Available from: https://doi.org/10.1111/syen.12117

Yang, Z. (2007) PAML 4: phylogenetic analysis by maximum likelihood. *Molecular Biology and Evolution*, 24(8), 1586–1591. Available from: https://doi.org/10.1093/molbev/msm088

Yang, Z. & Rannala, B. (1997) Bayesian phylogenetic inference using DNA sequences: a Markov Chain Monte Carlo Method. *Molecular Biology and Evolution*, 14(7), 717–724. Available from: https://doi.org/10.1093/oxfordjournals.molbev.a025811

13653113, 2026, 4, Downloaded from https://resjournals.onlinelibrary.wiley.com/doi/10.1111/syen.70073 by Readcube (Labtiva Inc.), Wiley Online Library on [06/11/2026]. See the Terms and Conditions (https://onlinelibrary.wiley.com/terms-and-conditions) on Wiley Online Library for rules of use; OA articles are governed by the applicable Creative Commons License

Yang, Z. & Rannala, B. (2006) Bayesian estimation of species divergence times under a molecular clock using multiple fossil calibrations with soft bounds. *Molecular Biology and Evolution*, 23(1), 212–226. Available from: https://doi.org/10.1093/molbev/msj024

Yin, J., Zhang, C. & Mirarab, S. (2019) ASTRAL-MP: scaling ASTRAL to very large datasets using randomization and parallelization. *Bioinformatics*, 35(20), 3961–3969. Available from: https://doi.org/10.1093/bioinformatics/btz211

Yu, G., Smith, D.K., Zhu, H., Guan, Y. & Lam, T.T.Y. (2017) Ggtree: an r package for visualization and annotation of phylogenetic trees with their covariates and other associated data. *Methods in Ecology and Evolution*, 8(1), 28–36. Available from: https://doi.org/10.1111/2041-210X.12628

Zerega, N.J.C., Clement, W.L., Datwyler, S.L. & Weiblen, G.D. (2005) Biogeography and divergence times in the mulberry family (Moraceae). *Molecular Phylogenetics and Evolution*, 37(2), 402–416. Available from: https://doi.org/10.1016/j.ympev.2005.07.004

Zhang, C. & Mirarab, S. (2022) Weighting by gene tree uncertainty improves accuracy of quartet-based species trees. *Molecular Biology and Evolution*, 39(12), msac215. Available from: https://doi.org/10.1093/molbev/msac215

Zhang, C., Ronquist, F. & Stadler, T. (2023) Skyline fossilized birth–death model is robust to violations of sampling assumptions in total-evidence dating. *Systematic Biology*, 72(6), 1316–1336. Available from: https://doi.org/10.1093/sysbio/syad054

Zhang, C., Stadler, T., Klopfstein, S., Heath, T.A. & Ronquist, F. (2016) Total-evidence dating under the fossilized birth–death process. *Systematic Biology*, 65(2), 228–249. Available from: https://doi.org/10.1093/sysbio/syv080

## SUPPORTING INFORMATION

Additional supporting information can be found online in the Supporting Information section at the end of this article.

**Figure S1.** Comparison of topology and support values among alignment and model strategies in the Bothriomyrmecini and Tapinomini. Main topology is consensus topology from UCE concatenation; alternate topologies are shown in insets. Grids at nodes show ultrafast bootstrap values and correspond to analyses given in the inset legend, with colours and symbols corresponding to inset scale; grid cells filled with horizontal lines indicate that the shown topology was not recovered in the given analysis.

**Figure S2.** Comparison of topology and support values among alignment and model strategies in the Leptomyrmecini. Main topology is consensus topology from UCE concatenation; alternate topologies are shown in insets. Grids at nodes show ultrafast bootstrap values and correspond to analyses given in the inset legend, with colours and symbols corresponding to inset scale; grid cells filled with horizontal lines indicate that the shown topology was not recovered in the given analysis.

**Figure S3.** Topology inferred from the 85% taxon occupancy UCE alignment in IQ-TREE2, unpartitioned, with a single GTR + F + G4 model. Numbers at nodes are ultrafast bootstrap support values.

**Figure S4.** Topology inferred from the 90% taxon occupancy UCE alignment in IQ-TREE2, unpartitioned, with a single GTR + F + G4 model. Numbers at nodes are ultrafast bootstrap support values.

**Figure S5.** Topology inferred from the 90% taxon occupancy UCE alignment in IQ-TREE2, partitioned by UCE locus with a GTR + F + G4 model for each partition. Numbers at nodes are ultrafast bootstrap support values.

**Figure S6.** Topology inferred from the 90% taxon occupancy UCE alignment in IQ-TREE2, partitioned by SWSC-en with merged partitions and models selected with ModelFinder. Numbers at nodes are ultrafast bootstrap support values.

**Figure S7.** Topology inferred in wASTRAL, weighted with SH-alrt supports and branch lengths from individual UCE locus trees with selected models inferred in IQ-TREE2. Numbers at nodes are local posterior probabilities.

**Figure S8.** Topology inferred in wASTRAL, weighted with ultrafast bootstrap supports and branch lengths from individual UCE locus trees with selected models inferred in IQ-TREE2. Numbers at nodes are local posterior probabilities.

**Figure S9.** Topology inferred in unweighted ASTRAL from individual UCE locus trees with selected models inferred in IQ-TREE2. Numbers at nodes are local posterior probabilities.

**Figure S10.** Topology inferred from 90% taxon occupancy exon alignment in IQ-TREE2, partitioned by locus with a GTR + F + G4 model for each partition. Numbers at nodes are ultrafast bootstrap support values.

**Figure S11.** Topology inferred from 90% taxon occupancy exon alignment in IQ-TREE2, with locus partitions merged and models selected in ModelFinder. Numbers at nodes are ultrafast bootstrap support values.

**Figure S12.** Topology inferred from 50% taxon occupancy exon alignment in IQ-TREE2, unpartitioned, with a single GTR + F + G4 model. Numbers at nodes are ultrafast bootstrap support values.

**Figure S13.** Histograms of locus concordance values for the 90% UCE alignment (top row), 90% exon alignment (middle row) and 50% exon alignment (bottom row). First column: gene concordance factor; second column: first discordance factor; third column: second discordance factor; fourth column: discordance factor due to polyphyly.

**Figure S14.** Calibration, effective prior, and posterior densities for the root node, estimated in MCMCtree. Vertical axis: probability density; horizontal axis: time in hecto-Megaannum (100 million years). Density colours correspond to inset legend. Thick dashed black line shows calibration density. Red vertical dashed lines bound the Grassy Lake amber interval; blue vertical dashed lines bound the Kachin amber interval.

**Figure S15.** Calibration, effective prior and posterior densities for the MRCA of the Bothriomyrmecini + Tapinomini, estimated in MCMCtree. Vertical axis: probability density; horizontal axis: time in hecto-Megaannum (100 million years). Density colours correspond to inset legend. Thick dashed black line shows calibration density. Red vertical dashed lines bound the calibrating Hat Creek amber interval.

**Figure S16.** Calibration, effective prior and posterior densities for the MRCA of the *Loweriella* genus group, estimated in MCMCtree. Vertical axis: probability density; horizontal axis: time in hecto-Megaannum (100 million years). Density colours correspond to inset legend. Thick dashed black line shows calibration density. Red vertical dashed lines bound the calibrating Ethiopian amber interval.

13653113, 2026, 4, Downloaded from https://resjournals.onlinelibrary.wiley.com/doi/10.1111/syen.70073 by Readcube (Labtiva Inc.), Wiley Online Library on [06/11/2026]. See the Terms and Conditions (https://onlinelibrary.wiley.com/terms-and-conditions) on Wiley Online Library for rules of use; OA articles are governed by the applicable Creative Commons License

**Figure S17.** Calibration, effective prior and posterior densities for the MRCA of the *Tapinoma* genus group, estimated in MCMCtree. Vertical axis: probability density; horizontal axis: time in hecto-Megaannum (100 million years). Density colours correspond to inset legend. Thick dashed black line shows calibration density. Red vertical dashed lines bound the calibrating Baltic amber interval.

**Figure S18.** Calibration, effective prior and posterior densities for the MRCA of the *Technomyrmex* genus group, estimated in MCMCtree. Vertical axis: probability density; horizontal axis: time in hecto-Megaannum (100 million years). Density colours correspond to inset legend. Thick dashed black line shows calibration density. Red vertical dashed lines bound the calibrating Ethiopian amber interval.

**Figure S19.** Calibration, effective prior and posterior densities for the MRCA of *Dolichoderus*, estimated in MCMCtree. Vertical axis: probability density; horizontal axis: time in hecto-Megaannum (100 million years). Density colours correspond to inset legend. Thick dashed black line shows calibration density. Red vertical dashed lines bound the calibrating Hat Creek amber interval.

**Figure S20.** Calibration, effective prior and posterior densities for the MRCA of the *Dolichoderus quadripunctatus* and *sulcaticeps* species groups, estimated in MCMCtree. Vertical axis: probability density; horizontal axis: time in hecto-Megaannum (100 million years). Density colours correspond to inset legend. Thick dashed black line shows calibration density. Red vertical dashed lines bound the calibrating Baltic amber interval.

**Figure S21.** Calibration, effective prior and posterior densities for the MRCA of the *Dolichoderus bispinosus* and *bidens* species groups sensu lato, estimated in MCMCtree. Vertical axis: probability density; horizontal axis: time in hecto-Megaannum (100 million years). Density colours correspond to inset legend. Thick dashed black line shows calibration density. Red vertical dashed lines bound the calibrating Dominican amber interval.

**Figure S22.** Calibration, effective prior and posterior densities for the MRCA of the Leptomyrmecini, estimated in MCMCtree. Vertical axis: probability density; horizontal axis: time in hecto-Megaannum (100 million years). Density colours correspond to inset legend. Thick dashed black line shows calibration density. Red vertical dashed lines bound the calibrating Chiapas amber interval.

**Figure S23.** Calibration, effective prior and posterior densities for the MRCA of the *Leptomyrmex* genus group, estimated in MCMCtree. Vertical axis: probability density; horizontal axis: time in hecto-Megaannum (100 million years). Density colours correspond to inset legend. Thick dashed black line shows calibration density. Red vertical dashed lines bound the calibrating Dominican amber interval.

**Figure S24.** Calibration, effective prior and posterior densities for the MRCA of the *Azteca* genus group, estimated in MCMCtree. Vertical axis: probability density; horizontal axis: time in hecto-Megaannum (100 million years). Density colours correspond to inset legend. Thick dashed black line shows calibration density. Red vertical dashed lines bound the calibrating Dominican amber interval.

**Figure S25.** Chronogram inferred without data under the conditional construction in MCMCtree. Blue distributions at nodes are effective prior distributions. Horizontal axis, top: absolute ages in Ma. Horizontal axis, bottom: geological epochs: Ea, Early (Lower) Cretaceous; La, Late (Upper) Cretaceous; P, Palaeocene; Eo, Eocene; O, Oligocene; Mi, Miocene.

**Figure S26.** Chronogram inferred without data under the multiplicative construction in MCMCtree. Blue distributions at nodes are effective prior distributions. Horizontal axis, top: absolute ages in Ma. Horizontal axis, bottom: geological epochs: La, Late (Upper) Cretaceous; P, Palaeocene; Eo, Eocene; O, Oligocene; Mi, Miocene.

**Figure S27.** Chronogram inferred under the multiplicative joint prior in MCMCtree with posterior distributions shown at nodes. Horizonal axis, top and bottom: absolute ages (Ma); horizontal axis, lower: geological periods and epochs. Purple distributions = 95% highest posterior density distribution for calibration nodes. Red bars = calibration priors. Blue distributions = 95% highest posterior density distribution for non-calibration nodes. Periods: K, Cretaceous; Pg, Palaeogene; Ng, Neogene. Epochs: LC, Lower Cretaceous, UC, Upper Cretaceous, Pal, Palaeocene, Eo, Eocene, Oli, Oligocene, Mio, Miocene. Geological periods: K, Cretaceous, Pg, Palaeogene, Ng, Neogene, Q, Quaternary.

**Figure S28.** Comparison of chronograms inferred under the conditional construction (black branches) and multiplicative construction (red branches) in MCMCtree. Horizonal axis, top and bottom: absolute ages (Ma); horizontal axis, lower: geological periods and epochs. Periods: K, Cretaceous; Pg, Palaeogene; Ng, Neogene. Epochs: LC, Lower Cretaceous, UC, Upper Cretaceous, Pal, Palaeocene, Eo, Eocene, Oli, Oligocene, Mio, Miocene. Geological periods: K, Cretaceous, Pg, Palaeogene, Ng, Neogene, Q, Quaternary.

**Figure S29.** Comparison of densities of posterior age estimates, major clade ages and major geological intervals, under the conditional construction (top panel) and multiplicative construction (lower panel) in MCMCtree. Vertical axis: probability density. Horizontal axis: age in Megaannum. Blue distributions: density of mean ages; dark grey distributions: density of lower bound estimates for 95% highest posterior densities; light grey distributions: density of upper bound estimates for 95% highest posterior densities. Grey bar with 45° dashed lines = Grassy Lake amber interval; grey bar with −45° dashed lines = Kachin amber interval. Dashed black vertical line: Cretaceous–Palaeogene boundary. Black vertical lines = mean root age estimates; red vertical lines = mean age estimate for crown Dolichoderinae; green vertical lines = mean age estimate for the MRCA of Bothriomyrmecini + Tapinomini; dark blue vertical lines = mean age estimates for the MRCA of Bothriomyrmecini; light blue vertical lines = mean age estimates for the MRCA of Tapinomini; purple vertical lines = mean age estimates for the MRCA of Dolichoderini + Leptomyrmecini; grey vertical lines = mean age estimates for the MRCA of Leptomyrmecini.

**Figure S30.** Biogeographic ancestral range reconstruction tree inferred in RevBayes under the DEC model using the conditional chronogram from MCMCtree. Horizontal axis, top and lower: absolute ages (Ma); horizontal axis, bottom: geological periods and epochs. Coloured circles at nodes represent inferred ranges, with internal areas corresponding to proportional likelihoods. Coloured circles at tips represent extant distributions as coded. Colours correspond to ranges, as detailed in the inset legend. R, Nearctic; T, Neotropical; P,

13653113, 2026, 4, Downloaded from https://resjournals.onlinelibrary.wiley.com/doi/10.1111/syen.70073 by Readcube (Labtiva Inc.), Wiley Online Library on [06/11/2026]. See the Terms and Conditions (https://onlinelibrary.wiley.com/terms-and-conditions) on Wiley Online Library for rules of use; OA articles are governed by the applicable Creative Commons License

Palearctic; A, Afrotropical; I, Indomalayan; U, Australasian. Geological periods: K, Cretaceous; Pg, Palaeogene; Ng, Neogene; Q, Quaternary. Geological epochs: LC, Lower Cretaceous; UC, Upper Cretaceous; Pal, Palaeocene; Eo, Eocene; Oli, Oligocene; Mio, Miocene.

**Figure S31.** Biogeographic ancestral range reconstruction tree inferred in RevBayes under the DEC + J model using the conditional chronogram from MCMCtree. Horizontal axis, top: absolute ages (Ma); horizontal axis, bottom: geological periods and epochs. Coloured circles at nodes represent inferred ranges, with internal areas corresponding to proportional likelihoods. Coloured circles at tips represent extant distributions as coded. Colours correspond to ranges, as detailed in the inset legend. R, Nearctic; T, Neotropical; P, Palearctic; A, Afrotropical; I, Indomalayan; U, Australasian. Geological periods: K, Cretaceous; Pg, Palaeogene; Ng, Neogene; Q, Quaternary. Geological epochs: LC, Lower Cretaceous; UC, Upper Cretaceous; Pal, Palaeocene; Eo, Eocene; Oli, Oligocene; Mio, Miocene.

**Figure S32.** Node labels for divergence dating inferences in MCMCtree, corresponding to numbers in Tables 5 and S11.

**Figure S33.** Node labels for biogeographic inferences, corresponding to numbers in Table S12.

**Table S1.** Collection data. **USI** unique specimen identifier. **AntWeb** embedded hyperlink to AntWeb specimen page of voucher. **Old_Name** other versions of the taxon name given in Genus and Species, as they may appear in supplementary files or data. **ExtractionID** unique identifying code referring to DNA extractions, assigned to voucher. **VoucherType** the voucher may be the **same specimen** from which DNA was extracted (most adults); an adult from the **same nest** as the extracted specimen (usually a pupa); or from the **same series** of collected individuals inferred to be nestmates (destructive extraction of adults). **Sequenced_Material** lifestage and caste of extracted specimen: **w** worker; **q** queen; **m** male; **p** pupa; **D** destructive extraction; **ND** nondestructive extraction; **PPND** previously pinned specimen, nondestructive extraction. **VoucherRepository** name of repository where vouchers are housed: **BEBC** Brendon E. Boudinot personal research collection; **CASC** California Academy of Sciences; **DZUP** Departamento de Zoologia (Museu de Entomologia Padre Jesus Santiago Moure), Universidade Federal do Paraná; **JTLC** John T. Longino personal research collection; **UCDC** Bohart Museum of Entomology, University of California, Davis. **Country** codes follow the International Organization for Standardization.

**Table S2.** Bioinformatic and accession information. **USI** unique specimen identifier. **Old_Name** other versions of the taxon name given in Genus and Species, as they may appear in supplementary files or data. **ExtractionID** unique identifying code referring to DNA extractions, assigned to voucher. **Lane** name of sequencing lane. **OE** original extraction: specimen originally extracted for Ward Lab UCE work **WL-UCE** or for the Ant Tree of Life project **AToL**, in which case aliquots were re-sequenced; or external reference provided. **Sequencing_Location** facility or institution where sequencing was performed. **LibPrep_Location** facility or group where library preparation (and target enrichment, where Strategy = TE) were performed. **Strategy** locus capture strategy; **TE** UCE target enrichment; **WG** low-coverage whole-genome sequencing. **Assembled_By** name of individual who assembled reads. **SRA_Accession** Sequence Read Archive unique identifier. **BioSample** BioSample unique identifier. **SRA_Proj** Sequence Read Archive project identifier. **BioProject** BioProject identifier. **Study** reference for source of reads, or * indicating this study. **Total_BP** total number of base pairs. **MeanContigLength** mean contig length in number of base pairs. **No_Contigs_Over_1kb** number of contigs greater than one kilobase in length. Rows filled with grey are sequences from external studies.

**Table S3.** Alignment statistics. **Alignment_name** name of alignment file in Supplementary Data. **Alignment_description** description of alignment. **No_of_taxa** number of taxa in alignment. **No_of_loci_-parts** number of loci or partitions. **Alignment_length_sites** number of nucleotide sites in alignment. **Total_matrix_cells** total number of data in alignment. **Undetermined_characters** number of undetermined sites. **Proportion_missing** proportion of missing data. **No_variable_sites** number of variable sites. **Proportion_variable_-sites** proportion of variable sites. **Parsimony_informative_sites** number of parsimony informative sites. **Proportion_parsimony_informative** proportion of parsimony-informative sites. **AT_content** proportion of adenine and thymine sites. **GC_content** proportion of guanine and cystosine sites. **A** number of adenine sites. **C** number of cystosine sites. **G** number of guanine sites. **T** number of thymine sites. – number of gaps.**?** number of undetermined sites.

**Table S4.** Per-sequence statistics for the 85% UCE alignment.

**Table S5.** Per-sequence statistics for the 95% UCE alignment.

**Table S6.** Per-sequence statistics for the 50% exon alignment.

**Table S7.** Per-sequence statistics for the 90% exon alignment.

**Table S8.** Adjacency matrices used in biogeographic inference. **Legend** gives abbreviations for areas. Columns with grey dashed fill give ages of breakpoints in Ma. **1** = areas considered adjacent within the time bin; **0** = areas not considered adjacent within the time bin.

**Table S9.** Summary of concordance factors for the 50% exon alignment, 90% exon alignment and 90% UCE alignment. Nodes numbers correspond to labels in fig. Values are coloured according to the scale in column **Scale**.

**Table S10.** All concordance factor statistics for the 50% exon alignment, 90% exon alignment and 90% UCE alignment. **Node** numbers correspond to labels in fig. **gCF** concordance factor (=gcf_N/gN%); g**CF_N** number of trees concordant with the branch; **gDF1** gene discordance factor for NNI-1 branch (=gDF1_N/gN%); **gDF1_N** number of trees concordant with NNI-1 branch; **gDF2** gene discordance factor for NNI-2 branch (=gDF2_N/gN %); **gDF2_N** number of trees concordant with NNI-2 branch; **gDFP** gene discordance factor due to polyphyly (=gDFP_N/gN %); **gDFP_N** number of trees decisive but discordant due to polyphyly; **gN** number of trees decisive for the branch; **UFB** ultrafast bootstrap support at given branch; **BPP** Bayesian posterior probability at given node; **Length** branch length.

**Table S11.** Posterior age estimates from MCMCtree. **Node Number** corresponds to labels in Figure S32; **C_mean** mean estimate from conditional construction; **C_95HPD_low** lower bound of the 95%

13653113, 2026, 4, Downloaded from https://resjournals.onlinelibrary.wiley.com/doi/10.1111/syen.70073 by Readcube (Labtiva Inc.), Wiley Online Library on [06/11/2026]. See the Terms and Conditions (https://onlinelibrary.wiley.com/terms-and-conditions) on Wiley Online Library for rules of use; OA articles are governed by the applicable Creative Commons License

highest posterior density from conditional construction; **C_95HPD_up** upper bound of the 95% highest posterior density from conditional construction; **M_mean** mean estimate from multiplicative construction; **M_95HPD_low** lower bound of the 95% highest posterior density from multiplicative construction; **M_95HPD_up** upper bound of the 95% highest posterior density from multiplicative construction.

**Table S12.** Posterior probabilities for ancestral areas inferred with BioGeoBEARS under models given in the top row. **Node** numbers correspond to labels in Figure S33; **end_state_1** most probable state; **end_state_1_pp** posterior probability of end state 1; **end_state_2** second most probable state; **end_state_2_pp** posterior probability of end state 2; **end_state_3** third most probable state; **end_state_3_pp** posterior probability of end state 3; **end_state_other** posterior probability of all other states. **R**, Nearctic; **T**, Neotropical; **P**, Palearctic; **A**, Afrotropical (including Malagasy); **I**, Indomalayan; **U**, Australasian. **n/a**, not applicable.

**Table S13.** AntWeb (www.antweb.org) photographer credits for images in Figure 2. **Unique_ID**, unique specimen identifier.

**File S1.** Supporting information.

**How to cite this article:** Lieberman, Z.E., Oberski, J.T. & Boudinot, B.E. (2026) The origin and evolution of Dolichoderinae, a dominant ant clade (Hymenoptera: Formicidae). *Systematic Entomology*, 51(4), e70073. Available from: https://doi.org/10.1111/syen.70073

13653113, 2026, 4, Downloaded from https://resjournals.onlinelibrary.wiley.com/doi/10.1111/syen.70073 by Readcube (Labtiva Inc.), Wiley Online Library on [06/11/2026]. See the Terms and Conditions (https://onlinelibrary.wiley.com/terms-and-conditions) on Wiley Online Library for rules of use; OA articles are governed by the applicable Creative Commons License